NTNU – Trondheim
Norwegian University of
Science and Technology

Validation of a Combined Wind and Wave Power Installation

Ingrid Brandtsegg Lome

Marine Technology
Submission date: June 2014
Supervisor: Sverre Steen, IMT
Co-supervisor: Jørgen Hals Todalshaug, MARINTEK

Norwegian University of Science and Technology
Department of Marine Technology

NTNU Trondheim
Norwegian University of Science and Technology
Department of Marine Technology

MASTER THESIS IN MARINE TECHNOLOGY

SPRING 2014

FOR

Ingrid Lome

Validation of a combined wind and wave power installation

Floating platforms for extraction of energy from both wind and waves has been a popular topic in European ocean research the later years. This project will consider a concept developed by NTNU and MARINTEK in cooperation with industry in the context of an EU research project.
The objectives of the master thesis are to investigate the feasibility and efficiency of the proposed system, and to propose improvements to the design. The following activities should be carried out in the master thesis:

- Improve the numerical simulation model, in order to make it more complete and more correct. The numerical simulation model shall cover both the complete unit, and one side of the unit, which is the object of the planned test.
- Design a test set-up and test program that can be performed in the MCLab at the Marine Technology Centre. The specific objective of the test must be made very clear (since it will not be the same as for the entire master thesis).
- Perform the model test
- Analyze the model test results, and use the analyzed results to evaluate, validate and possibly tune the simulation model.
- Evaluate the feasibility and efficiency of the proposed concept, and give recommendations.

In the thesis the candidate shall present his personal contribution to the resolution of problem within the scope of the thesis work.

Theories and conclusions should be based on mathematical derivations and/or logic reasoning identifying the various steps in the deduction.

The thesis work shall be based on the current state of knowledge in the field of study. The current state of knowledge should be established through a thorough literature study, the results of this study shall be written into the thesis. The candidate should utilize the existing possibilities for obtaining relevant literature.

The thesis should be organized in a rational manner to give a clear exposition of results, assessments, and conclusions. The text should be brief and to the point, with a clear language. Telegraphic language should be avoided.

The thesis shall contain the following elements: A text defining the scope, preface, list of contents, summary, main body of thesis, conclusions with recommendations for further work, list of symbols and acronyms, reference and (optional) appendices. All figures, tables and equations shall be numerated.

NTNU Trondheim
Norwegian University of Science and Technology
Department of Marine Technology

The supervisor may require that the candidate, in an early stage of the work, present a written plan for the completion of the work. The plan should include a budget for the use of computer and laboratory resources that will be charged to the department. Overruns shall be reported to the supervisor.

The original contribution of the candidate and material taken from other sources shall be clearly defined. Work from other sources shall be properly referenced using an acknowledged referencing system.

The thesis shall be submitted electronically (pdf) in DAIM:

- Signed by the candidate
- The text defining the scope (signed by the supervisor) included
- Computer code, input files, videos and other electronic appendages can be uploaded in a zip-file in DAIM. Any electronic appendages shall be listed in the main thesis.

The candidate will receive a printed copy of the thesis.

Supervisor	: Professor Sverre Steen
Advisor	: Jørgen Hals, MARINTEK
Start	: 14.01.2014
Deadline	: 10.06.2014

Trondheim, 14.01.2014

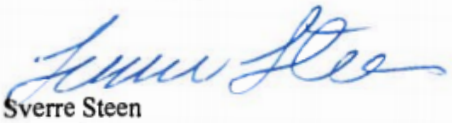

Sverre Steen
Supervisor

Preface

This master thesis in marine hydrodynamics concludes the Master Degree program of Marine Technology at the Norwegian University of Science and Technology. It accounts for 30 credits and has been carried out from January to June 2014. This thesis has been in cooperation with MARINTEK and Pelagic Power as a part of the EU research project MARINA Platform. A pre-study of the subject was done during the fall of 2013.

First, I would like to thank my supervisor at NTNU, Sverre Steen for guidance throughout the semester. He has been of great help, especially with planning of the model test set-up. Also, my advisor Jørgen Hals Todalshaug at MARINTEK has been very helpful and has answered all my questions regardless of how stupid they were.

During the experimental campaign Torgeir Wahl helped me with almost everything, I would not have been able to carry out the model tests without his help. Great thanks is also given to MARINTEK for allowing me to use the Marine Cybernetics Lab and the guys at the workshop for assembling and dismounting the model, and making new parts that were needed. Without the W2Power design by Pelagic Power and Inrigo AS building and financing the model, there would not have been a thesis. I am thankful for this opportunity to learn more about wave power.

Finally, thanks to Helle Tessand Baalsrud and Hege Eskild for proofreading my thesis and the girls whom I share an office with for being discussion partners and offering large amounts of moral support.

The softwares used were unknown to me before this work started, and much time was spent trying to figure out how to implement all desired features. Unfortunately, lack of time made the numerical modelling difficult and the final models not as good as I had hoped.

The work with this thesis has been extremely educational. I have learned a lot about wave power production and experienced the practical side of engineering, which I have enjoyed to the fullest.

MTS, Trondheim, June 10th 2014

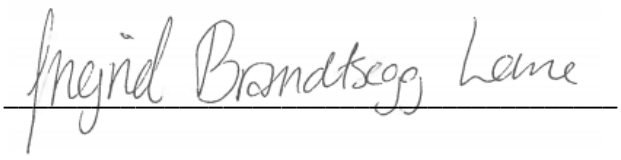

Ingrid Brandtsegg Lome

Summary

To meet the increasing energy demand of the world it is important to develop technology for harvesting energy from renewable sources. One of the largest renewable energy sources is the world's oceans, where wind, wave and thermal energy are considered the main sources. Offshore wind and wave technology is emerging; several designs are under development and prototype testing of some technologies has given positive results. It is beneficial to install wind turbines and wave converters on the same foundation as this can reduce costs and facilitate connection to shore.

A validation of the combined wind and wave power production platform W2Power has been carried out in this thesis. W2Power is a triangular semi-submersible platform with two wind turbines and ten wave energy converters along the sides. The work has consisted of planning and performing an experimental campaign and making numerical simulation models of the platform. For the experimental campaign only one side of the platform has been considered, this to reduce costs and increase test model accuracy. The main objectives of the experimental campaign were estimation of power production and investigation of the interaction between the wave energy converters. The wave energy converters were tested for operational conditions, both regular and irregular waves. A total of three simulation models have been made using the softwares GeniE, HydroD (Wadam) and SIMA. Of these, two models are of the experimental set-up, where one is tuned to produce the same results as the model tests and one is untuned for comparison, and one model of the entire platform. The two wind turbines integrated in the W2Power design have not been taken into account.

The model tests were not performed with optimal load resistance in the air cylinders due to a calculation error made in the beginning of the experimental campaign. This resulted in the air cylinders acting more as springs than dampers, overestimating the actual forces and slightly underestimating the responses of the buoys. Some measurements with optimal load resistance exist, and the estimation of produced power was done based on these. An electricity production of 10 – 400 GWh per year was estimated as a total for all ten wave converters connected to the platform. The expected electricity output of the platform should be in the range of 1 – 10 GWh per year, when compared with other wave energy devices, making the estimations unexpectedly high.

The RAOs computed in Wadam for the buoys alone, i.e. not connected to the platform framework, concord with the calculated RAOs from the model test. The heave peak period in Wadam is 6 seconds versus 5.5 seconds for the measured results, while the surge peak periods are 5 versus 5.5 seconds. The heave peak amplitudes varies from 1.9 m/m for 0^o incoming angle to 1.3 m/m for 90^o and from 0.7 m/m to 0.4 m/m in surge. This concordance implies that the hydrodynamics of the buoys is correctly modelled. The responses measured during the model test and the calculated RAOs revealed that a shadowing effect between the buoys exist: the buoy interacting with the incoming waves first have higher response and forces than the other buoys.

The analyses done with the numerical simulation model in SIMA did not give satisfactory results. The rotation point was modelled so that the rotation arms of the buoys were flexible instead of stiff arms rotating about a point. To achieve correct responses large forces were applied to the fixed elongation couplings representing the air cylinders. This led to large vertical forces on the rotation arm that were not consistent with the measured forces. However, the simulated horizontal forces acting on the platform framework were of equal magnitude as the measured for most conditions analysed. The response of the buoys had to be reduced to simulate correct vertical forces, making the numerical model inconsistent with the measured responses.

Based on the model test and the estimation of produced power, it was concluded that the W2Power design is feasible.

Sammendrag

Det er viktig å utvikle ny teknologi for å høste energi fra fornybare kilder slik at det økende energibehovet i verden kan tilfredsstilles. En av de største fornybare energikildene er verdenshavene, hvor vind, bølger og termisk energi er ansett som hovedkilder. Offshore vind- og bølgeteknologi på vei fremover: flere konsepter er under utvikling og tester av prototyper har for noen teknologier gitt positive resultater. Fordelene med å installere vindturbiner og bølgekraftomformere på samme fundament er kostnadsreduksjon og enklere kobling til strømnettet.

En validering av det kombinerte vind- og bølgekraftverket W2Power har blitt utført i denne oppgaven. W2Power er en triangulær halvt nedsenkbar plattform med to vindturbiner og ti bølgekraftomformere langs sidene. Arbeidet har bestått av å planlegge og utføre et modellforsøk og å lage numeriske simuleringsmodeller av plattformen. I modellforsøket er det kun én side av plattformen som har blitt behandlet, dette for å redusere kostnader og øke nøyaktigheten til modellen. Formålene med modellforsøket var å estimere produsert kraft og å undersøke hvordan bølgekraftomformerne påvirket hverandres bevegelser. Bølgekraftomformerne ble testet for normal driftstilstand i både regulære og irregulære bølger. Totalt ble det laget tre numeriske modeller ved hjelp av programvarene GeniE, HydroD (Wadam) og SIMA. Av disse var to modeller av forsøksoppsettet, hvor en ble justert slik at den ga like resultater som forsøket og den andre forble ujustert og brukt til sammenligning. Den tredje modellen var av hele plattformen. De to vindturbinene integrert i plattformdesignet har ikke blitt tatt hensyn til i arbeidet.

Modellforsøket ble ikke utført med optimal lastresistans i luftsylindrene på grunn av en regnefeil som ble gjort i begynnelsen av forsøket. Dette førte til at luftsylindrene oppførte seg mer som fjær enn dempere, noe som ga overestimerte krefter på konstruksjonen og underestimert respons til bøyene. Noen målinger med korrekt optimal lastresistans eksisterer, disse ble brukt i beregningene av produsert kraft. En årlig elektrisitetsproduksjon på 10 – 400 GWt ble estimert for alle ti bølgekraftomformerne samlet. Sammenlignet med andre bølgekraftomformere burde den forventede elektrisitetsproduksjonen fra plattformen være rundt 1 – 10 GWt per år, noe som gjør produksjonsestimatet uforventet høyt.

Transferfunksjonene for respons beregnet i Wadam for bøyene uten kobling til plattformen stemmer overens med beregningene gjort på grunnlag av modellforsøket. Topp-perioden i hiv er 6 sekunder i Wadam mot 5.5 sekunder for de målte resultatene, mens topp-periodene i jag er 5 mot 5.5 sekunder. Topp-amplituden i hiv varierer fra 1.9 m/m for 0^o innkommende bølge-vinkel til 1.3 m/m for 90^o og fra 0.7 m/m til 0.4 m/m i jag. Denne overensstemmelsen betyr at hydrodynamikken til bøyene er modellert korrekt. Responsene målt under forsøket og de beregnede transferfunksjonene for respons viste at en skygge-effekt mellom bøyene eksisterer: den bøya som bryter bølgene først har større bevegelse og blir påført større krefter enn de andre bøyene.

Analysene som ble gjort med de numeriske simuleringsmodellene i SIMA ga ikke tilfredsstillende resultater. Rotasjonspunktet var modellert slik at rotasjonsarmene var fleksible, istedenfor stive armer roterende rundt ett punkt. For å oppnå korrekte responser måtte store krefter påføres det som representerte luftsylindrene i modellen. Dette førte til store vertikale krefter på rotasjonsarmen som ikke stemte overens med kreftene fra modellforsøket. De simulerte horisontale kreftene på plattformen var imidlertid av samme størrelsesorden som de målte kreftene for de fleste analyserte tilstandene. Responsen til bøyene måtte reduseres for å simulere korrekte vertikale krefter, noe som gjorde at responsen i den numeriske modellen ikke lenger var lik den målte.

Basert på modellforsøket og beregningen av produsert kraft ble det konkludert at teknologien bak W2Power er mulig.

Table of Content

List of figures

List of tables

Symbols and acronyms

SYMBOL	DIMENSION	EXPLANATION
H	m	Wave height
H(ω)	m/m or N/m	Transfer function
H_s	m	Significant wave height
S_{xx} (ω)	m^2s	Input (wave) spectrum
S_{YY} (ω)	m^2s or N^2s	Output spectrum
T	s	Wave period
T_p	s	Peak period
$x_{1/3}$	m or N	Significant value
γ	-	Peak-enhancement factor
ζ_a	m	Wave amplitude
λ	-	Scale factor
ξ	-	Damping ratio
σ	m or N	Standard deviation
ω	1/s or rad/s	Wave frequency

ACRONYM	EXPLANATION
WT	Wind turbine
WEC	Wave energy converter
IEA	International Energy Association
EWEA	European Wind Energy Association
BRIC	Brazil, Russia, India, China
RAO	Response Amplitude Operator

1. Introduction

1.1 Background and motivation

The primary energy (energy found in nature that has not been subjected to conversion) consumption in the world in 2012 was 12 477 Mtoe or almost 150 000 TWh. Of this about 15 % was converted and used as electricity [1].

The demand for primary energy in the world will increase during the next decades. This is, among other factors, due to expected increase in population and the dynamism of economies in areas with great potential such as the BRIC countries. The world's demand for electricity is growing with almost two times the rate of its total energy consumption [2] as more and more technologies are electrified (e.g. cars, heating).

According to the New Policies Scenario stated by the International Energy Association [2] the global energy demand will grow more than one third from today's level by 2035. The world today is failing to put the global energy system onto a more sustainable path, even when accounting for all new developments and policies. It is expected that renewables will account for almost one third of the world's total electricity output and approach coal as the primary source of global electricity in 2035 [2]. At this point the contribution from offshore wind will be around 20 % of the total produced wind power. The contribution from marine energy ought to increase from the 2030s and onward to around 5 – 8 % of the electricity worldwide [3].

Some of the main reasons for developing renewable energy power plants are lower greenhouse gas emissions, reduction in local pollution and a reliable supply of energy as several countries wish to reduce their dependence on oil and gas [4]. Ocean energy technologies have a potential to contribute significantly to the reduction of greenhouse gas emissions as they have low lifecycle emissions [5].

To reduce greenhouse gas emissions and slow down the heating of the earth, not all petroleum and gas found can be extracted. Instead, technology for exploiting other energy sources should be developed further, such as offshore wind and wave energy. It is uncertain how much oil and gas that is left to be exploited, but there are still considerable amounts left. Even so, when Norway run out of oil and gas, or when the government decides to leave the rest in the ground, it is important that Norway already has the expertise and technology to provide other methods to produce power.

The Directive of the European Parliament and of the Council on the promotion of the use of energy from renewable sources of 2011 states that the countries within the EU shall contribute to increase the share of renewable energy used for electricity to 20 % by 2020 [6]. A suggestion of at least 27 % renewables by 2030 was recently made by the EU, which will be debated in the European Council and European Parliament before set into action [7]. The countries of the EU have also agreed to reduce CO_2 emissions by 20 % compared to 1990 levels by 2020. Today, the emissions are around 18 % below 1990 levels, and the new climate goal up for debate is set to a reduction of 40 % by 2030 [7]. By 2050 the target is to reduce Europe's greenhouse emissions by 80 – 95 % compared to 1990 levels [8].

The world's oceans are a huge source of energy, not only when it comes to oil and gas, but also for offshore wind and wave power. For wind turbines two of the biggest advantages compared to onshore turbines are that the wind is much stronger offshore and that turbines of larger dimensions can be installed due to reduced visual impact as they can be installed far away from shore [9]. The drawback is that the installation, connection to shore and maintenance is significantly higher for offshore turbines [4].

The technologies within the fields of offshore wind and wave power are developing rapidly. When it comes to offshore wind power, the knowledge from onshore wind power is combined with offshore oil and gas technology. At the end of 2013 a total of 2 080 offshore bottom fixed wind turbines were installed and grid connected in Europe. These wind turbines have a cumulated installed capacity of 6.6 GW spread between 69 wind farms. These wind farms produce 24 TWh in a normal wind year, which is enough to cover 0.7 % of the EU's total electricity consumption. The outlook for 2014 and 2015 by the European Wind Energy Association states that the 12 offshore projects that currently are under construction will increase the installed capacity by 3 GW, bringing the European cumulative capacity to 9.6 GW [10].

To this day, no floating wind turbines have been installed. However, Statoil is currently developing Hywind; the world's first floating wind turbine. The demo concept was installed off the coast of Karmøy in 2010 and a new demonstration park off the coast of Aberdeenshire, Scotland, is planned [11]. The wave power technology is still considered immature, but concepts such as the Pelamis [12] and Oyster [13] have been pilot tested and proved that they can produce power to the grid. The potential of wave power have been estimated to be in the range of 2 – 3 TW [14], [15], where the exploitable limit have been suggested as 10 – 25 % [16]. Technologies combining wind and wave power are also developing, among these the W2Power design.

1.2 Objective

The objectives of the master thesis are to investigate in the feasibility and efficiency of the W2Power installation and to propose improvements to the design.

1.3 Scope and limitations

The design of the platform is in the starting phase, and it has not been done any model tests assessing the response of the buoys. Therefore, only operational conditions will be considered in this analysis. Extreme conditions together with wind and current will not be addressed.

The model test and the main numerical simulation will only be of one of the three sides of the platform. This because it would be costly to build a model of the entire platform and time consuming beyond the time available to make a full simulation model implemented with all desired features.

2. Literature review

The following sections give a short description of the status and potential of offshore wind and wave power, the EU project MARINA Platform and the W2Power design.

2.1 Status and potential of offshore wind and wave power

Wind generated waves propagate as gravity waves and have almost no energy loss as long as the water depth is superior to the wavelength. The energy of the waves is mechanical and consists of the kinetic energy associated with the velocity field of the water particles and the potential energy associated with the deformation of the fluid environment on the surface. Wave power is defined as the flow of energy passing through a surface perpendicular to the propagation of the waves per unit time. For convenience it is usually referred to as power per unit length of the wave front instead of per unit area of the wave front. This conversion is done by integrating the power per surface from the bottom of the ocean to the surface [5], [17].

The marine energy is widely available around the world and, particularly offshore wind power, represents an enormous potential source [3]. It is not easy to calculate an exact value of the energy potential from wind and waves, but most studies conclude that the wave energy potential alone is in the same range as the electrical energy consumption of the world today. Isaacs and Seymour (1973) [18] estimated the global wave power potential to be in the range of 1 – 10 TW. Several attempts have been done to map the offshore wave energy during the last 15 years. By using two of these, the WERATLAS and WorldWaves, Mørk et al. (2009) [14] found the global net resource to be almost 3 TW. Here, net resource means excluding areas where $P \leq 5$ kW/m and areas covered with ice. Another study, performed by Gunn and Stock-Williams (2012) [15] using outputs from the NOAA Wavewatch III global model, states that the global wave power resource is 2.11 ±0.05 TW. How much of the global potential that is possible to extract heavily depends on the conversion technology used. Somewhere between 10 and 25 % have been suggested as the exploitable limit by Barstow et al. (2008) [3].

The research within the field of wave energy conversion got a real boost during the oil crisis of 1973. [17]. Many designs have been tested, but so far nobody has found a solution that has a low enough cost per kWh and can withstand the loads from the waves and the environment over longer time periods. In Ocean Wave Energy [19] S. Salter writes that to be able to make wave energy converters (WECs) that are commercially feasible we first have to make the devices survive, then make them effective. In addition, he says the costs must be reduced by a factor of about two to make it interesting for investors and electricity users.

WECs can be classified in different manners: by geometry, where they are located (shoreline, near-shore, offshore) or by their hydro-mechanical conversion. The latter is the most used classification and was adopted by Falcão (2009) [20]. This classification with sub-classes is shown in figure 1, also including some examples of promising technologies that are under development.

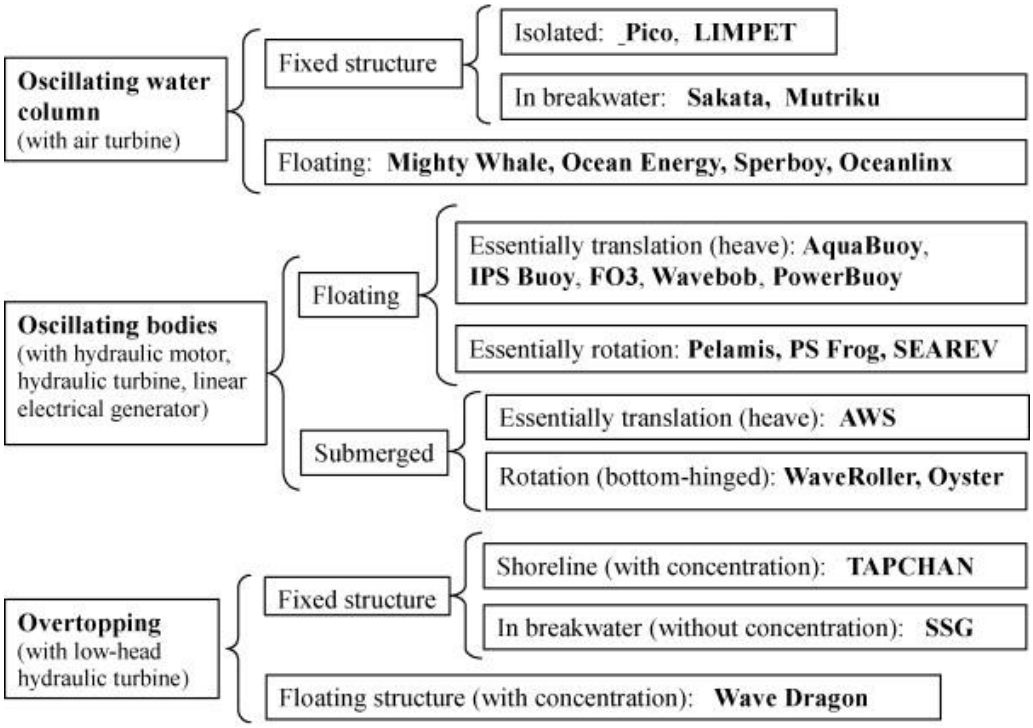

Figure 1: Classification of wave converters, adopted by Falcão [20]

Full-scale testing have only been carried out for a handful WEC devices, but the pre-commercial trials of individual modules and small arrays are expected to accelerate through this decade [5]. The Pelamis design [12] is one of the most developed and tested WEC devices today. It is an oscillating floating body that captures the energy from the waves as they pass along the length of the device. It was the first commercial scale WEC to generate electricity to a national grid from offshore waves (2004-2007). In 2008 three devices were installed and operated on the northwest coast of Portugal. These generated sustained power to the grid, but due to the financial collapse of one of the parent companies, the project ended earlier than planned. After extensive testing the Pelamis has been upgraded many times, currently the Pelamis P2 is being tested for a number of commercial projects. Other near-commercial technologies are the oscillating body devices PowerBuoy, Wavebob, Oyster and Waveroller, and the overtopping devices WaveDragon and WavePlan [5].

The onshore wind technology is considered mature and has been converted to apply for the offshore environment, giving the offshore wind technology a great head start. The main difference between onshore and offshore wind is of course the waves acting on the structure. Commercial offshore wind farms today are mainly located at shallow waters near shore. This facilitates the installation, the maintenance and repair and connection to shore, since the wind turbines (WTs) are bottom mounted. To be able to combine wave and wind power extraction the WTs must be installed at a location where there are waves of a certain height. This implies deeper water, which again makes the installation of the WTs more complicated, as they have to be floating. Several designs have been developed for offshore floating WTs, among others the Hywind project by Statoil [11]. To make maintenance and repairs easier and to save costs on power cables to shore and connections between the turbines several designs with two or more WTs on the same floater has been developed. Examples of this are the Hexicon multi-turbine platform [21] and the Windsea semi-sub with three WTs [22]. However, not many designs with multiple WTs are commercially available.

The MARINA Platform project has evaluated around a hundred different concepts for combined wind and ocean power production units. The majority of concepts with positive evaluation is categorized as “integrated combinations of fixed foundations with a single WT and multiple WECs” [23]. With only one WT the risk of one turbine being in the wake of the other is eliminated and the WT will have maximum incoming flow at all times (implied that it is faced in the direction of the incoming wind). The force from the waves acting on the WECs are oscillating, and they will thus produce electrical power oscillations. This may degrade the power quality from a single device, and it would therefore be convenient to develop designs with multiple devices to obtain a smoother cumulative power generation [5].

Semi-subs used in the oil and gas industry are in general rectangular, but for offshore wind the majority of the concepts developed are of triangular shape. This will give a moderate draft and a smaller water plane area compared to a barge, which may reduce interaction forces from incoming waves. A semi-sub has larger wave loads and motions than a spar buoy, which is beneficial when combining it with WECs. Some of the concepts developed are semi-subs with a curved front side and with the possibility of installing multiple WTs. Regarding the WEC devices several combinations have been considered. The most important is however to optimize the layout of the devices around the platform so they will capture as much wave energy as possible. [23].

Due to the lack of deployment experience, it is difficult to assess the environmental impacts from offshore wind and wave technologies. Possible impacts are competition for space, noise and vibration, electromagnetic fields, disruption to biota and habitats, water quality changes and possible pollution. Which of the listed impacts that are the most significant will vary with technology and location of the energy-harvesting units. [5].

2.2 MARINA Platform

The MARINA (Marine Renewable Integrated Application) Platform project is an EU founded project started in 2009. It is a collaboration between twelve European countries and is planned to continue until June 2014 [24]. The project combines the deep-water engineering experience from the oil and gas development during the last 40 years and state of the art concepts for offshore wind and ocean energy extraction.

The aim of the project is to bring offshore renewable energy applications closer to the market. This is done by investigating several designs of combined wind and ocean energy converters/multipurpose platforms and from these find the most promising solutions. The project has established a set of criteria on which the designs have been evaluated. By using these criteria the project will create a novel set of design and optimization tools. These tools address, among other things, new platform design, component engineering, risk assessment, spatial planning and platform-related grid connections. The main focus of the tools is system integration and reduction of costs.

By using the tools established two or three multipurpose renewable energy platforms will be realised, meaning they will go through preliminary engineering designs. Then the designs will be validated by advanced modelling and tank testing at a reduced scale and eventually be constructed as pilot scale platforms for testing at sea [25].

At this stage the about 100 initial designs have been narrowed down to ten, which will be investigated further. One of these designs is the W2Power platform that will be evaluated and discussed in this thesis.

2.3 W2Power

2.3.1 Description of the design

The W2Power is a triangular semi-submersible platform that combines WTs and WEC devices. The platform is equipped with two counter-rotating 3.6 MW WTs. At the column at the third corner (B in Figure 2) the power take-off system for the WECs will be placed. Instead of a WT, this corner will have a helipad to ensure easy access for inspections and maintenance. This corner will also be used for anchoring and will provide a pivot point for the platform, ensuring that the wind turbines operates under the optimal wind direction condition at all times.

The areas near the sea surface contain large amounts of energy and it is therefore important to protect the wave power conversion system. This is done by placing the system inside buoys so that large waves will submerge the buoys and not damage the system. Arrays of buoys containing wave pumps will be installed along the sides of the structure, four on the side AC and three on each of the sides AB and BC. In total, the WECs will have an installed capacity of 3 – 5 MW, bringing the total capacity of the platform to 10 – 12 MW. It may however be more convenient to use the average delivered effect of the WECs instead of their capacity. The developers of the concepts estimate somewhere between 150 – 200 kW as a yearly average for the delivered capacity per buoy.

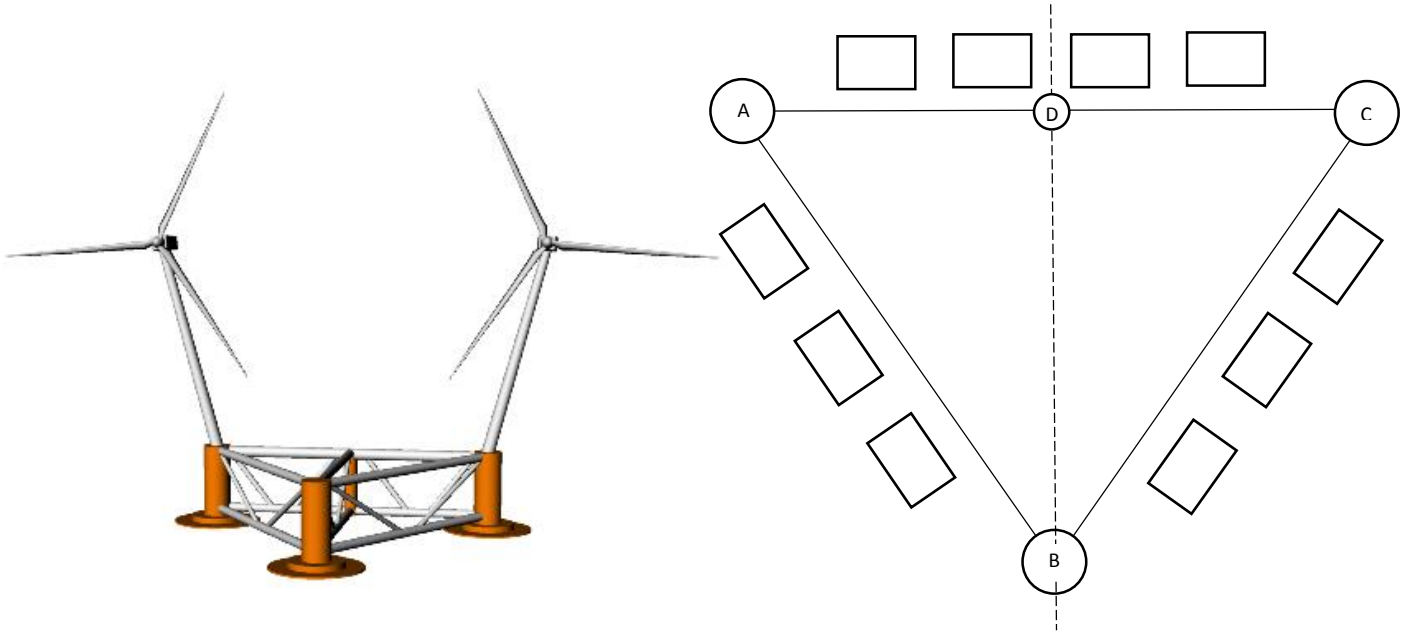

Figure 2: The W2Power design. Left: The platform without buoys [26]. Right: A schematic of the platform with buoys seen from above.

The semi-sub will be a triangle where side AC is 90 meter and the sides AB and BC are 80 m. The columns in the corners have a diameter of 9 m and a height of 25 m, of which the draft is 15 m. The diameter of column D is 5 m. The WT towers are 67.5 m high with an inclination of 15^{o} and a rotor diameter of 107 m [26]. The design of the platform framework has not yet been determined, figure 2 shows a suggestion from the early design phase.

The combination of wind and wave energy harvesting makes the W2Power able to produce more stable flow of electricity than a device for only wind or wave energy extraction. Waves are more predictable than wind, as they appear before the wind and does not die out as fast as the wind does. Different price estimates have been done, giving 0.049 €/kWh [27] and 0.18 €/kWh [23]. The expected yearly electricity production based on meteorological data from the North Sea is 40 GWh and the power generated will be exported to shore via subsea cables. Other applications for the

platform may be desalinization and to produce electricity for use at oil platforms instead of transporting the energy to shore [27].

If the performance of the WECs is optimal when integrated between the legs of a semi-sub must be assessed. Interference problems between the WTs must also be addressed [23].

The W2Power is designed to absorb energy in both heave and surge, as the buoy moves in a circular path shown in figure 3. For energy considerations, heave and surge are not coupled motions. When seen from a bird's-eye view their wave patterns will be different, as opposed to e.g. surge and pitch.

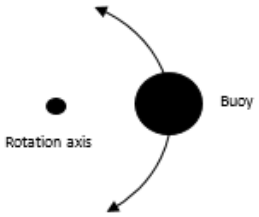

Figure 3: Rotation path buoy

2.3.2 Previous work

The platform concept was tested in a 1:3 scale in 2008. The tests revealed some difficulties in installing the buoys, but it also confirmed that the technology is functional. This was however with a different type of WEC. The test also proved that the platform itself can survive a storm strong enough to rip the mooring chains apart.

Several model tests have been carried out over the last couple of years for a 1:100 scale model. The measurements done during these tests include:

- Global motion response of platform only in operation and extreme conditions
- Global motion response of platform with buoys (without PTO) in operation and extreme conditions
- Decay test of platform with and without buoys

3. Method

The numerical simulation models of the platform were made using the DNV software GeniE and HydroD. GeniE was used to construct the substructures of the platform; the columns that make the three corners of the platform and the ten buoys containing the WECs. Finite element models of the substructures were made and exported to HydroD. In HydroD the hydrodynamic analysis of the substructures were done in Wadam, which is implemented in HydroD. Here the hydrostatic stiffness coefficients were obtained together with the frequency dependent hydrodynamic added mass and damping.

Once the hydrodynamic analysis finished, all the substructures were imported to the MARINTEK graphical user interface SIMA and analysed using SIMO and RIFLEX. The platform framework was implemented here, and the numerical simulation models assembled. Three numerical models were made; two of the side AB of the platform for use in the comparison with the model test (one tuned to fit the results and one untuned) and one of the entire platform to make the basis for a more thorough analysis of the system.

A model test was performed at the MC lab at MARINTEK to study one side of the platform with the corresponding three WECs. This test was used to investigate in the buoys ability to produce power, the interaction between the buoys and the interaction between the buoys and the platform framework. In addition, the model test was used to validate the numerical simulation models.

4. Software

4.1 GeniE

GeniE is a part of the Sesam software package developed by DNV. It is a tool for engineering and strength analysis of ships and offshore structures. The modelling of the structural part of the model can be done either by importing from other systems or other Sesam programs, by using wizards or building the model from scratch.

The program can be used for both fixed and floating structures, and the same concept model can be used as a basis for hydrostatic, hydrodynamic and structural analysis. GeniE allows you to generate a finite element or a panel model where the mesh can be automatically generated or controlled by the user. The model will then be exported as a .fem file and can be opened in the desired program (e.g. HydroD) for further analysis [28], [29].

4.2 HydroD/Wadam

HydroD is a part of the Sesam software package developed by DNV, which is used for hydrodynamic and stability analyses of large fixed and floating structures of arbitrary shape. The hydrodynamic model can be created in HydroD or imported from GeniE. It is possible to do stability analysis, frequency domain analysis and time domain analysis. Wadam (Wave Analysis by Diffraction and Morison Theory) is used to perform the frequency domain analysis and is integrated in HydroD. The analysis capabilities in Wadam include calculation of hydrostatic data and inertia properties, and of global responses (e.g. first and second order wave exciting forces and moments, hydrodynamic added mass and damping and first and second order rigid body motions). The loads are automatically transferred to a finite element model for subsequent analysis that includes inertia loads and pressure loads among others [30].

It is possible to do a multi-body analysis with up to 15 different bodies for analyses in the frequency domain, where full hydrodynamic interaction between the bodies is included. The user may specify an additional coupled damping and restoring matrix for the bodies.

Statistical post-processing can be done to find typical result attributes like global response data or detailed results for selected panels/points. The results may also be used directly as input to a mooring or coupled motion analysis (DeepC/SIMO) [31].

4.3 SIMO and RIFLEX

SIMA (Simulation Workbench for Marine Applications) is the graphical user interface for both SIMO and RIFLEX developed by MARINTEK. It provides a common interface for the analysis software modules and it presents visualizations of the simulation model as it is being prepared.

SIMO (Simulation of Marine Operations) is a time domain simulation program for study of motions and station keeping of multi-body systems. It uses linear wave theory to simulate the responses of the bodies. The program can be applied for analyses on surface vessels, positioning and complex marine operations. Several force modes can be used to simulate a range of effects: hydrostatic stiffness, damping, wave forces and slow drift forces among others [32].

RIFLEX (Riser System Analysis Program) is used for analysis of slender marine structures such as flexible risers, metallic catenary risers, mooring lines and umbilicals. The structural analysis is based on finite element modelling. A range of load models may be applied, e.g. external/internal hydrostatic pressure effects described by the effective tension concept and hydrodynamic loading described by the generalized Morsion's equation [33].

5. Numerical simulation model

Three numerical simulation models have been developed. Two of the side AB of the platform with its three WECs, where one is tuned to fit the measured results and one untuned for comparison, and one of the entire platform with ten WECs. The WTs are not considered in this analysis and were therefore not modelled. They will however effect the weight of the structure, but this will not be of importance since the platform framework will be kept fixed during the simulations. The reason for the three models is that only the side AB of the platform will be studied in the experimental campaign, and it will be convenient to compare the tuned and untuned model in the validation process. The findings from the model test will be used to improve the numerical model of the entire platform.

The substructures of all models are the same, it is the composition of the structure when doing the analyses in SIMA that differs.

5.1 Environment

All environmental data is based on the findings in the MARINA Platform report "Environmental Data at Five Selected Sites for Concept Comparison" [34]. This report is prepared to define the environmental conditions at five selected European sites suitable for offshore wind and wave energy extraction. Of the five sites, only two have a sufficient water depth for floating structures. One of these sites is located 30 km off the northwest coast of Norway and the other 40 km off the west coast of Spain.

In the Wadam analysis a wave amplitude of 1 m and periods from 1 – 16 s, with a leap of 1 s, was used. The waves had incoming angles of 0 – 360°, with a leap of 10°. The SIMA analyses were carried out for the same regular waves and sea states as the model test, these will be described in section 6.7. Wind and current are not applied.

5.2 Creating the model – GeniE

The ten buoys containing the WECs and the three corner columns (column A, B and C, ref. figure 2) of the platform were built from scratch in GeniE. The load condition for the wetted surfaces were applied to all parts below the mean draft (T = 15 m). A mesh of size one meter was applied to all components to create the finite element models needed for HydroD analysis. This is illustrated in figure 4.

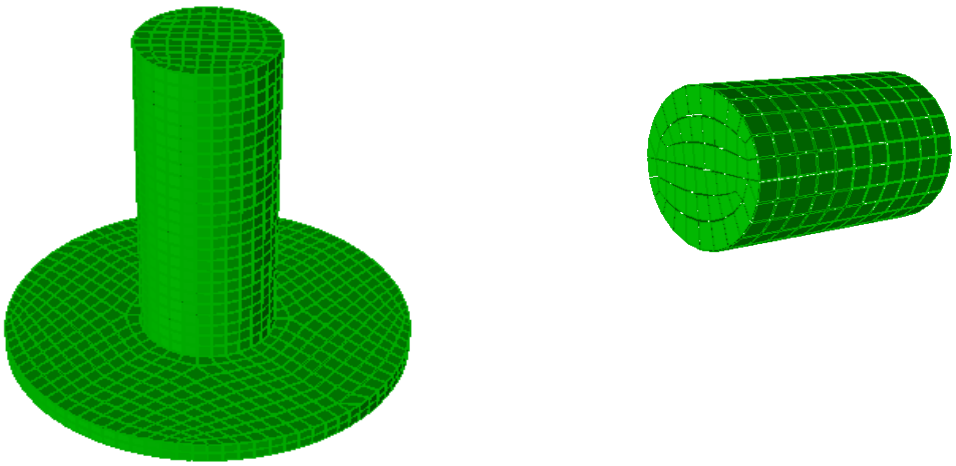

Figure 4: The GeniE models of the two substructures of the platform design; the columns A, B and C and the buoy containing the WEC.

5.3 Calculating the hydrodynamic coefficients – HydroD (Wadam)

Wadam calculates loads using Morison's equation for slender structures and first and second order 3D potential theory for large volume structures. It is also possible to do analysis with both of the mentioned methods simultaneously. For this analysis only 3D potential theory has been used.

The hydrodynamic coefficients were found independently for each of the components modelled in GeniE. This was done by importing the .fem file from GeniE as a panel model and applying a load condition corresponding to the wetted surface of the structure. The mass model was then calculated from the buoyancy of the structure before the analysis was run.

5.4 Calculating the responses of the design – SIMA

One at the time, the sub-structures of the design were imported to SIMA and placed in the correct position. The framework of the platform and the rotation arms of the buoys were made using RIFLEX lines. The rotation points of the buoys were modelled as flex joints. This was not optimal, as the flex joints make the RIFLEX lines flexible instead of having stiff lines rotate about a given point. The movement of the buoys will be correct, but the cross section of the rotation arm will have an impact on the response of the buoy and the forces caused by the waves acting on it. A schematic of the buoy with rotation arm and rotation point is presented in figure 5.

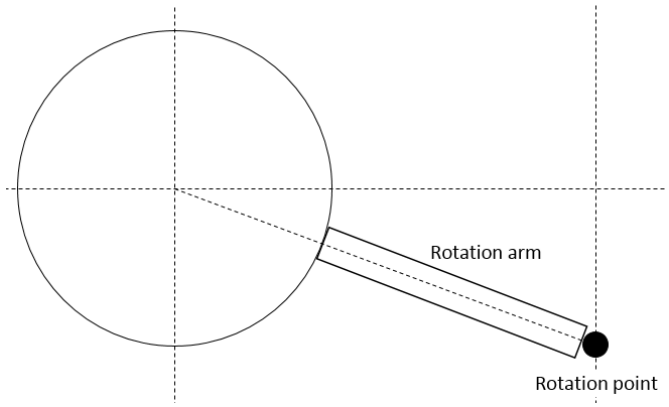

Figure 5: Buoy with rotation arm and rotation point

5.4.1 Model of the platform side AB with WECs

A numerical model of the actual model test setup was made. This model only contains three WECs and a simplified framework. As the main objective of the model test is to investigate in the response of the WECs and their hydrodynamic influence on each other, the corner columns were not modelled. To tune the numerical model to give as equal responses as the model test as possible, the air cylinders attached to each buoy were implemented as fixed elongation couplings. An additional model without fixed elongation couplings was also made to investigate in the effect of these. Both models are shown in figure 6.

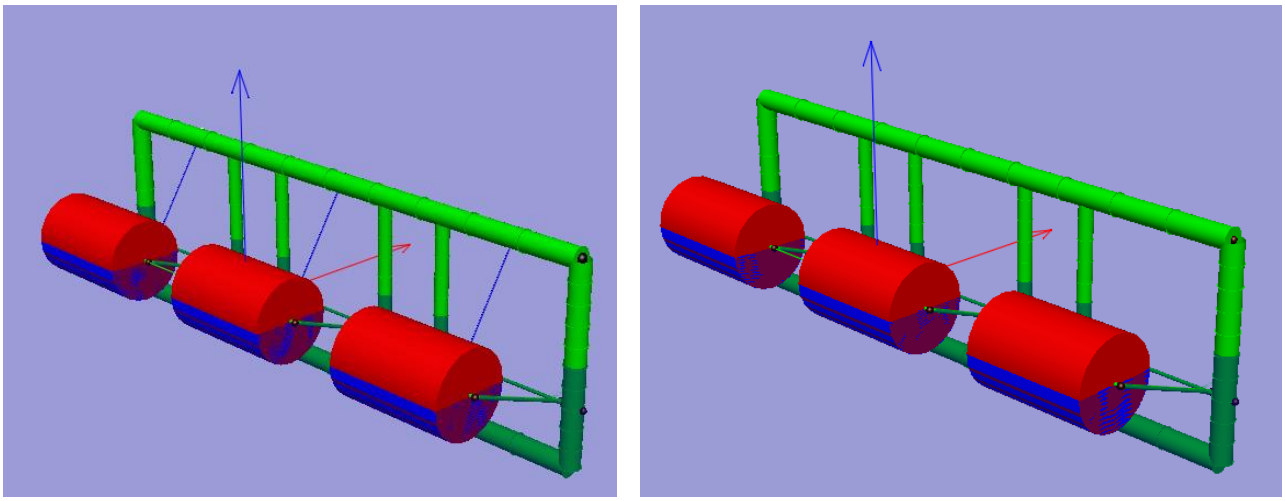

Figure 6: SIMA model of one side of the platform. Left: tuned model. Right: untuned model.

5.4.2 Model of the entire platform with WECs

Due to time limitations the model of the entire platform is not as complete as desired. The model contains the framework and the ten WECs, but not the WTs. The framework is fixed, and only the WECs are allowed to move as the waves pass. The final framework and how the WECs are connected to the platform have not been decided, a suggestion is presented in figure 7.

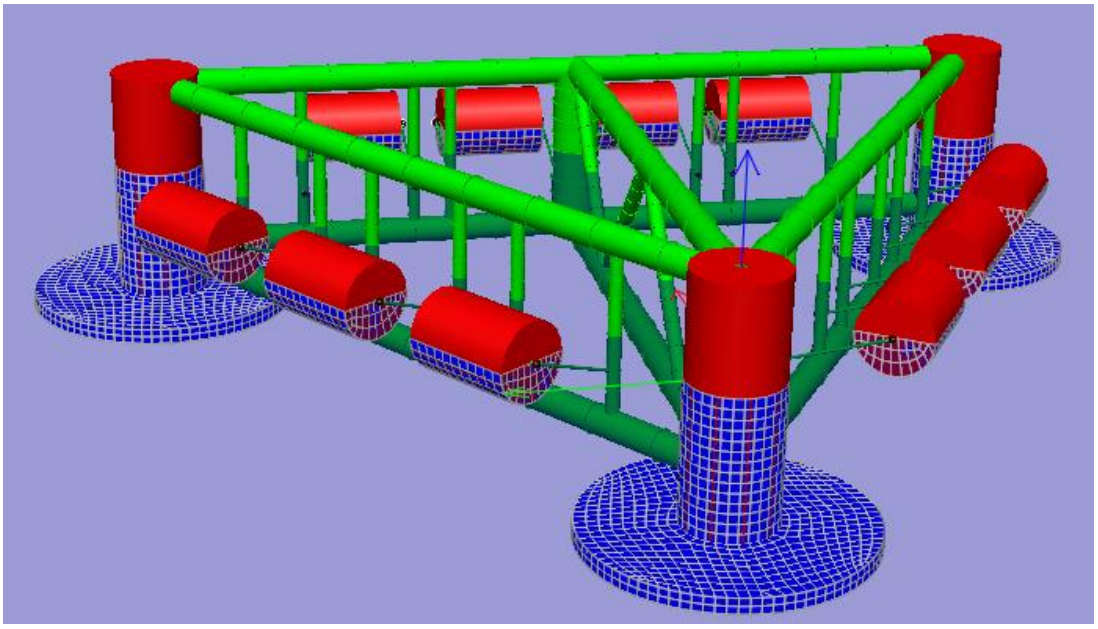

Figure 7: SIMA model of entire platform

6. Experimental campaign

6.1 Introduction

Due to the complexity of the design, only the side AB (ref. figure 2) of the platform with its three WECs was modelled for the test. To model the entire platform would be very costly and, because of the limited dimensions of the towing tank, not give accurate enough measurements. If the scale of the model is too small it will be very difficult to model the power take-off of the buoys correctly.

The test has covered typical operational conditions regarding waves. No wind or current conditions have been investigated.

The model test was performed at the Marine Cybernetics (MC) Lab at MARINTEK, Trondheim, March 31st – April 15th 2014.

6.2 Objectives

The main objectives of the model test was to investigate in the response and power production output of the buoys and to validate the numerical simulation model. In addition, the hydrodynamic interaction between the buoys have been investigated. How their presence will affect each other may have significant effect on how much power that can be produced. This interaction cannot be calculated by SIMA directly, and it is therefore important to find out if the numerical models must be adjusted to take this effect into account.

The objectives of the model test with the three WECs can be summarized as follows:

- Measure the response of the buoys and calculate the produced power
- Measure the vertical forces from the waves on the rotation arms
- Measure the horizontal forces from the buoy on the framework of the platform
- Validate the numerical simulation model made in SIMA with respect to response of the buoys and forces acting vertically on the rotation arms and horizontally on the framework
- Investigate the hydrodynamic interaction between the buoys, i.e. if there is a shadowing effect between the buoys affecting their response

6.3 Lab/tank facilities

Figure 8 shows a schematic of the tank at the MC Lab with the towing carriage, wave maker and wave beach. The length of the tank is 40 m, breadth 6.45 m and max water depth 1.5 m. The wave maker is a 6 m width single paddle who can generate regular waves up to 0.25 m with periods from 0.3 – 3 s. Sea states with maximum significant wave height is 0.15 m and peak periods between 0.6 – 1.5 s can also be generated.

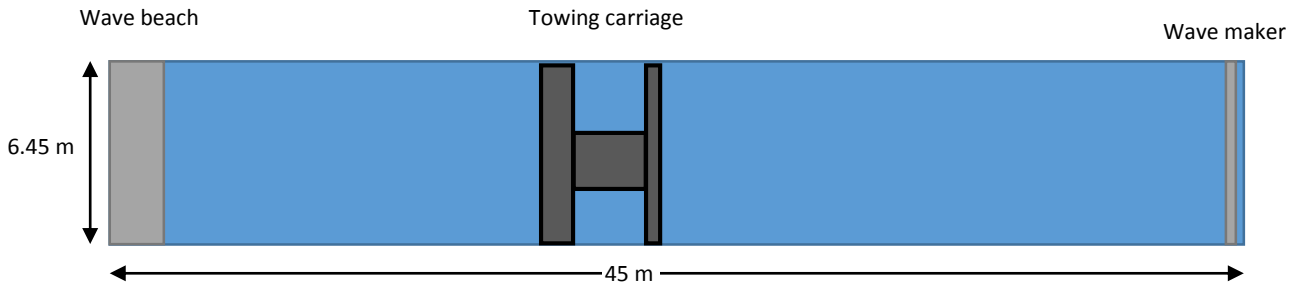

Figure 8: Test facilities, MC Lab. Not to scale.

6.4 Model description

The test set-up is illustrated in figure 9 and includes the following components:

- Three buoys
- Simplified framework representing the platform

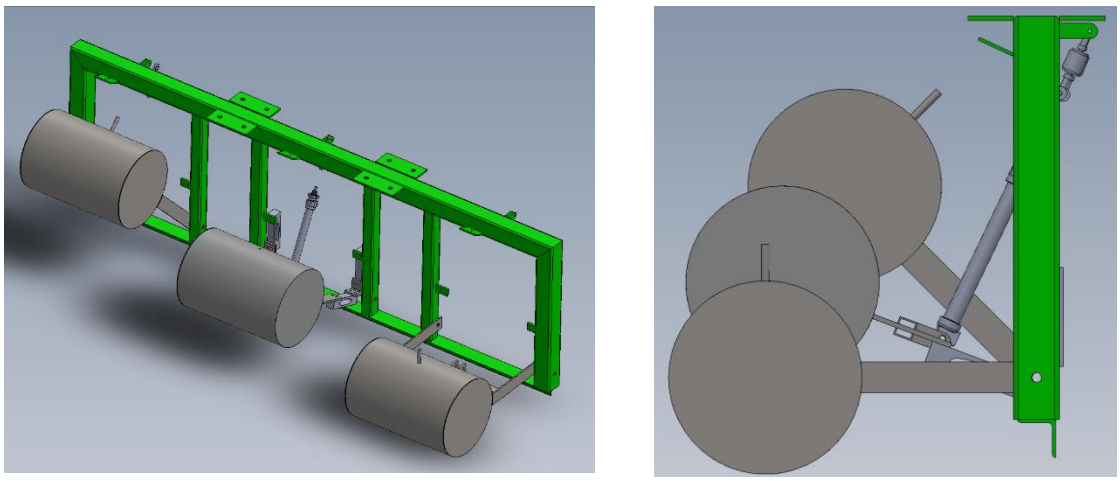

Figure 9: eDrawing 3D model of the test model. Drawing developed by Inrigo AS.

The platform framework is simplified to reduce size and cost of the test model. Since the framework is to be held fixed during the entire test its weight is not important.

The model is mounted under the towing carriage, to a plate that can be rotated. Only one of the buoys are equipped with transducers. The two remaining buoys are connected to the frame at the rotation axis and they both have air cylinders to secure sufficient damping. It is possible to change the position of the buoy with transducers so that measurements can be done for all three positions.

Froude scaling was applied and the model was constructed in a linear scale of 1:30, and manufactured by Inrigo AS. The complete model with air cylinders and transducers was assembled at the MC Lab. Photos of the model test set-up can be found in Appendix A.

6.4.1 Buoy description

Table 1 presents the main dimensions of the buoys.

Table 1: Main dimensions of buoys

	Unit	Model	Full-scale
Number of buoys		3.00	3.00
Diameter	m	0.250	7.50
Length	m	0.367	11.00
Distance between buoys	m	0.283	8.50
Distance platform - buoy	m	0.333	10.00
Vertical position from rotation axis	m	-0.125	-3.75
Distance rotation point – center of buoy	m	0.356	10.68
Volume	m^3	0.018	485.97
Volume displacement	m^3	0.009	242.98
Displacement	kg	8.999	242 982.56

Figure 10 shows the buoy position numbering at 90° incoming wave angle.

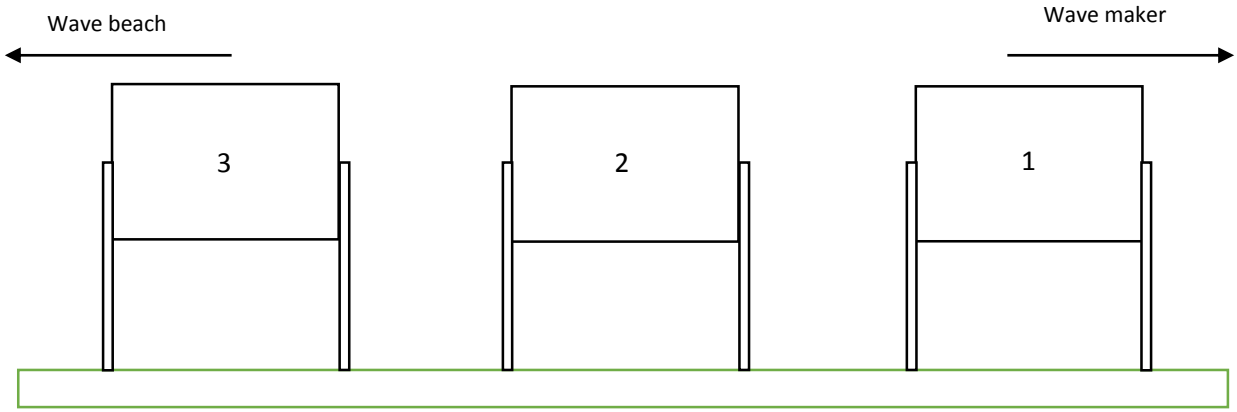

Figure 10: Buoy positions at 90 degrees incoming wave angle

6.4.1.1 Ballast

The buoys weigh about 6 kg and had to be ballasted to float on the correct waterline. Ballasting was done by attaching weights on the top of the buoys. This caused the center of gravity to shift slightly upwards. No calculations of how large this shift was have been done. Table 2 presents the ballast applied to each buoy.

Table 2: Ballast applied to each buoy

	Ballast
Buoy 1	3.33 kg
Buoy 2	3.35 kg
Buoy 3	3.38 kg

6.4.2 Frame description

Table 3 presents the main dimensions of the frame.

Table 3: Main dimensions model frame

	Unit	**Model**	**Full-scale**
Length	m	1.81	54.3
Total height	m	0.58	17.4
Height lower brace	m	0.05	1.5
Height upper profile	m	0.06	1.8
Width upper profile	m	0.06	1.8
Breadth side profile	m	0.06	1.8
Width side profile	m	0.06	1.8
Breadth middle profile	m	0.04	1.2
Width middle profile	m	0.04	1.2
Height middle profile	m	0.47	14.1
Distance lower brace - rotation axis	m	0.055	1.65

6.5 Instrumentation and data acquisition

6.5.1 Instrumentation

The following instruments are mounted to the test model:

- Four load cell force transducers; two measuring the vertical force on each of the two rotation arms of the buoy and two measuring the horizontal force on the framework
- One potentiometer for position measures of the buoy
- One force transducer connected to the air cylinder
- Three air cylinders; one at each buoy
- Pressure regulators at the end of the hoses connected to the outlets of the air cylinders

In addition, a wave probe is mounted between the model and the incoming waves.

The buoy on which the measurements are done are equipped with four load cells, one force transducer and one potentiometer. Two of the load cells are connected to the rotation arms of the buoy to measure vertical forces, the two others to the framework to measure horizontal forces. The last force transducer is connected between the top of the air cylinder and the frame, while the potentiometer is connected to the upper part of the frame and the cross beam between the rotation arms, making the string parallel to the air cylinder.

Figure 11 and figure 12 show the transducer set-up, references to the wave maker and wave beach when the model is at 90° incoming wave angle.

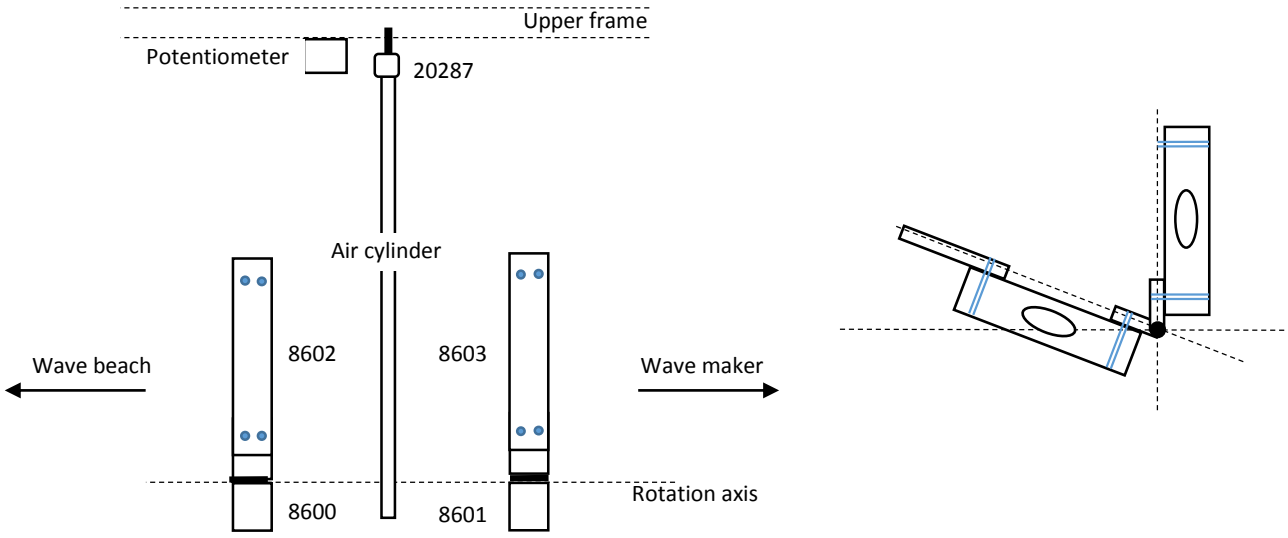

Figure 11: Left: Instrumentation set-up as seen from the buoy. Right: Load cell transducer set-up as seen from the side.

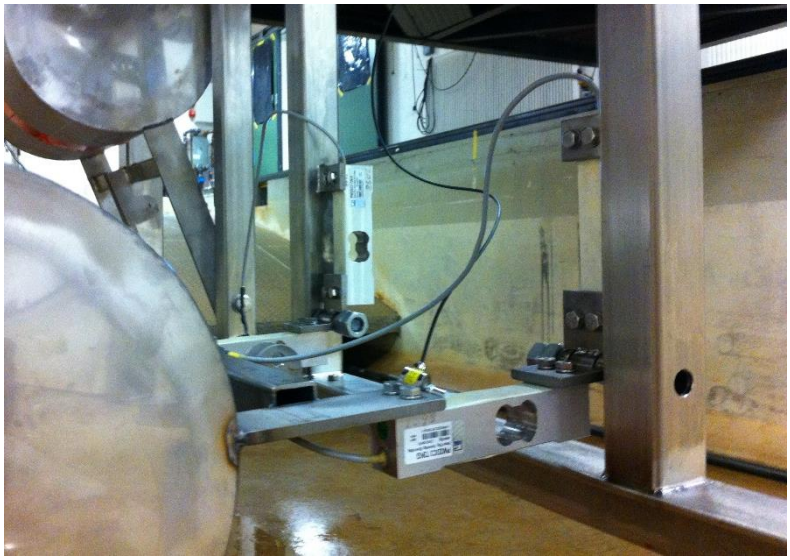

Figure 12: Load cell transducer set-up

6.5.2 Data acquisition

All measurements were sampled at a rate of 200 Hz (36.5 Hz full-scale). A 40 Hz low-pass Butterworth filter was applied before the analog/digital conversion.

6.6 Test program

6.6.1 Variation in load resistance of air cylinder

Pressure regulators connected to hoses, which again is connected to the outlets of the air cylinders, controls the load resistance. The opening of the pressure regulators were varied in six steps from completely opened to completely closed for five wave conditions.

The load resistance of the air cylinders is a function of the wave period. The load resistance was varied and tested for the following wave height and wave periods

Table 4: Wave configurations for variation of load resistance

Model scale		**Full-scale**	
H [m]	**T [s]**	**H [m]**	**T [s]**
0.100	1.278	3.0	7.0
0.100	1.643	3.0	9.0
0.100	2.008	3.0	11.0
0.100	2.373	3.0	13.0
0.100	2.739	3.0	15.0

6.6.2 Decay tests

A decay test for each buoy position was performed. The buoy moves in heave and surge, but it is not possible to do separate decay tests with the present configuration of the model.

6.6.3 Operational conditions

The tests for operational conditions were performed for all three buoy positions and for seven different angles between 0^o and 90^o, with a leap of 15^o. Due to symmetry of the design this covered all possible incoming angles for the two sides of the platform with three WECs.

Table 5 presents the operational conditions with wave set numbering. The numeration for regular and irregular waves is the same. Reference for the buoy position numbering is made to figure 10.

Table 5: Operational conditions and wave set numbering

Wave set	Buoy position	Incoming wave angle	Wave set	Buoy position	Incoming wave angle	Wave set	Buoy position	Incoming wave angle
1	2	0°	**8**	1	0°	**15**	3	0°
2	2	15°	**9**	1	15°	**16**	3	15°
3	2	30°	**10**	1	30°	**17**	3	30°
4	2	45°	**11**	1	45°	**18**	3	45°
5	2	60°	**12**	1	60°	**19**	3	60°
6	2	75°	**13**	1	75°	**20**	3	75°
7	2	90°	**14**	1	90°	**21**	3	90°

Regular wave tests require about five minutes per wave, which adds up to 80 minutes per wave set of 16 waves. A total of 28 hours was estimated for all regular wave tests. Each sea state was simulated for one hour full-scale, which corresponds to almost 11 minutes in model scale. The set of six sea states that was tested had an estimated duration of 85 minutes when the time needed for the water to calm is included. Estimated time for all irregular waves was 30 hours.

6.7 Environmental conditions

6.7.1 Regular waves

Based on scatter diagrams for the possible installation sites [34], previous experiments with the W2Power [35] and the tank capacity the waves listed in table 6 were tested.

Table 6: Environmental conditions regular waves

Incoming angles	0,15,30,45,60,75,90			
	Model scale		**Full-scale**	
wave #	**H [m]**	**T [s]**	**H [m]**	**T [s]**
1	0.033	1.095	1.0	6.0
2	0.033	1.278	1.0	7.0
3	0.033	1.643	1.0	9.0
4	0.033	2.008	1.0	11.0
5	0.033	2.373	1.0	13.0
6	0.033	2.739	1.0	15.0
7	0.067	2.739	2.0	15.0
8	0.100	1.278	3.0	7.0
9	0.100	1.643	3.0	9.0
10	0.100	2.008	3.0	11.0
11	0.100	2.373	3.0	13.0
12	0.100	2.739	3.0	15.0
13	0.133	1.278	4.0	7.0
14	0.133	2.008	4.0	11.0
15	0.167	1.643	5.0	9.0
16	0.167	2.008	5.0	11.0

6.7.2 Irregular waves

JONSWAP spectra are used to simulate the full-scale sea states. The spectrum parameter is given by

$$S(\omega) = 5\pi^4 \frac{H_S^2}{g^2 T_p^4}(1 - 0.287 \ln \gamma) g^2 \omega^{-5} e^{\left(-\frac{5}{4}\left(\frac{\omega}{\omega_p}\right)^{-4}\right)} \gamma^{e^{\left(\frac{\left(\frac{\omega}{\omega_p}-1\right)^2}{2\sigma^2}\right)}}$$

Equation 1: JONSWAP spectrum

Where $\omega_p = 2\pi/T_p$ is the angular spectral peak frequency, σ is the spectral width parameter, σ = 0.07 for $\omega \leq \omega_p$ and σ = 0.09 for $\omega > \omega_p$. γ is the peak-enhancement factor and depends on H_s and T_p with the following relation

$$\gamma = \begin{cases} 5 & for \quad \frac{T_P}{\sqrt{H_S}} \leq 3.6 \\ \exp\left(5.75 - 1.15\frac{T_P}{\sqrt{H_S}}\right) & for \quad 3.6 < \frac{T_P}{\sqrt{H_S}} \leq 5 \\ 1 & for \quad 5 < \frac{T_P}{\sqrt{H_S}} \end{cases}$$

Equation 2: Peak-enhancement factor as a function of H_S and T_P

The sea states were chosen considering the maximum capacity of the wave maker of the MC Lab. The following six sea states were tested:

Table 7: Environmental conditions irregular waves

Incoming angles	0,15,30,45,60,75,90				
	Model scale		**Full-scale**		
Sea state	**H_s [m]**	**T_p [s]**	**H_s [m]**	**T_p [s]**	**γ**
A	0.025	1.095	0.75	6.0	1.00
B	0.025	1.461	0.75	8.0	1.00
C	0.075	1.095	2.25	6.0	3.16
D	0.075	1.461	2.25	8.0	1.00
E	0.125	1.095	3.75	6.0	5.00
F	0.125	1.461	3.75	8.0	2.72

6.8 Time schedule for model test

Table 8 shows a proposed schedule for the 16 days of testing. A complete log can be found in Appendix B.

Table 8: Tentative schedule for model test

Date	What
Mon 31	Installation of the model
Tue 1	Calibration of instruments + Ballasting
Wed 2	Variation of load resistance air cylinder + Decay test 2
Thu 3	Regular wave set 1-5
Fri 4	Regular wave set 6-7. Irregular wave set 1-3
Sat 5	Irregular wave set 4-7 + change position of buoy
Sun 6	Buffer day to finish the week's planned tests.
Mon 7	Decay test 1 + Regular wave sets 8-12
Tue 8	Regular wave set 13-14. Irregular wave set 8-10.
Wed 9	Irregular wave set 11-14 + change position of buoy
Thu 10	Decay test 3 + Regular wave set 15-19
Fri 11	Regular wave set 20-21. Irregular wave set 15-17.
Sat 12	Irregular wave set 18-21.
Sun 13	Buffer day to finish the week's planned tests.
Mon 14	Dismounting + Wave measurements
Tue 15	Buffer day

7. Results

7.1 Model test

7.1.1 Optimal load resistance

The optimal load resistance of the air cylinders was found by comparing average produced power for different opening configurations of the pressure regulators. Power is the rate of transfer of energy, $P = \frac{dW}{dt} = Fv$ [36]. The average power of a time series over one period is given by

$$P_{average} = \frac{1}{T}\int_0^T Fv\, dt$$

Equation 3: Average power over one period

This calculation was done for five different wave periods, all with a wave height of 0.1 m. The average power over one period is plotted against the valve opening in figure 13.

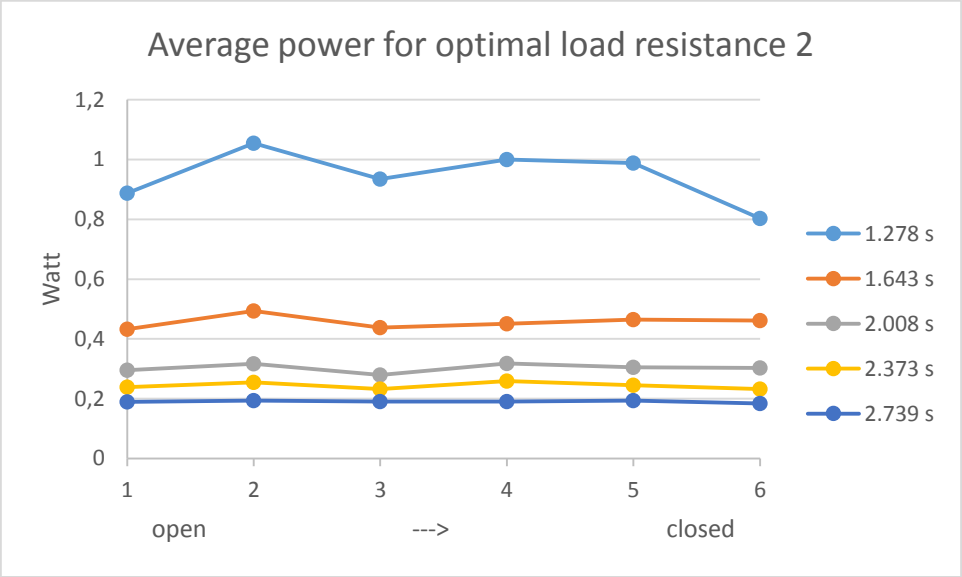

Figure 13: Optimal load resistance in air cylinders, average power over one period as a function of valve opening for five different wave periods.

As can be seen from figure 13, the second configuration (valves slightly shut) is the most advantageous when considering produced power. However, at the time of the model test, when these calculations were first done, they were not done correctly. Based on the calculations it was assumed that pressure valve configuration six (valves completely shut) was the most advantageous. In addition, the measured signals and the observed movements of the buoys were in general smoother for this configuration. All tests carried out during the experimental campaign were therefore performed with the valves completely shut. It was not discovered until after the model test was finished that the used valve configuration was not optimal and that the air cylinders had acted more as springs than dampers.

7.1.2 Air cylinder characteristics

The axial force in the air cylinder depend on two terms: the damping times the velocity and the spring stiffness times the position. It has been assumed that the axial force is given by the following linear expression

$$F(t) = R\,v(t) + k\,x(t)$$

Equation 4: Axial force air cylinder

The constants R and k have been found by reading off the measured force for zero position and zero velocity respectively:

$$R|_{x(t)=0} = \frac{F(t)}{v(t)} \qquad k|_{v(t)=0} = \frac{F(t)}{x(t)}$$

Equation 5: Damping and spring stiffness in air cylinder

This has been done for three different waves at 0^o incoming angle for buoy position one and two. At this angle position one and three are the same, and the force at position three has not been included in the investigation although separate measurements exist. Table 9 presents the obtained values.

Table 9: Damping and spring stiffness of air cylinder, model scale. The values in the column "in" is when the buoy is moving upwards (the piston going into the cylinder) and "out" when the buoy moves downwards.

			k [kg/s^2]		R [kg/s]	
Buoy 1	**T [s]**	**H [m]**	**z_{max}**	**z_{min}**	**In**	**Out**
Wave 1	1.095	0.033	407	538	97	74
Wave 8	1.278	0.100	434	520	36	36
Wave 15	1.643	0.167	416	566	40	47
Buoy 2						
Wave 1	1.095	0.033	166	757	113	12
Wave 8	1.278	0.100	335	549	57	33
Wave 15	1.643	0.167	362	535	51	34

It is clear that the contribution to the axial force is much larger from the spring stiffness than from the damping. For buoy position one the spring stiffness is around 400 kg/s^2 when the piston is at top position and around 550 kg/s^2 at minimum position. At buoy position two, the spring stiffness is slightly lower for the cylinder at max position while within the same range at minimum position than at buoy position one. The values for wave 1 at position two differs significantly from the others. One of the reasons for this is that the axial force for this wave oscillates about – 3.2 N instead of about a value close to zero as it does for the other waves tested.

It must be stressed that these values are approximations, the axial force is most likely not linearly dependent on the damping and spring stiffness. The spring stiffness is probably dependent on the initial volume and change in volume of the air cylinder.

7.1.3 Effect of incorrect damping

The incorrect damping in the air cylinders has an impact on the responses and forces of the buoys. To quantify the size of this impact, comparisons of regular wave measurements and the runs for finding the optimal load resistance have been done. Five waves have been considered, all with a model scale

height of 0.1 m and periods varying between 1.278 and 2.739 seconds at 0° incoming wave angle. The maximum and minimum values from the transducers have been compared and the deviation in percent calculated. Table 10 presents the average deviation of each transducer, reference is made to figure 11 for transducer positions. Positive values represent higher values with incorrect damping.

Table 10: Average deviation in percent between correct and incorrect damping for all transducers

Transducer	8600	8601	8602	8603	20287	Displace	Wave
maximum	31.14 %	198.43 %	18.42 %	-31.11 %	80.05 %	-10.03 %	-0.91 %
minimum	28.62 %	56.01 %	-29.10 %	6.47 %	162.77 %	-18.39 %	-8.87 %

The deviations are in some cases large. Some of the deviation is because of uncertainty in the measurements; the wave measurements should for example not be affected by incorrect damping. From the table it is seen that the displacement of the buoy is always smaller with incorrect damping, while the axial force in the air cylinder (transducer 20287) is larger. The transducers that measure the vertical forces on the rotation arm (8600 and 8601) gives larger values with incorrect damping. No clear tendency is observed for transducers measuring the horizontal force on the platform framework (8602 and 8603).

Based on the deviations listed above it is reasonable to say that the force measurements presented in the following sections are overestimations of the real forces.

7.1.4 Decay tests

Two decay tests were performed for each position of the buoy to ensure correct measurements. The aim of the decay test is to find the damping of the buoys, and was done according to theory from C.M. Larsen, 2012 [37].

A usual measure of the damping is the natural logarithm of this ratio, called the logarithmic decrement:

$$\Lambda = \frac{1}{n}\ln\left(\frac{u_i}{u_{i+n}}\right) = \xi\omega_0 T_d \cong 2\pi\xi$$

Equation 6: Logarithmic decrement

Where u_i is the amplitude at oscillation i, ω_0 the natural frequency, ξ the damping ratio and T_d the damped natural period. This approximation is valid for small values of ξ. The damping is found from the critical damping:

$$c = c_{crit}\xi = 2m\omega_0\xi$$

Equation 7: Damping

Where m is the mass of the system, which for oscillations in water also includes the hydrodynamic mass.

The average natural frequency and period, damping factor and damping for the three positions are presented in table 11.

Table 11: Damping ratio, natural frequency and period and damping for the three buoy positions

		Model scale			Full-scale		
	ξ [-]	**ω_0 [1/s]**	**T_0 [s]**	**c [kg/s]**	**ω_0 [1/s]**	**T_0 [s]**	**c [kg/s]**
Buoy position 1	0.1040	0.3949	2.5322	1.3303	0.0721	13.8695	6 558
Buoy position 2	0.1869	0.8101	1.2344	4.9056	0.1479	6.7614	24 182
Buoy position 3	0.0943	0.3941	2.5373	1.2042	0.0720	13.8973	5 936
Buoy position 2 w/o air cylinder	0.0850	0.7840	1.2754	2.1602	0.1431	6.9859	10 649

As seen from table 11, the values of position one and three are quite similar, while the values of position two deviates a lot from the others. The natural frequency and the damping ratio of position two are around two times the values of the other positions. The damping ratio at position two without the air cylinder connected is however similar to position one and three. That position one and three are similar is no surprise, the model was turned 180° and the buoy itself was not moved.

7.1.5 Deviation from middle position

It has been investigated whether or not the buoys rotate about their equilibrium position (at the calm free surface, z = 0). This has been done by calculating the mean values of the response in z direction for all regular waves. Buoy position one and three have no or very little deviation from middle position, and the buoys oscillate slightly below the calm surface. As the waves become larger, the deviation increases, at the most – 4.6 mm. The deviations from middle position for buoy position two are for some waves quite large, at the most – 46 mm. A clear tendency of positive/negative deviations or for which wave the deviations increase cannot be seen.

7.1.6 Response amplitude operator (RAO)

7.1.6.1 Regular waves

The RAO is the ratio between the response amplitude and the input amplitude [38]:

$$RAO = \frac{Y_a}{\zeta_a}$$

Equation 8: RAO regular waves

Where ζ_a is the wave amplitude and Y_a the response amplitude. Y_a is found from the measured maxima and minima of the steady part of the response signal.

Heave

The RAOs for motion in heave for six different frequencies are shown for the three buoy positions in figure 14. The results are presented as full-scale values for easy comparison with SIMA. Plots of the RAOs for the remaining angles can be found in Appendix C.

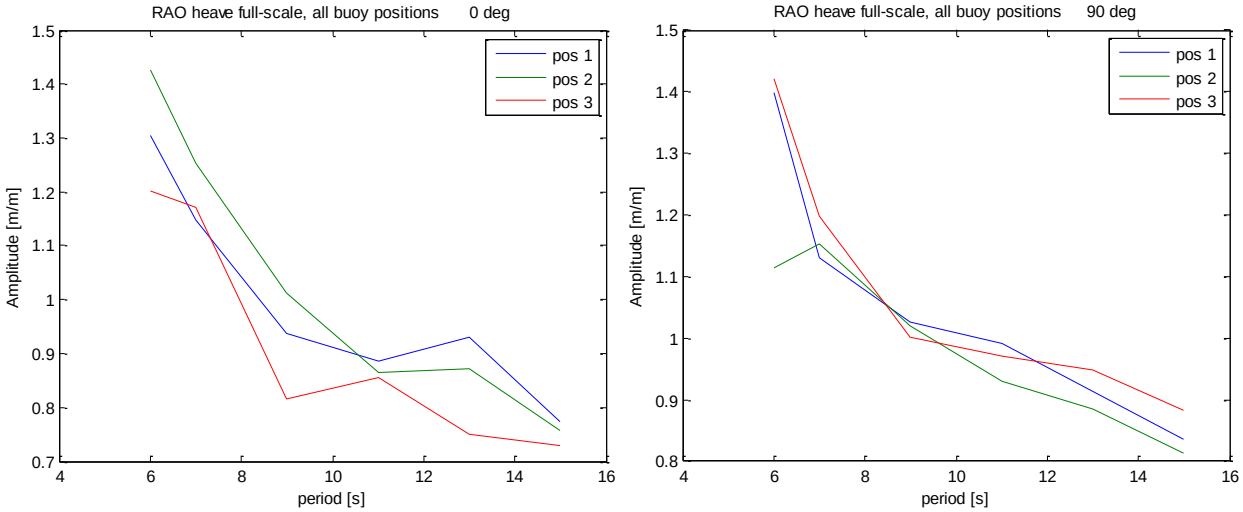

Figure 14: RAO heave regular waves, 0 and 90 degrees, full-scale measurements

The values of the RAOs are around one, which is as expected; the buoy moves with the surface elevation caused by the incoming waves. The peak period for the three positions is not always within the range of periods tested. It is reasonable to believe that the peaks will appear at periods somewhere between 4 and 5.5 seconds. The RAO for buoy position one is more or less the same for all angles, while it for the other positions has some variations for the shortest periods. Buoy position two has a peak at 7 s for 90°, and position three a peak at 7 s for 60° and 75°. For periods longer than 9 s, the difference in amplitude is not significant between the angles.

A comparison of response amplitude of the different positions shows that there are small differences between the positions. No clear tendencies can be observed, position one does not always have the highest amplitudes and the angle of the incoming waves seem to have some impact, but not of significance. The response amplitudes of wave 12 (H = 3 m) is shown in figure 15 as an example.

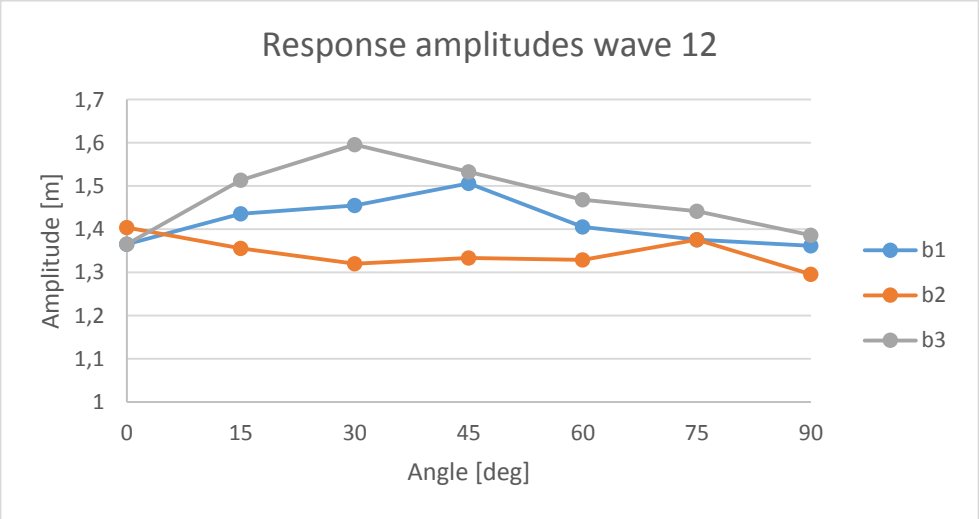

Figure 15: Response amplitudes wave 12

Surge

The shape of the RAOs in surge are almost equal to those in heave, the peaks appear at the same angles. The response in surge is much smaller than in heave, around 0.35 m/m, which is not surprising considering that the buoy movement in surge, measured in meters, is between 20 and 50 % of the movement in heave. The RAOs for motion in surge for six different periods are shown for the three buoy positions in figure 15. Plots of the RAOs for the remaining angles can be found in Appendix D.

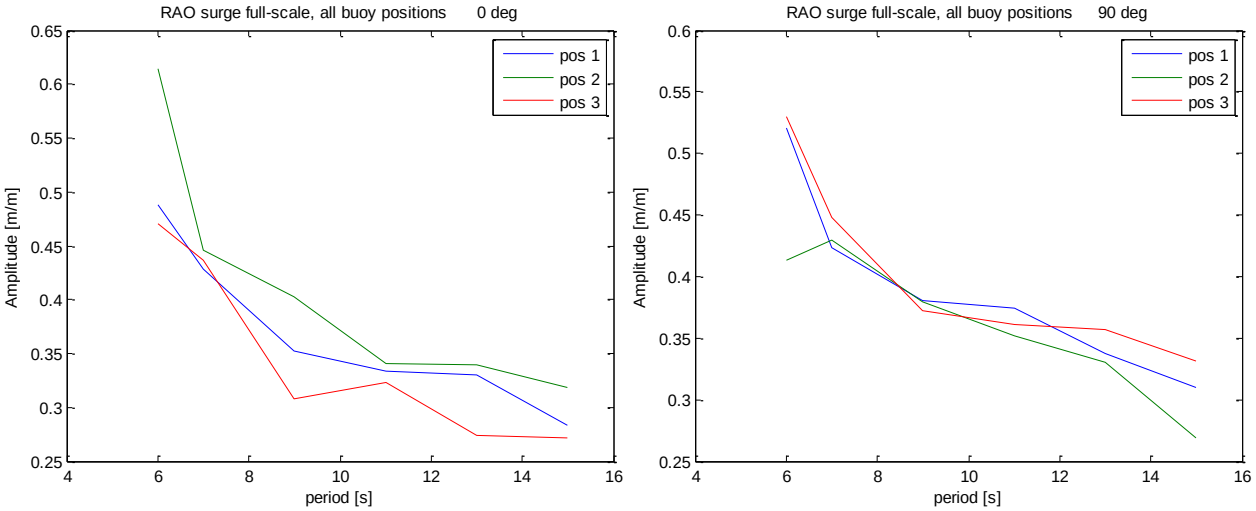

Figure 16: RAO surge regular waves, 0 and 90 degrees, full-scale measurements

7.1.6.2 Irregular waves

Tests have not been run for sea state B (H_s = 0.75 m, T_p = 8 s, full-scale), as it was observed that the responses were small and similar to those of sea state A. The test of sea state E at 0° incoming wave angle was aborted after about two minutes due to extremely large responses. Sea state E for 0° – 60° for buoy position one was therefore not run in fear of breaking the test model and transducers.

To find the standard deviation and significant value of the response, one has to find the moments of the spectrum. The nth moment of the spectrum is given by

$$m_n = \int_0^\infty \omega^n S(\omega) d\omega$$

Equation 9: Spectral moment

Where m_0 is the variance of the displacement, m_2 the mean square velocity and m_4 the mean square acceleration of the response. The standard deviation of the response is calculated as $\sigma = \sqrt{m_0}$ and the significant value of the response as $x_{1/3} = 4\sqrt{m_0}$. [38].

Heave

For small (0° – 15°) and large values (75° – 90°) of the incoming wave angle there is not much difference in the response amplitude between the different buoy positions. The largest differences are observed around 45° for all sea states, with some variation in the magnitude of the difference. In general, for these angles the amplitude measured at buoy position one is larger than at position two, which again is larger than amplitudes at position three. As the wave period increases above eight

seconds the value of the response amplitude approaches one for all buoy positions. The highest peak amplitude value is usually found at 0°.

The response peak periods vary between 3.5 and 6.6 seconds, for most conditions it is around 5.5 seconds. In general the peak period increases with increasing angle. There are no clear differences between the sea states.

Figure 17 shows the RAOs in heave for sea state C for 45° and 90°. RAOs for other sea states and angles can be found in Appendix E.

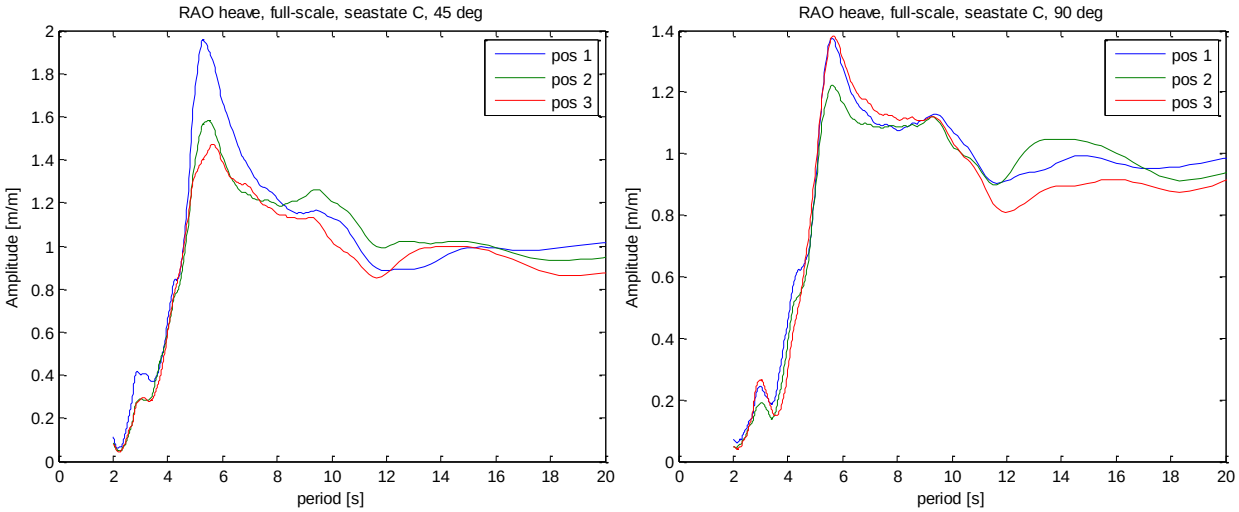

Figure 17: RAO heave irregular waves, sea state C, 45 and 90 degrees, full-scale values

The significant values of the heave frequency spectra, $x_{1/3}$, are highest for small angles: between 1.3 and 1.4 times the significant wave height of the sea state, H_S. $x_{1/3}$ approaches H_S for the largest angles. Buoy positions two and three have similar significant values, while the values for position one are slightly higher. For buoy position one, sea state C (H_s = 2.25 m), a peak is observed at 60° incoming wave angle. This is illustrated in figure 18.

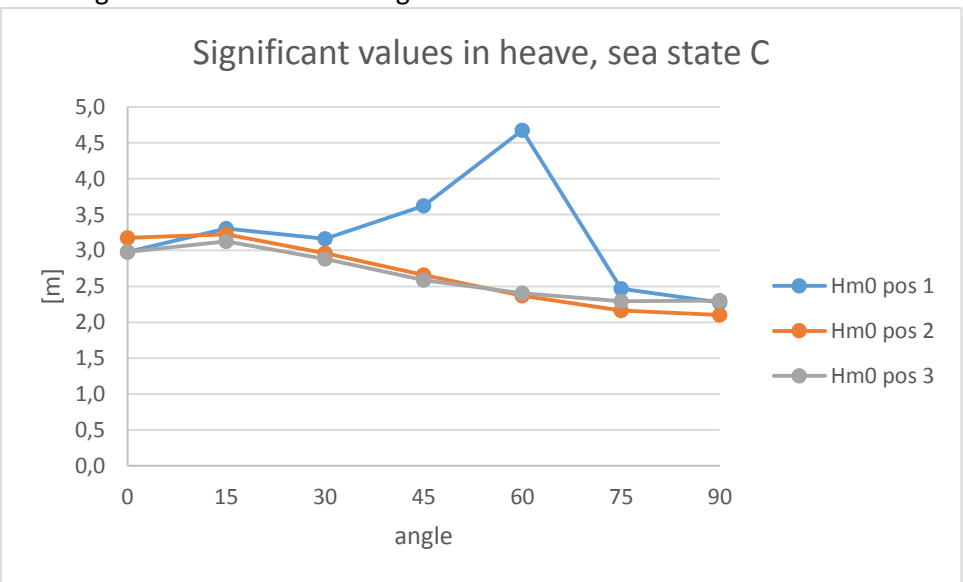

Figure 18: Significant values, sea state C. Full-scale values.

Surge

The RAOs in x direction show that there is not much difference in measured surge response between the buoy positions. The difference is however highest for 45° and 60°. The most prominent peak is found at 5 – 6 seconds for all sea states and angles. For higher periods the RAO stabilizes at around 0.4 m/m. For some sea states and angles, e.g. sea state C, 45°, the RAO increases again as the period increases. This is most likely because of small values in the calculations: something small divided by something smaller gives a very high quotient. Figure 19 shows the RAO for sea state C at 45 and 90° incoming wave angle. RAOs for other sea states and incoming wave angles can be found in Appendix F.

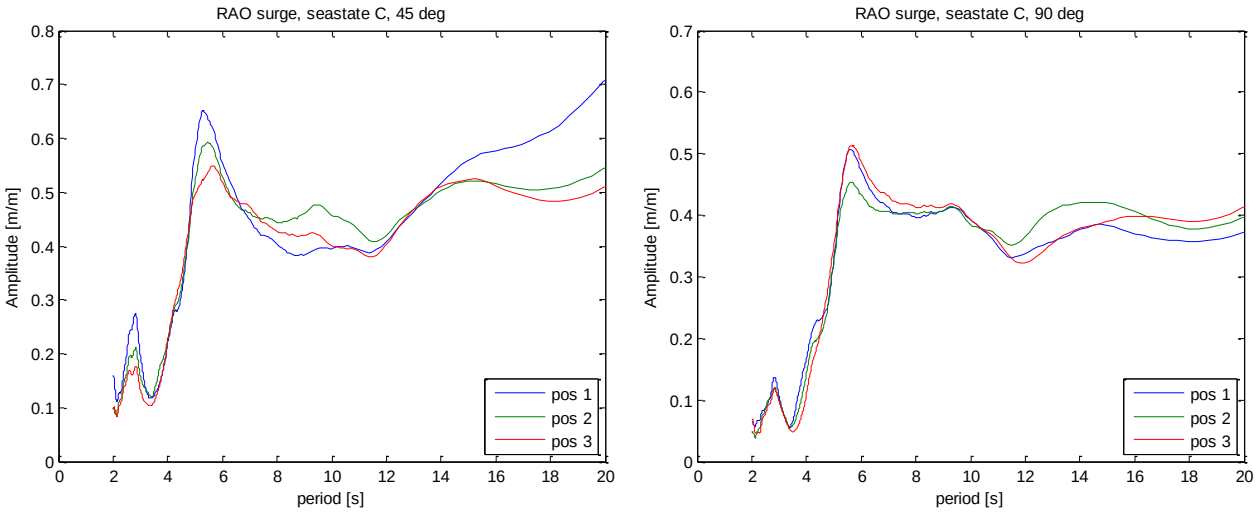

Figure 19: RAO surge irregular waves, sea state C, 45 and 90 degrees, full-scale values

7.1.7 Produced power

The produced power depends on the damping of the air cylinder. The damping force and the velocity of the stroke must be in phase for power to be produced. Unfortunately, the pressure regulators connected to the air cylinders were closed more than they should have been during the model tests. Because of this, most of the axial force on the cylinder is spring forces instead of damping forces. With spring forces dominating little or no power is produced. However, based on the runs done for optimal load resistance and three other runs with the pressure regulator valves open, rough estimates of produced power have been done. Table 12 presents average produced power over one wave period calculated according to equation 3 for both model and full-scale.

Table 12: Average produced power over one wave period

model			full-scale		
H [m]	**T [s]**	**P [W]**	**H [m]**	**T [s]**	**P [W]**
0.100	1.278	1.0047	3.0	7.0	152 294.65
0.100	1.643	0.4797	3.0	9.0	72 713.99
0.100	2.008	0.3241	3.0	11.0	49 127.80
0.100	2.373	0.2519	3.0	13.0	38 183.56
0.100	2.739	0.1975	3.0	15.0	29 937.49
0.033	2.373	0.0502	1.0	13.0	7 609.43
0.067	2.739	0.0893	2.0	15.0	13 536.29
0.167	2.008	0.0876	5.0	11.0	13 278.60

The power, P, is the power harvested from the waves that can be transformed to electricity. The efficiency of the buoys varies between 1 and 20 %, dependent on wave period. A rough estimate of the total yearly electricity production of the WECs has been done with the assumptions of 3500 operating hours, a generator efficiency of 30 % and other losses set to 50 %. This gives a yearly production between 10 and 400 GWh, which is unexpectedly high. These estimations are based on regular waves only, and without much knowledge about the conversion to electricity. It must therefore be stressed that the obtained values only give an indication about the possible produced power.

7.1.8 Vertical forces on rotation arm

7.1.8.1 Regular waves

The magnitude of the vertical forces acting on the rotation arm from the waves and how these forces vary with wave angle have been investigated for five different regular waves. A typical result is shown for transducer 8600 in figure 20 with full-scale values of the force. Plots for the other buoy positions and for transducer 8601 are found in Appendix G.

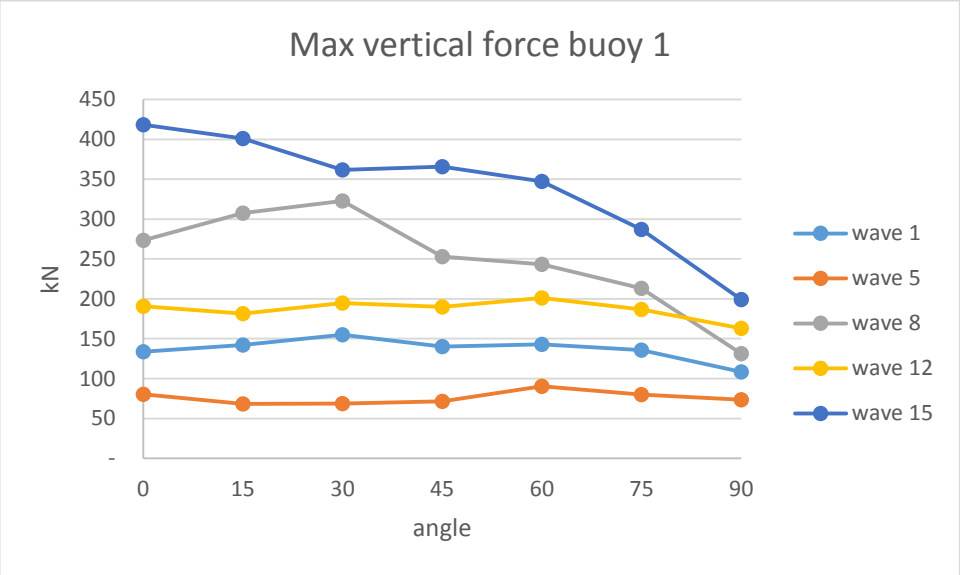

Figure 20: Max vertical force at rotation point at buoy position one for all incoming wave angles. Full-scale values.

The vertical force does not vary much with incoming wave angle for less energy dense waves (waves 1, 5 and 12). For the waves with more energy the force declines as the angle increases. This is because the measurements presented are from the rear rotation arm relative to the incoming waves, this being in the shadow of the buoy. For measurements from the fore rotation arm the trend is opposite: the force increases as the angle increases.

A comparison of the vertical forces for the different buoy positions has been done, but no clear tendencies discovered. For some waves the forces are quite equal, for others the forces at position one are largest, while for others again the forces are largest forces occur at position three. One would believe that the forces are smaller at position three, at least for 45 and 60°, since the shadowing effect is largest here.

7.1.8.2 Irregular waves

The vertical force transfer functions are similar to the RAOs in heave, the largest forces are found around wave periods of 5 – 6 seconds. Figure 21 shows the full-scale transfer functions for transducer 8601 at 45 and 90° angle. For 0° the transfer functions are quite similar. As the incoming wave angle increases it is clear that the vertical forces at position one is higher than at the other positions. Position two and three have similar peak amplitude values for all angles and sea states. Two possible explanations are found: the shadowing effect is small/nonexistent between the two rare positions or the responses at position two are smaller then they should be due to higher resistance in the rotation point.

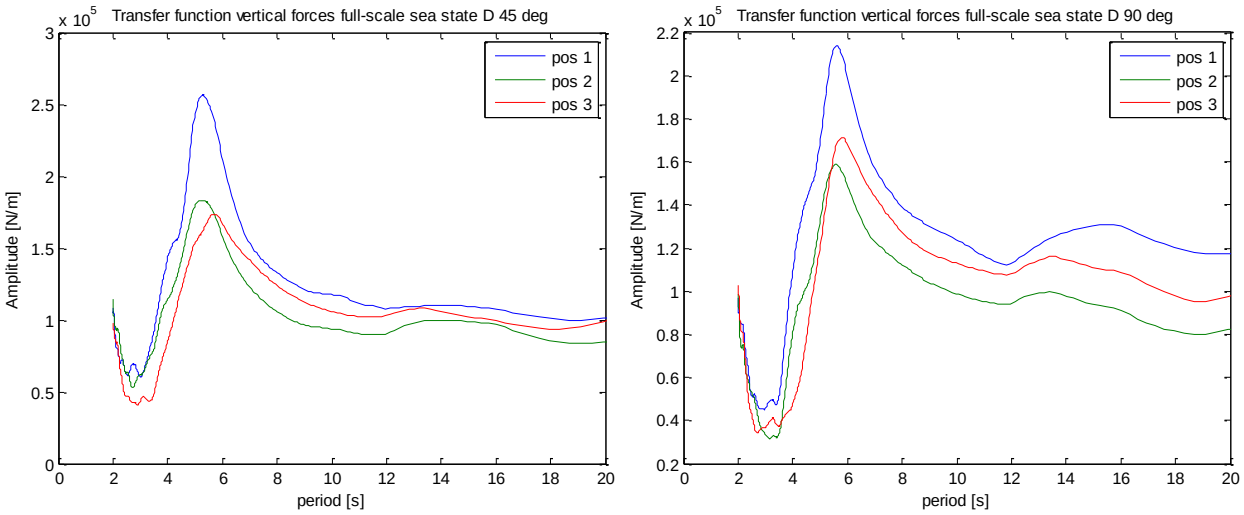

Figure 21: Transfer function vertical force for sea state D, 45 and 90 degrees incoming wave angle, full-scale values

The significant values of the vertical force frequency spectra have been calculated according to the theory presented in section 7.1.6.2, but with S(ω) being the output spectrum of the forces. In general they decrease as the incoming wave angle increases. Figure 22 shows full-scale significant values for sea state D as a function of incoming angle. Both transducers measuring the vertical force at the rotation arm are included in the plot.

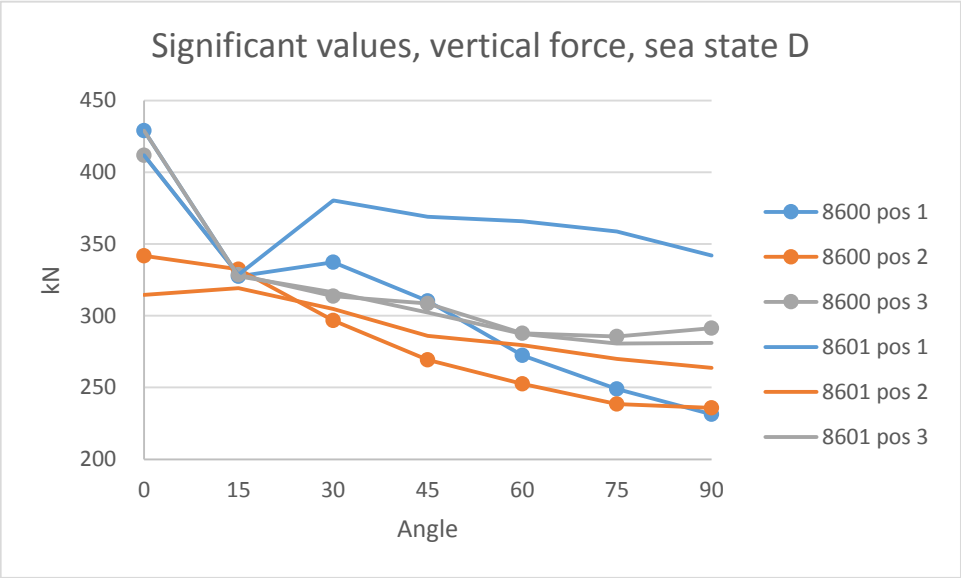

Figure 22: Significant values of vertical forces measured by transducers 8600 and 8601, sea state D, full-scale vertical forces

The significant values at position two and three are slightly higher for transducer 8601, this is reasonable since this is closer to the wave maker for angles larger than 0°. Transducer 8601 at position one has larger significant values than the other positions. The reason for this is that the transducer is connected to the model at the place where the waves interact first, i.e. where the largest wave forces occur. Plots of significant values for sea states C and F can be found in Appendix H.

7.1.9 Horizontal forces on platform framework

7.1.9.1 Regular waves

Investigation of the horizontal forces acting on the platform framework from the buoy at the rotation point has been performed in the same way as for vertical forces. Figure 23 shows the max forces measured at the fore rotation point, transducer 8603, at buoy one scaled to full-scale.

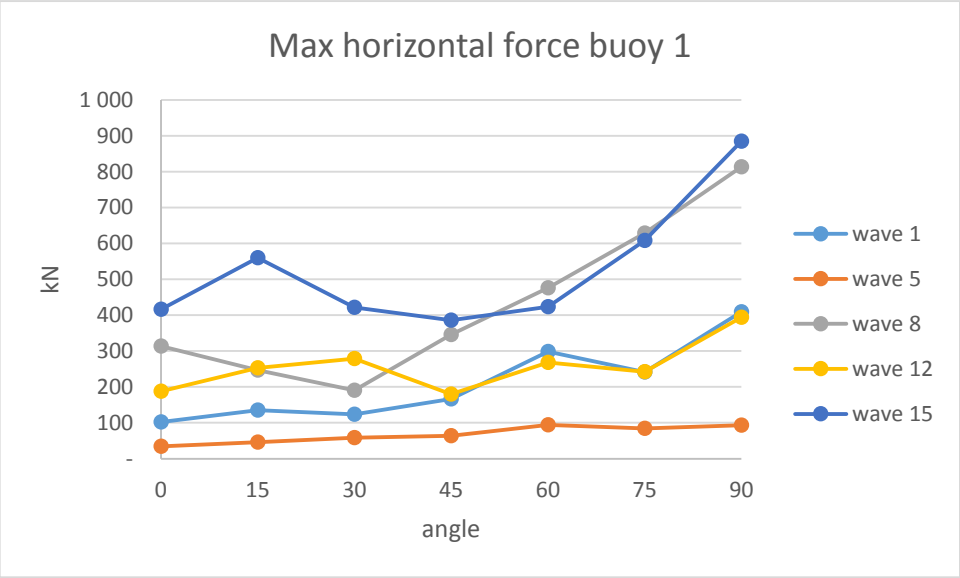

Figure 23: Max horizontal force at rotation point at buoy position one for all incoming wave angles. Full-scale values.

For all waves the force increases as the angle increases. This is as expected since the waves interact more and more with this side of the buoy as the angle increases. Not much difference in magnitude of the forces have been observed when comparing the different positions. Which of the positions that have the largest measured forces varies, and it is not possible to say if the forces always are larger at position one (as would be reasonable to believe). Figures that illustrate this are found in Appendix I.

7.1.9.2 Irregular waves

The transfer functions for the horizontal forces acting on the platform framework are not as consistent as the vertical forces when comparing different angles. For several angles, more than one peak is observed. In general, the forces are larger at position one than position two, which again is larger than at position three. This implies that there is a shadowing effect. Figure 24 shows the full-scale transfer functions of transducer 8603 for sea state D at 45° and 90°.

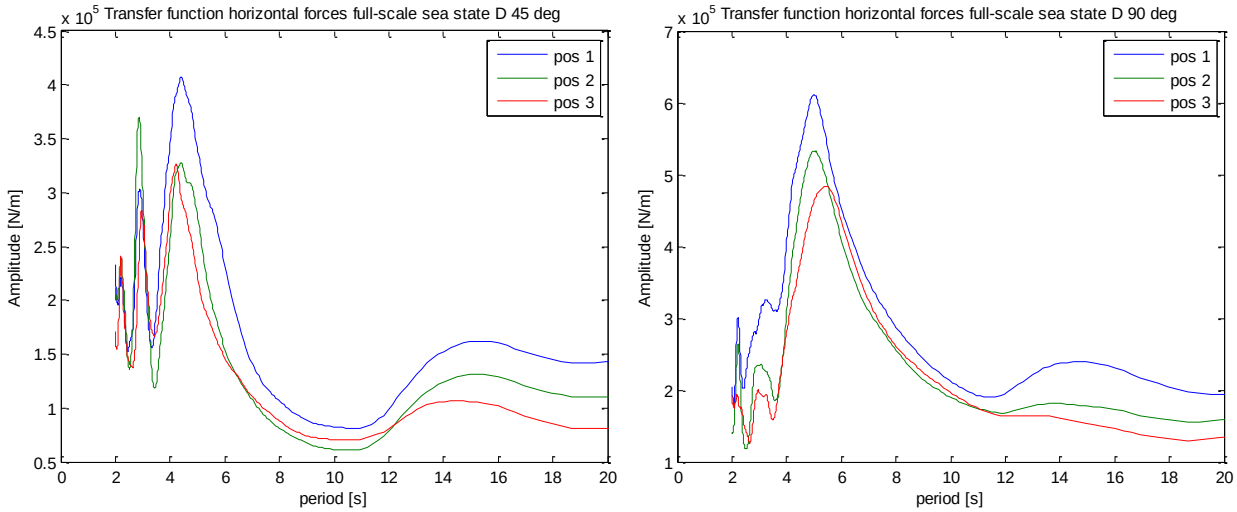

Figure 24: Transfer function horizontal forces, sea state D, 45 and 90 degrees incoming wave angle. Full-scale values.

The significant values of the force frequency spectra have been calculated. The values for all three positions coincide with the findings for regular waves and the transfer functions: the forces are larger at transducer 8603 at 90° and the forces are in general largest at position one. This is illustrated in figure 25. Significant values of the horizontal force for sea states C and F are found in Appendix J.

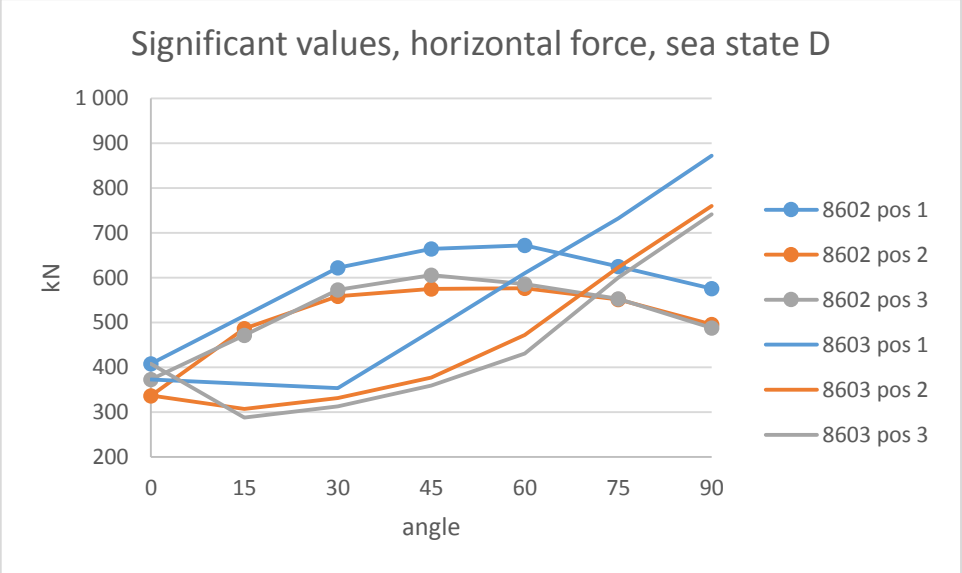

Figure 25: Significant values of horizontal forces measured by transducer 8602 and 8603, sea state D, 45 and 90 degrees incoming wave angle. Full-scale values.

7.1.10 Uncertainty analysis

The error of a measured result is the difference between the measurement and its true value. Bias errors are systematic errors in the measurements, e.g. incorrect calibration or accuracy of the geometrical shape of the model. This will not be of importance in this work since all results are compared with measurements with the same systematic error. Precision errors are scatter in the result, and are found by repeating the same measurement and comparing the results. The statistical representation of error is the uncertainty and is usually represented by a confidence interval.

Uncertainties have been calculated for maximum and minimum values of all transducers with a confidence interval of 95 %. For a set of N = 12 samples the corresponding value of t in the Student's t distribution is 2.2. The analysis has been done for regular waves 8 and 14. Table 13 presents the uncertainties in percent.

Table 13: Uncertainties of N=12 samples for regular waves 8 and 14 together with mean uncertainty of the two waves.

Transducer	wave 8	wave 14	mean
8600, vertical force	10.38 %	7.63 %	9.01 %
8601, vertical force	11.03 %	4.42 %	7.72 %
8602, horizontal force	7.64 %	8.93 %	8.28 %
8603, horizontal force	5.16 %	7.74 %	6.45 %
20287, axial force in air cylinder	4.76 %	2.74 %	3.75 %
displacement	4.58 %	11.22 %	7.90 %
wave	2.32 %	1.99 %	2.15 %

7.1.11 Uncertainties

7.1.11.1 Errors due to structural modelling

During the tests it was observed a variation in resistance at the rotation point for the different buoy positions. This is clearly seen in the results of the decay tests: at position two the damping ratio of the buoy is about twice the value of positions one and three. When the buoy was shifted from position two to position one, inaccuracies in the connection points at the framework was discovered. These were a bit further apart at position one, making the hinge with the rotation point shift slightly from horizontal position. This was fixed before the tests continued, but if the final positions of the rotation points were equal to those of position two is uncertain. Also, for some runs the buoys that were not equipped with transducers moved less than they should. The reason for this is varying friction at their rotation point, they moved as they should after small adjustments. This was not always discovered right away, and has to some extent affected the movement of the buoy with transducers: the waves diffracted by one buoy sets the other in motion. It can also have an impact on the shadowing effect, the waves brake differently around an object almost at rest versus an object in motion.

The water depth in the tank varied between 1.325 and 1.34 m because of spilling of water when running the highest waves. This led to a variation in the draft of the model which again led to a variation in angle between the rotation arm and platform framework for the buoy at z = 0. This could lead to differences in the mean position of the transducers, but the error was to a high degree avoided by frequent zero measurements.

7.1.11.2 Errors due to environmental modelling

An error that can occur, especially for short and steep waves in a long and narrow tank, is change in wave properties as the wave propagate from the wave maker. To investigate if the changes have been significant during the model test the wave parameters and spectral shape of the applied JONSWAP spectra have been compared to theoretical values (equation 1 and equation 2, section 6.7.2). In general, the measured values are slightly lower than the theoretical, but the deviations are not significant. As an example, the significant wave height differs with 1 – 3 mm. The spectral shapes are more or less equal, though the measured spectra are not as smooth as the theoretical. However, for sea state E, deviations around ten times larger than for the other sea states are observed. This is the sea state with the steepest waves, so it is not unexpected that the largest deviations are found here.

The model will reflect and generate waves. These waves may reach the tank wall and be reflected back to the model. For regular waves this will not be a problem, the time series are short, and the waves will not have time to reach back to the model before the measurements are finished. For irregular waves tank wall effects might be of importance. No measurements have been done specifically to address this effect. However, the height of reflected and diffracted waves have been calculated for regular waves by comparing the wave height with and without the model in the tank. The heights varies between 0 and 26 mm, which is at the most 13 % of the wave height. It is reasonable to assume that these results also apply for irregular waves. It is not easy to quantify how much of the energy in the waves that are reflected back to the model, but this could for some of the runs be of significance. In this validation the measurements are compared to each other, and since the tank wall effects will be similar for all runs, no more emphasis is given to this matter.

7.1.11.3 Instrumentation and measuring errors

Zero readings have been done before each wave set to avoid errors because of drift in the measured signal from the transducers. Slow variations in temperature causes this drift, and is especially important for transducers immersed in water due to change of cooling because of change in water velocity.

For some of the calculations, e.g. axial force in air cylinder as a function of damping and spring stiffness, it is important that the measurements were done at the exact same time instant to obtain accurate results. The error caused by this is considered to be small.

7.2 Numerical simulation model

Effort has been made to tune the simulation model of side AB to produce the same results as the model test. It has proven to be difficult to obtain equal results, both due to the inconsistent responses for some waves and buoy positions and time limitations. The fixed elongation couplings have been adjusted individually for each buoy position and wave to produce responses as similar as possible to the measured responses. The starting point for the adjustments have been the length of the coupling and the damping found in section 7.1.2. Mainly the force has been varied to tune the response, but for some conditions the distance and the damping had to be adjusted as well. A list of fixed elongation settings are found in Appendix K. As the fixed elongation couplings have only been tuned with respect to the measured responses at 0^{o}, inaccurate results can be expected for high incoming wave angles. Full-scale dimensions have been used in the numerical simulation model.

No analyses have been carried out for the numerical model of the entire platform.

7.2.1 Response amplitude operator

The RAOs of the three buoy positions are equal; the same Wamit-file has been imported from Wadam to SIMA for all positions.

Figure 26 show the RAO in heave for 0°, 30°, 60° and 90° obtained from Wadam. The peak period is 5 seconds and the peak amplitude decreases as the angle increases. These results are similar to those obtained in the model test.

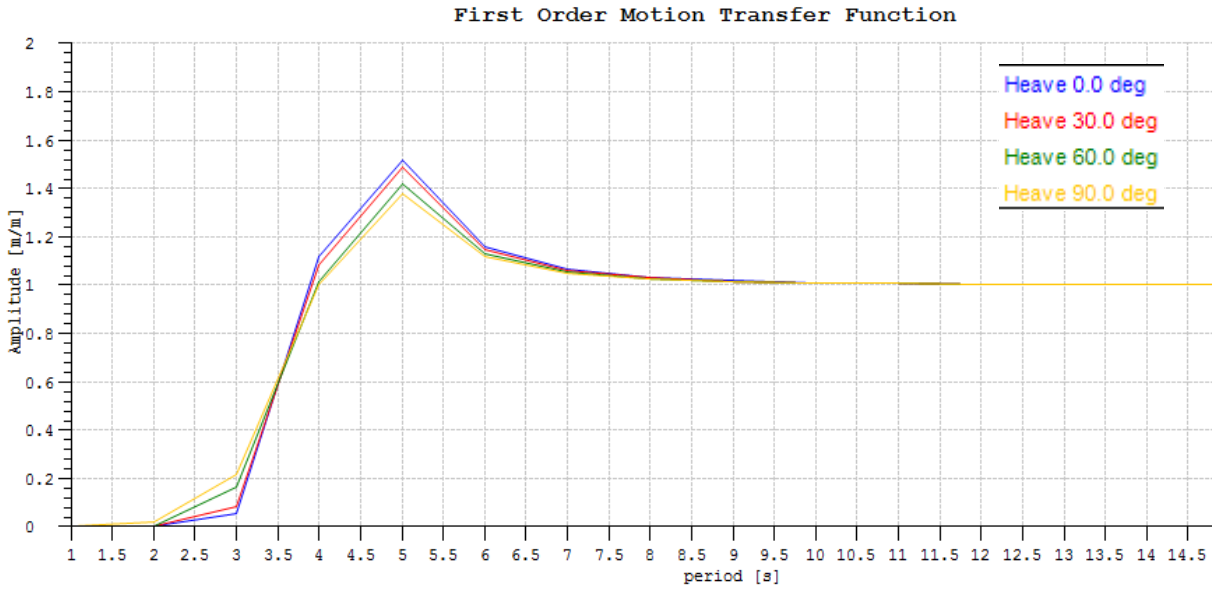

Figure 26: RAO heave, results from Wadam

The RAOs in surge are presented in figure 27. For 90° the amplitude is so small that it does not show with the present scale. A peak is observed at 6 seconds before the amplitudes increase as the wave period increases.

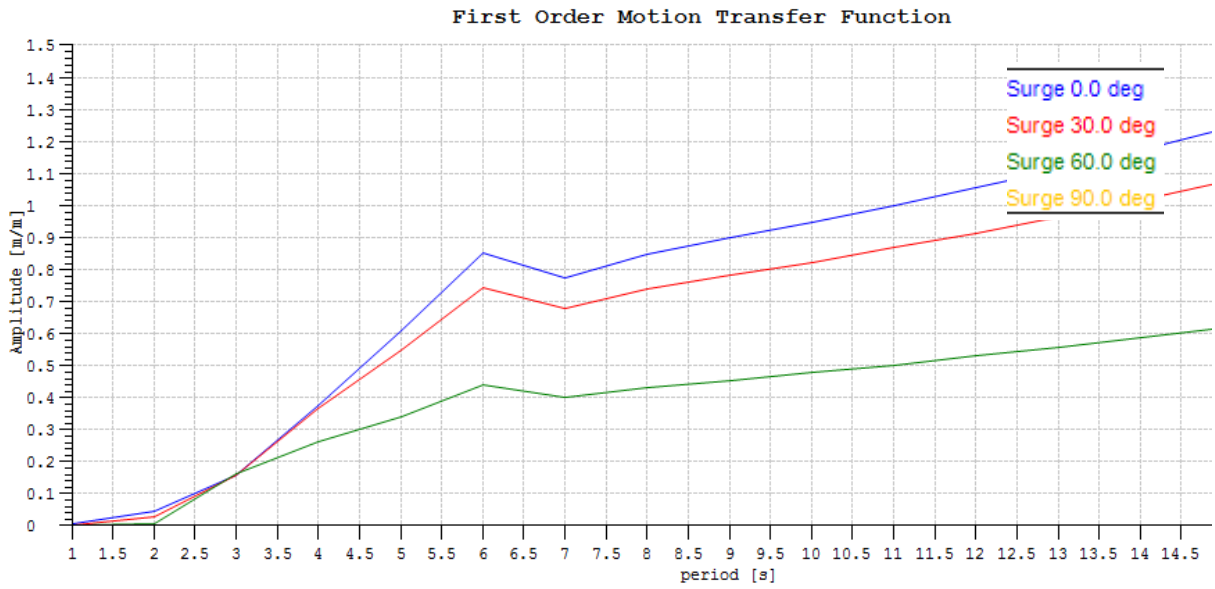

Figure 27: RAO surge, results from Wadam

7.2.2 Forces

7.2.2.1 Regular waves

Figure 28 shows the maximum value of the vertical forces at buoy position one for five regular waves at different incoming wave angle. The forces barely vary with the angle, which could imply that the waves pass through the buoys instead of around them.

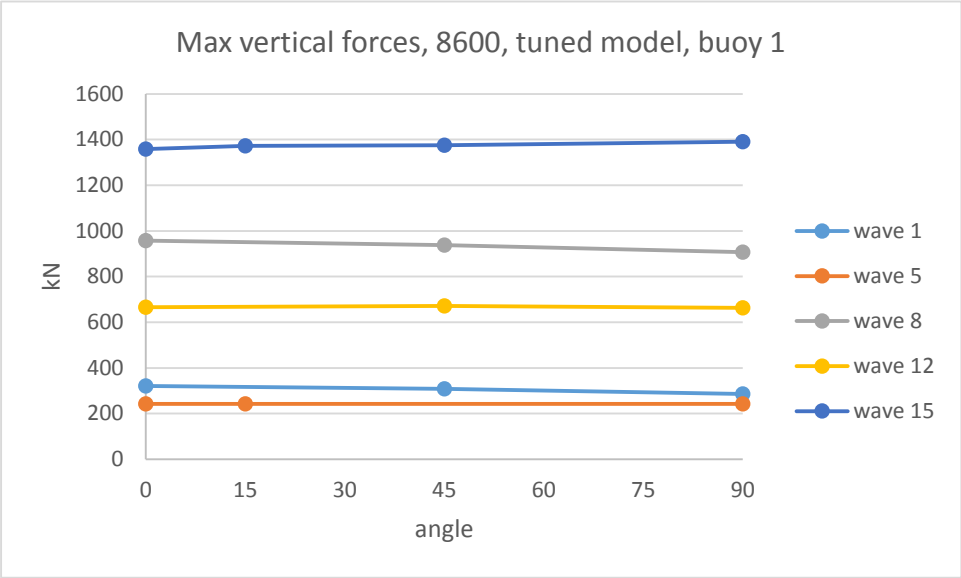

Figure 28: Max vertical forces at buoy position one for the tuned SIMA model. Position on SIMA model corresponds to transducer 8600.

The forces at buoy position two and three are equal to those of position one for all waves considered except wave 15. Here, the tendencies are the same, but the values for position two is around 2000 kN and position three 1600 kN.

The maximum value of the horizontal forces at buoy position one for five regular waves are plotted in figure 29.

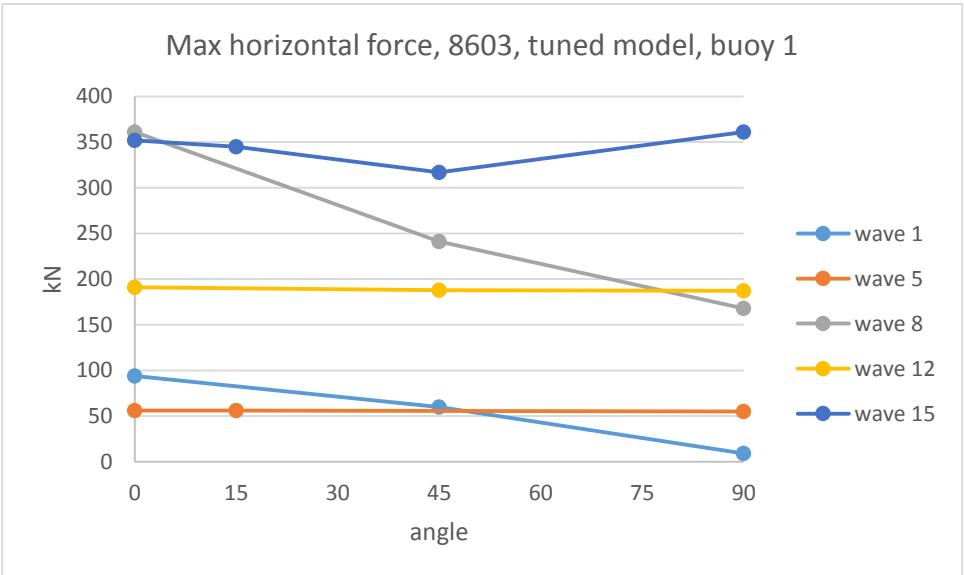

Figure 29: Max horizontal forces at buoy position one for the tuned SIMA model. Position on SIMA model corresponds to transducer 8603.

For wave 5 and 12 the maximum force does not vary much with incoming wave angle, while some variation is seen for the other waves. 8603 is the transducer closest to the wave maker during the model test, and it was expected that the forces would be highest at 90° incoming wave angle. Instead, for wave 1 and 8 the force is lower at this angle. Wave 15 has the expected tendency, but the increase in force is quite small. It is clear that the shadowing effect is not accounted for in the numerical model.

The tendencies of the horizontal forces as the incoming wave angle increases are the same for all three buoy positions, and the values are equal for all waves except wave 15. The highest forces occur at buoy position two, with almost 500 kN at 0° angle. At buoy position three the maximum force at 0° is 450 kN. At 90° angle, the vertical force at position three are 100 – 150 kN higher than at the two other positions.

7.2.2.2 Irregular waves

The fixed elongation couplings have been adjusted with the starting point at the values for the wave that has most similar height and period as the analyzed sea sate. Running the irregular analysis in SIMA have been challenging, as errors occurred if the damping was not high enough. To achieve correct response the force in the fixed elongation couplings has to be large and the damping small. With these settings, large forces act on the rotation arm. Decreasing the stiffness rotation around local y-axis for the rotation point modelled as a flex joint have been tried, but with little success.

Figure 30 presents the significant values of the vertical forces acting on the rotation arm corresponding to force transducers 8600 and 8601 for the three buoy positions.

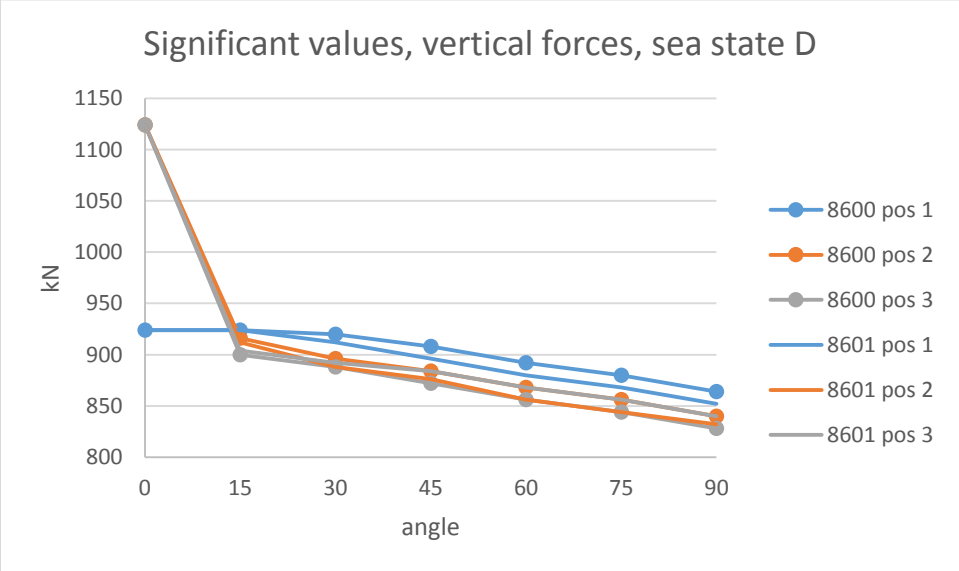

Figure 30: Significant values of vertical forces for sea state D. Positions on SIMA model correspond to transducers 8600 and 8601.

The significant values are approximately equal for all three positions, with the exception of 0° incoming wave angle. This is strange, at 0° the forces should be equal for all buoy positions since the incoming waves interact equally with all three buoys. The large deviation might be caused by errors in the SIMA model. To investigate this, the settings for each buoy were double checked and the analysis run again obtaining the same result. The tendency as the incoming wave angle increases is

clear: the significant values decrease. The forces are in the same range as for regular wave 8, this coincides well as the wave period and height of the regular wave are similar to peak period and significant wave height of sea state D.

The significant values of the horizontal forces for sea state D are presented in figure 31.

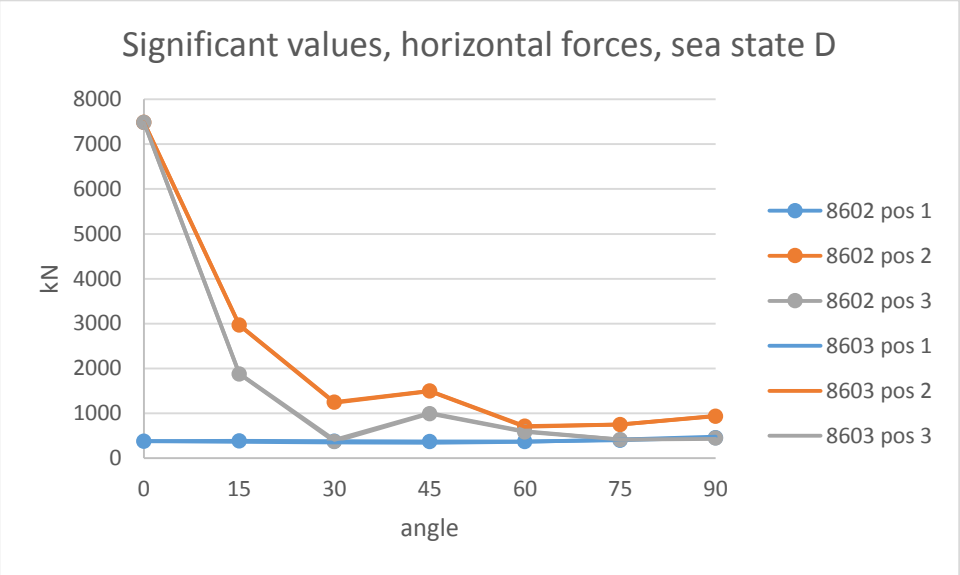

Figure 31: Significant values of horizontal forces for sea state D. Positions on SIMA model correspond to transducers 8602 and 8603.

The forces at buoy position one are much smaller that at the two other positions for low angles. This is unexpected, as all settings for the three buoys are equal. The tendency of position two and three are the same: the significant value decreases significantly from 0° to 30° incoming wave angle before it settles around 1000 kN. The significant value at position one increases slightly with increasing angle, and is around 400 kN for all angles. An increase of almost 100 kN is observed from 60° to 90°.

7.3 Comparison of numerical model and model test

7.3.1 Response

Comparison of the responses of the model test and the numerical model has been done by comparing the time series of the responses in regular waves and by looking at the peak values of the buoy's RAOs. Figure 32 and figure 33 shows the time series of the heave motion for wave 5 at 0° incoming wave angle for model test and numerical model respectively.

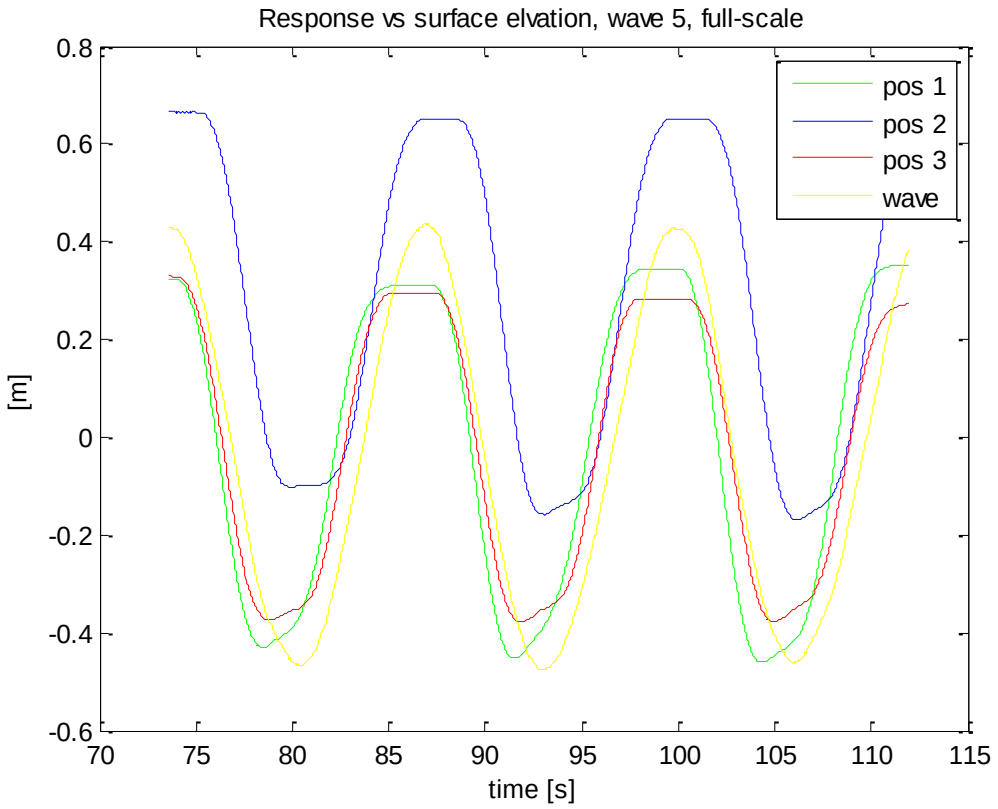

Figure 32: Response vs surface elevation for wave 5 at 0 degrees incoming angle, model test results, full-scale values

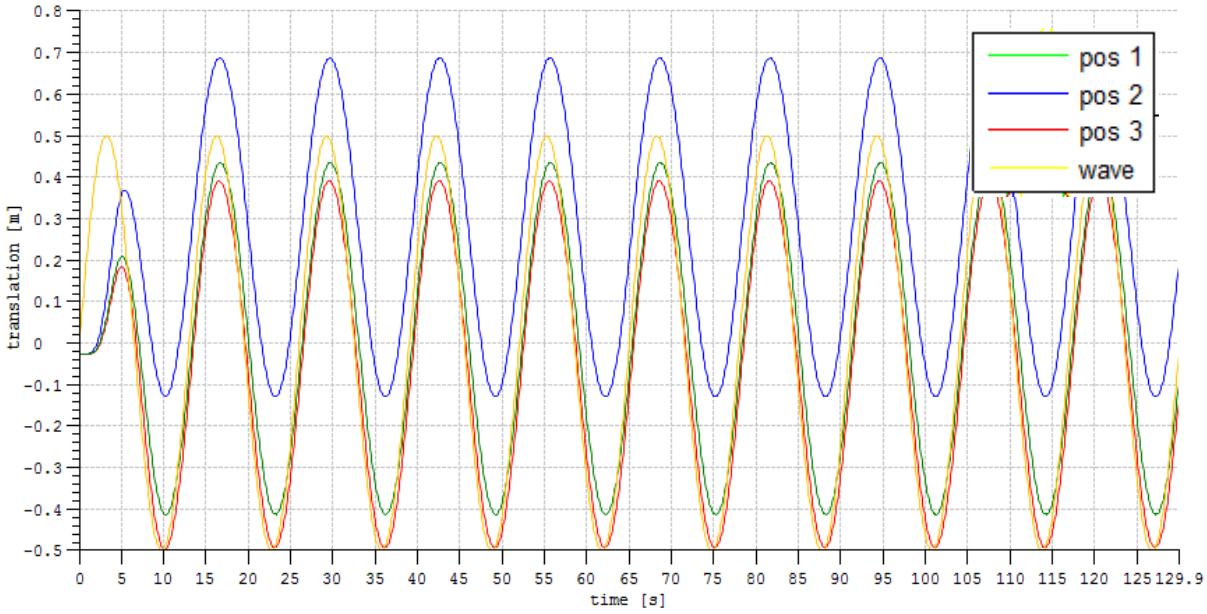

Figure 33: Response vs surface elevation for wave 5 at 0 degrees incoming angle, results from numerical model

At buoy position three the simulated motion has a lower minimum value, -0.5 m versus- 0.35 m for the model test, and at position one the maximum value is 0.45 m for the simulated model versus 0.35 m for the model test. Other than this, the heave response in the numerical model coincides well with the response measured in the model test. It should also be noted that the buoys remain at maximum and minimum position for some time during the model test, while their movement is smoother in the simulation.

The responses for wave 15 are shown for the model test in figure 34 and the simulation model in figure 35. The responses does not coincide as well as for wave 5. Higher responses and waves with more energy were more complicated to tune than low waves with little energy.

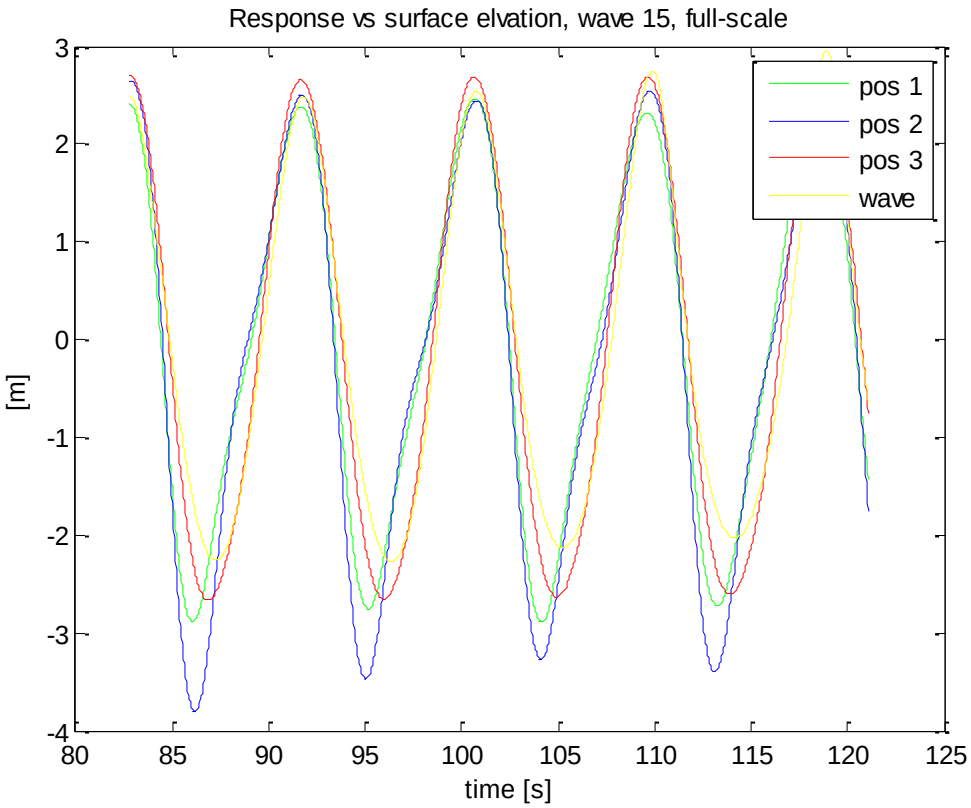

Figure 34: Response vs surface elevation for wave 15 at 0 degrees incoming angle, model test results, full-scale values

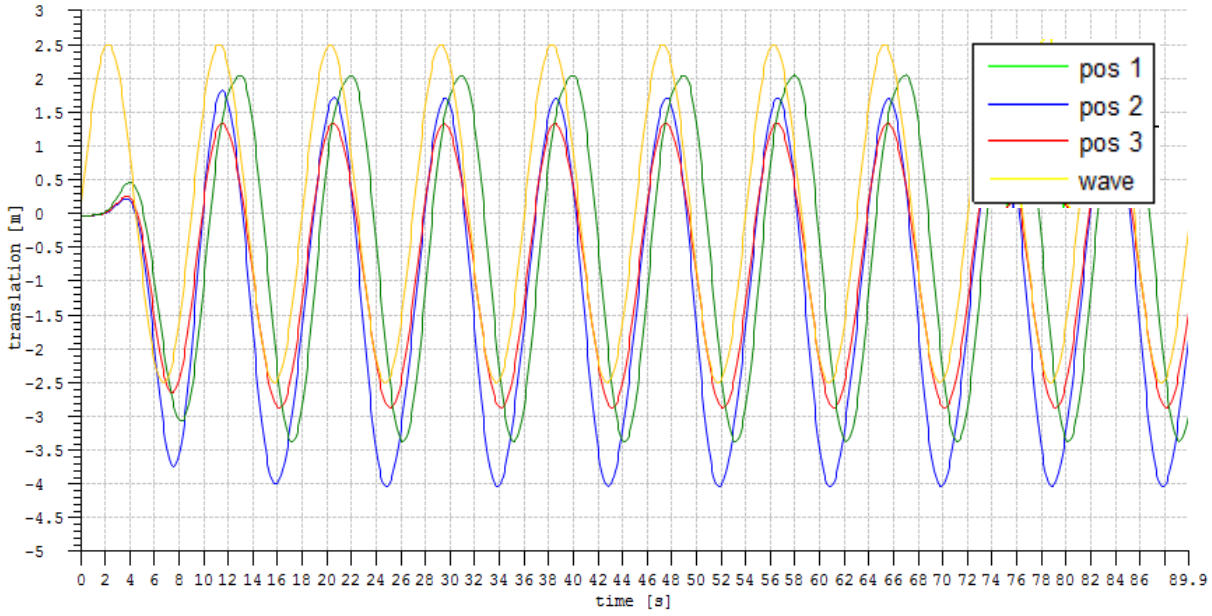

Figure 35: Response vs surface elevation for wave 15 at 0 degrees incoming angle, results from numerical model

During the model test the heave motion of the buoys followed the surface elevation above the mean free surface, while the response was larger below the mean free surface. The responses in the numerical analysis coincides well with the model test for buoy position one and two below the mean free surface, while it is inaccurate above.

The time series of the response of the numerical model without tuning (implementation of fixed elongation coupling to represent the air cylinders) have also been studied. The results show heave responses with smaller amplitude than the wave amplitude for the three buoy positions for all angles. The responses declines slightly for increased incoming wave angle.

Table 14 presents the peak periods, T_{peak}, and peak amplitude, ζ_{peak}, of the RAOs for incoming wave angles 0°, 30°, 60° and 90° from Wadam and the model test. The values form the model test is for sea state D, as this is most similar to the environment used in the Wadam analysis.

Table 14: Comparison of the peak period and amplitude of the RAOs obtained from Wadam analysis and model test.

	0°		30°		60°		90°	
	T_{peak} [s]	ζ_{peak} [m/m]	T_{peak} [s]	ζ_{peak} [m/m]	T_{peak} [s]	ζ_{peak} [m/m]	T_{peak} [s]	ζ_{peak} [m/m]
Heave								
Wadam	5.0	1.517	5.0	1.486	5.0	1.417	5.0	1.379
Model test position 1	5.609	1.963	5.248	1.801	5.574	1.550	5.680	1.293
Model test position 2	5.574	1.871	5.439	1.718	5.680	1.338	5.828	1.186
Model test position 3	5.609	1.963	5.644	1.683	5.680	1.390	5.827	1.290
Surge								
Wadam	6.0	0.850	6.0	0.745	6.0	0.440	2.0	0.001
Model test position 1	5.574	0.749	5.248	0.672	5.539	0.577	5.680	0.478
Model test position 2	5.574	0.698	5.439	0.635	5.644	0.497	5.790	0.439
Model test position 3	5.574	0.749	5.644	0.626	5.680	0.518	5.827	0.478

The comparisons presented in the above table shows that the tendency of the peak amplitudes is the same for the model test and Wadam: it decreases with increasing incoming wave angle. The value of the amplitudes are higher in the model test for low angles, while the numerical model has the highest amplitudes for high angles. The peak period in heave and surge are approximately the same for the model test, around 5.5 seconds, whereas they are 5 and 6 seconds respectively in the Wadam calculations. In the Wadam analysis, the buoy is not connected to the platform, being freer to move in surge than the buoy in the model test. The peak period in the model test are equal because a large heave motion leads to a large surge motion.

7.3.2 Forces

To investigate if a tuned model is better than an untuned model, results from two numerical simulation models are presented in the following. The tuned model has implemented fixed

elongation couplings with force and damping values set to be as equal to the air cylinders of the test model as possible. These have only been tuned for an incoming wave angle of 0°, which have led to responses with some deviation from the model test for higher angles. In the untuned model there is no additional damping of the buoys or applied forces.

When comparing the vertical forces acting on the rotation arms large differences are observed between the model test and the numerical models. The largest differences are found for vertical forces, where the numerical models computes values between 100 and 500 % larger than the measured values for regular waves and up to almost 200 % for irregular waves. Table 15 presents the maximum vertical forces at buoy position one for 0°, 45° and 90° incoming wave angle for the model test and the tuned and untuned simulation models.

Table 15: Comparison of max vertical forces for transducer 8600 and corresponding elements of the tuned and untuned numerical model

buoy 1, max values 8600 = max vertical forces [kN]							
wave 1	**model test**	**tuned numerical**	**untuned numerical**	**wave 12**	**model test**	**tuned numerical**	**untuned numerical**
0	134	321	301	**0**	191	666	612
45	140	309	278	**45**	190	671	610
90	108	286	252	**90**	163	663	610
wave 5				**wave 15**			
0	80	243	220	**0**	418	1358	1031
45	72	242	223	**45**	366	1375	1079
90	71	243	224	**90**	199	1391	1085
wave 8							
0	273	958	646				
45	253	938	685				
90	131	907	681				

For regular waves the untuned numerical model gives slightly better results than the tuned model. The tendency seen for the measured results for waves 1, 5 and 8, with almost no change in maximum force as the incoming wave angle increases, also applies for the numerical models. For waves 12 and 15, the measured results decrease as the angle increases, while the forces are almost constant in the numerical simulation models. When looking at the significant values of the vertical force for sea state D (figure 22), the values obtained from the untuned numerical model do not deviate much from the measured results. For 0° incoming wave angle the numerical calculations are 15 – 30 % larger, increasing to around 50 % for 90°. The tuned numerical model computes significant values in the range 100 – 250 % larger than the measured values.

The simulated horizontal forces obtained from the tuned model are in general of the same magnitude as the measured forces for 0° incoming wave angle. For high angles the measured values increase for all waves investigated, while the maximum values obtained from the simulation models either decrease or remain around the same value. Overall, the tuned numerical model gives better results than the untuned for regular waves. Table 16 presents maximum horizontal forces for 0°, 45° and 90° for waves 1, 5, 8, 12 and 15.

Table 16: Comparison of max horizontal forces for transducer 8603 and corresponding elements of the tuned and untuned numerical model

Buoy 1, max values 8603 = max horizontal forces [kN]							
wave 1	model test	tuned numerical	untuned numerical	wave 12	model test	tuned numerical	untuned numerical
0	103	94	93	**0**	188	191	220
45	167	60	65	**45**	179	188	210
90	409	9	29	**90**	394	187	211
wave 5				**wave 15**			
0	34	56	62	**0**	416	352	584
45	64	55	60	**45**	386	317	656
90	94	55	57	**90**	885	361	549
wave 8							
0	314	361	306				
45	346	241	229				
90	813	168	141				

The irregular wave analyses with the untuned numerical model computes significant values of the horizontal force close to the measured values. A tendency of a decrease in significant value with increasing incoming wave angle occurs for the tuned and untuned numerical model and the model test. However, the values of the different buoy positions differs more for the model test. The tuned numerical model computes significant values between 70 and 1500 % larger than the model test for buy position two and three. The largest deviations occur at 0^o incoming wave angle. For buy position one, significant values around 400 kN are computed by the tuned simulation model. This is concordant with the measured values, although the numerical values do not increase for high angles as the measured do.

In the numerical models, both the tuned and the untuned, small or no differences are observed between the forces on the fore and aft rotation arm of each buoy. The measurements done in the model test however show that there is a shadowing effect, making the forces acting on the aft rotation arm, seen from the wave maker, smaller.

The untuned model computes lower significant values of the force than the tuned model because the response of the buoys is much smaller. Even though the forces are of correct magnitude, the simulated response does not consist with the measured response.

The large forces obtained in the numerical analyses can to some extent be explained by the modelling of the rotation point. As this is modelled as a flex joint in SIMA, the rotation arm is made flexible and the bending of this causes large forces. The forces can be reduced by increasing the diameter of the cross section of the rotation arm. This would lead to a smaller response that would not coincide with the measured response without increasing the forces in the fixed elongation couplings representing the air cylinders. Increasing these forces will lead to increased forces acting on the rotation arm.

8. Discussion

8.1 Optimal load resistance

The optimal load resistance of the air cylinders that was found during the model test turned out to be wrong. The pressure regulating valves should not have been completely closed. After more thorough investigation it is clear that the air cylinders have been acting more like springs than dampers. The axial force of the air cylinder was in phase with the position, and not the velocity, of the cylinder stroke. The produced power is found by integrating the force times the velocity, and when these are not in phase, little or no power is produced. The incorrect damping has also caused overestimation of forces and a slight underestimation of responses.

8.2 Air cylinder characteristics

The damping and spring stiffness of the air cylinder depend on whether the piston is going in or out of the cylinder. This is because of difference in cylinder volume: the volume is smaller when the piston goes out because of the piston rod occupying space. For both buoy positions investigated the spring stiffness is larger when the piston is on its way out of the cylinder, while the damping is smaller.

Finding an accurate model of the damping in the air cylinders will be very time consuming. It is reasonable to believe that it will be non-linear. In addition to the damping from the pressure loss over the valve there will be a frictional loss between the piston and the cylinder. These will both be complex and difficult to find. There is also an uncertainty related to the friction/resistance in the hinges at the rotation point. To be certain to find a correct and accurate model additional measurements with the cylinder alone and the cylinder with the buoy are necessary.

Tuning the numerical model in SIMA has been difficult because of the variation in damping and spring stiffness. As they vary for both wave and incoming angle, no general values were possible to obtain. The numerical model was only tuned with respect to 0^{o} incoming wave angle because of time limitations. Better results would have been obtained if the fixed elongation couplings were adjusted individually for each angle.

8.3 Response amplitude operator

For regular waves, the RAOs were calculated for periods between six and 15 seconds. The period selection was based on the scatter diagrams of the two possible installation sites (ref. section 5.1). These sites have their highest density for wave periods around 10 – 14 seconds, and almost no waves shorter than six seconds. The amplitude increased for decreasing wave period, but for some incoming wave angles the peak was not within the measured periods. It is reasonable to believe that the peak period of the RAO is around five seconds, corresponding to the peak period for irregular waves. In future studies shorter wave periods should be tested for to assure a correct value of the peak period at an early stage in the study.

The RAOs computed in Wadam cohere with the RAOs calculated from the measurements done during the experimental campaign. This implies that the hydrodynamics of the buoys is correctly modelled. Unfortunately, due to time limitations, RAOs from the SIMA analyses have not been computed. As the response of the buoys is similar for irregular waves for the tuned SIMA model and the measured results, it is reasonable to assume that their RAOs will be similar. When the buoy is connected to the rotation arm, it cannot translate in surge as freely as in Wadam. This will lead to a peak period in surge close to that in heave, as seen in the results from the model tests.

8.4 Produced power

Produced power has only been estimated for regular waves at 0° incoming wave angle. As the main incoming angle will be around 35° and the waves will be irregular, the values obtained does not give an accurate description of the real world. A yearly electricity production of 10 – 400 GWh is much higher than what can be expected. The installed capacity per buoy will be between 300 and 500 kW, accumulating to a total of 3000 – 5000 kW for the entire platform. Compared to other wave power production devices [39], this will give a yearly electricity production in the range of 1 – 10 GWh. However, the estimations prove that the WEC design is feasible and that power will be produced with the design as it is without further modifications. This result shows great promise for wave power in the future.

The highest production estimates are found for a wave period of seven seconds, this is close to the peak period of the RAOs. Production estimates for wave periods of five and six seconds should be done, but no measurements exist for these periods.

8.5 Forces

The vertical forces acting on the buoy's rotation arms and the horizontal forces acting on the platform framework depend on the damping of the system. As it was discovered that the air cylinder configuration used during the model test was wrong, so are the forces. It is reasonable to assume that the measured forces are overestimations of the actual forces that will occur with correct damping. This assumption is based on investigation of eight regular waves with optimal load resistance versus the applied load resistance.

The results from the analyses done in SIMA do not cohere with the experimental results. The computed forces are in general larger than the measured, especially for energy dense waves. However, a few exceptions exist: horizontal forces at all buoy positions for regular waves and horizontal forces for irregular waves at position one. For these runs, the simulated forces are of the same magnitude as the measured.

The measured forces are believed to be overestimations of the actual forces that will occur with a correctly adjusted test model. With this in mind, the SIMA models are even more incorrect and thus give larger deviations when compared to these forces. On the other hand, if the model test had been carried out with optimal pressure valve configurations, the tuning of the fixed elongation couplings would also have been different. If these results would have better or worse than those obtained has not been investigated.

9. Conclusions and recommendations

The W2Power design is feasible. The platform will produce power, but how much is still uncertain. The estimations done propose a total electricity production of all ten wave converters to be in the range of 10 – 400 GWh per year. This is a rough estimate, and unexpectedly high. A more reasonable estimate, based on other wave converter designs, is 1 – 10 GWh. The highest power output is obtained for waves with a period of seven seconds. Shorter periods may be more advantageous, but this has not been tested. Based on the scatter diagram of the two possible installation sites it is recommended to either tune the wave converters so the maximum power output occurs at a higher wave period or change the installation site to a location with shorter waves.

A shadowing effect between the buoys was observed during the model tests, especially for incoming wave angles 45 and 60°. The measured responses and forces were in general higher for the buoy interacting first with the incoming waves. How large this effect is has been difficult to quantify, as the response of the buoys were affected by variation in the resistance in the rotation points. Especially was this the case for buoy position two, where periodic deviations from middle position were observed for several of the conditions tested.

During the post-processing of the experimental results it was discovered that the load resistance in the air cylinders used throughout the entire experimental campaign was wrong. The air cylinders acted more as springs than dampers, this leading to overestimated forces from the waves acting on the model and underestimated responses.

The numerical simulation models have correct hydrodynamic properties. The RAOs computed in Wadam concord with the calculations from the model test. The responses of the buoys and the horizontal forces acting on the platform framework are in general satisfactory for the tuned numerical model, while the vertical forces on the rotation arm are very large compared to measured forces. The simulated forces are more in accordance with the measured for the untuned numerical model. However, for this numerical model the responses are lower than the measured, and the model does not give an accurate picture of the model test set-up. It is recommended that the rotation point of the buoy is modelled differently. For the performed analyses, the rotation arms were made flexible to produce the correct responses instead of implementing an actual rotation point with stiff lines connected. No simulations have been performed for the numerical model of the entire platform.

10. Future perspectives

The further work should consist of improving the numerical models and performing a new experimental campaign.

The numerical simulation model of the test set-up should be improved to give correct forces and response simultaneously. This can be achieved by changing the modelling of the rotation point of the buoys. In addition, the effect of the platform framework being freely floating versus held fixed should be investigated. The same improvements should be done for the model of the entire platform. Here the wind turbines, or at least something representing the weights of them, must be accounted for. This is however only important for the floating platform. Fatigue analyses should also be carried out.

In the new experimental campaign, more emphasis should be given to correct damping in the air cylinders to assure correct measurements. In addition, it is important that the resistance in the rotation points are equal for all three buoy positions to avoid errors and uncertainties caused by this. One option could be to not account for the shadowing effect and only do measurements with one buoy to do improved estimates of the produced power. The test should also cover extreme conditions if this is possible without breaking the test model and transducers.

Bibliography

[1] "BP, Statistical Review of World Energy 2013," [Online]. Available: http://www.bp.com/en/global/corporate/about-bp/statistical-review-of-world-energy-2013.html. [Accessed 23rd September 2013].

[2] "World Energy Outlook 2012," International Energy Agency, 2012.

[3] G. Beslin and J. Ruer, "Marine Energy and Industrial Actors," in *Marine Renewable Energy Handbook*, B. Multon, Ed., Wiley, 2012, pp. 67-99.

[4] K. Tvedt, "Energi og klima: Norsk klimastiftelses nettmagasin," 2012. [Online]. Available: http://energiogklima.no/wp-content/uploads/2012/04/Fornybar-Energi-et-bakgrunnsdokument-for-7fjellskonferansen.pdf. [Accessed 23rd January 2013].

[5] S. Lewis, J. Estefen, J. Huckerby, W. Musial, T. Pontes and J. Torres-Martinez, "Ocean Energy," in *IPCC Special Report on Renewable Energy Sources and Climate Change Mitigation*, O. Edenhofer, R. Pichs-Madruga, Y. Sokona, K. Seyboth, P. Matschoss, S. Kadner, T. Zwickel, P. Eickemeier, G. Hansen, S. Schlömer and C. von Stechow, Eds., Cambridge and New York, Cambridge University Press, 2011, pp. 497-530.

[6] "Europaportalen, Fornybardirektiv 2," [Online]. Available: http://www.regjeringen.no/nb/sub/europaportalen/eos/eos-notatbasen/notatene/2008/apr/fornybardirektiv-2.html?id=522812. [Accessed 30th September 2013].

[7] EU, "EU - Press releases database," 22nd January 2014. [Online]. Available: http://europa.eu/rapid/press-release_IP-14-54_en.htm. [Accessed 23rd January 2014].

[8] "European Commision," [Online]. Available: http://ec.europa.eu/clima/policies/brief/eu/index_en.htm. [Accessed 30th September 2013].

[9] P. E. Morhorst, J. Lemming and N.-E. Clausen, "Development of Offshore Wind Power - Status and Perspectives," in *Offshore Wind Power*, J. Twidell and G. Gaudiosi, Eds., Multi-Science Publishing, 2008, pp. 1-13.

[10] G. Corbetta, "The European offshore wind industry - key trends and statistics 2013," European Wind Energy Association, 2014.

[11] "Statoil," [Online]. Available: http://www.statoil.com/no/technologyinnovation/newenergy/renewablepowerproduction/offshore/hywind/pages/hywindputtingwindpowertothetest.aspx. [Accessed 30th September 2013].

[12] "Pelamis Wave Power," [Online]. Available: http://www.pelamiswave.com/pelamis-technology. [Accessed 23rd September 2013].

[13] “Aquamarine Power,” 13th May 2013. [Online]. Available: http://www.aquamarinepower.com/news/aquamarine-power-secures-full-consent-for-40mw-lewis-wave-energy-farm/. [Accessed 10th December 2013].

[14] G. Mørk, S. Barstow, A. Kabuth and M. T. Pontes, “Assessing the global wave energy potential,” June 2010.

[15] K. Gunn and C. Stock-Williams, “Quantifying teh global wave power resource,” *Elsevier,* 23rd February 2012.

[16] S. Barstow, G. Mørk, D. Mollison and J. Cruz, “The Wave Energy Resource,” in *Ocean Wave Energy*, J. Cruz, Ed., Springer, 2008, pp. 93-130.

[17] J. Aubry, H. B. Ahmed, B. Multon, A. Barbarit and A. Clément, “Wave Energy Converters,” in *Marine Renewable Energy Handbook*, Wiley, 2012.

[18] J. D. Isaacs and R. J. Seymour, “The Ocean as a power resource,” *International Journal of Environmental Studies,* pp. 201-205, 1973.

[19] S. Salter, “Looking Back,” in *Ocean Wave Energy*, Springer, 2008.

[20] A. F. d. O. Falcäo, “Wave energy utilization: A review of the technologies,” *Elsevier,* 22nd October 2009.

[21] “Hexicon,” [Online]. Available: http://hexicon.eu/solutions.html. [Accessed 23rd September 2013].

[22] “Windsea,” [Online]. Available: http://windsea.no/the-concept/. [Accessed 23rd September 2013].

[23] I. Martinez and C. López Pavón, “Recommended concepts for further documentation and analysis,” Marina Platform, 2011.

[24] "European Commision, CORDIS, MARINA Platform," 12th December 2013. [Online]. Available: http://cordis.europa.eu/projects/rcn/93425_en.html. [Accessed 20th May 2014].

[25] “Marina Platform,” [Online]. Available: http://marina-platform.info/index.aspx. [Accessed 30th September 2013].

[26] *Scaling data used for Mn Call 1 Tank test,* 2012.

[27] “Pelagic Power: W2Power,” [Online]. Available: http://www.pelagicpower.no/index.html. [Accessed 17th September 2013].

[28] “DNV: GeniE,” [Online]. Available: http://www.dnv.com/binaries/genie_feb_2012_highres_tcm4-75120.pdf. [Accessed 21st October 2013].

[29] DNV, “Sesam User Manual GeniE vol. 1,” DNV, 2011.

[30] DNV, “Sesam User Manual Wadam,” DNV, 2013.

[31] “DNV: HydroD,” [Online]. Available: http://www.dnv.com/binaries/hydrod_feb_2012_highres_tcm4-75882.pdf. [Accessed 21st October 2013].

[32] MARINTEK, “Sintef, SIMO fact sheet,” [Online]. Available: http://www.sintef.no/upload/MARINTEK/PDF-filer/FactSheets/Simo.pdf. [Accessed 30th October 2013].

[33] MARINTEK, “Sintef, RIFLEX fact sheet,” [Online]. Available: http://www.sintef.no/upload/MARINTEK/PDF-filer/FactSheets/RIFLEX.pdf. [Accessed 25th November 2013].

[34] L. Li, Z. Gao and T. Moan, “Environmental Data at Five Selected Sites for Concept Comparison,” MARINA Platform, 2012.

[35] J. Hals, “Plan for W2Power UEdin tests, MARINET call 1, Test round 2,” 2013.

[36] P. A. Tipler and G. Mosca, “Chpt. 6: Work and Kinetic Energy,” in *Physics for Scientists and Engineers*, W. H. Freeman and Company, 2008, pp. 173-195.

[37] C. M. Larsen, “System with one degree of freedom. System med en frihetsgrad.,” in *Marine Dynamics lecture notes*, Department of Marine Technology, 2012, pp. 7-30.

[38] S. Steen, Lecture notes: Experimental Methods in Marine Hydrodynamics, NTNU, 2012.

[39] D. Krohn, M. Woods, J. Adams, B. Valpy, F. Jones and P. Gardner, “Wave and Tidal Energy in the UK,” RenewableUK, 2013.

Appendix

Appendix A: Pictures from experimental campaign

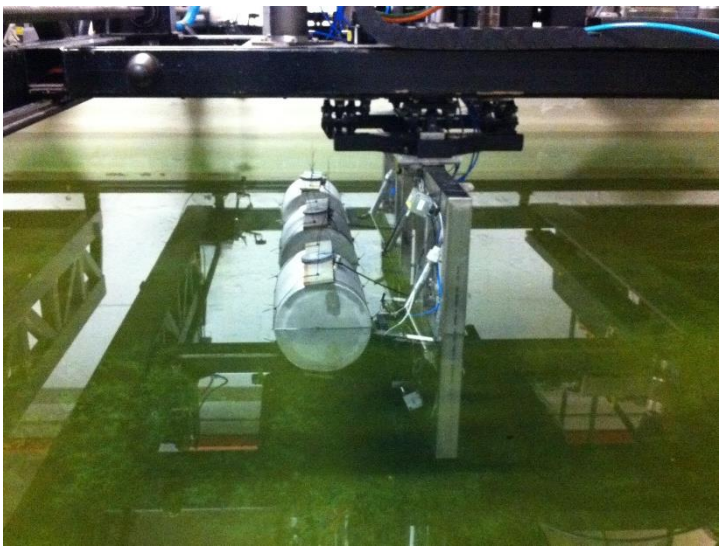

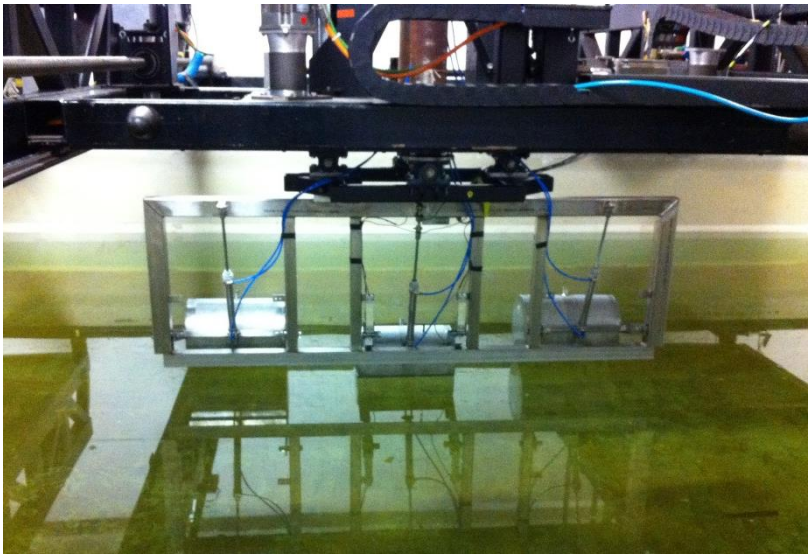

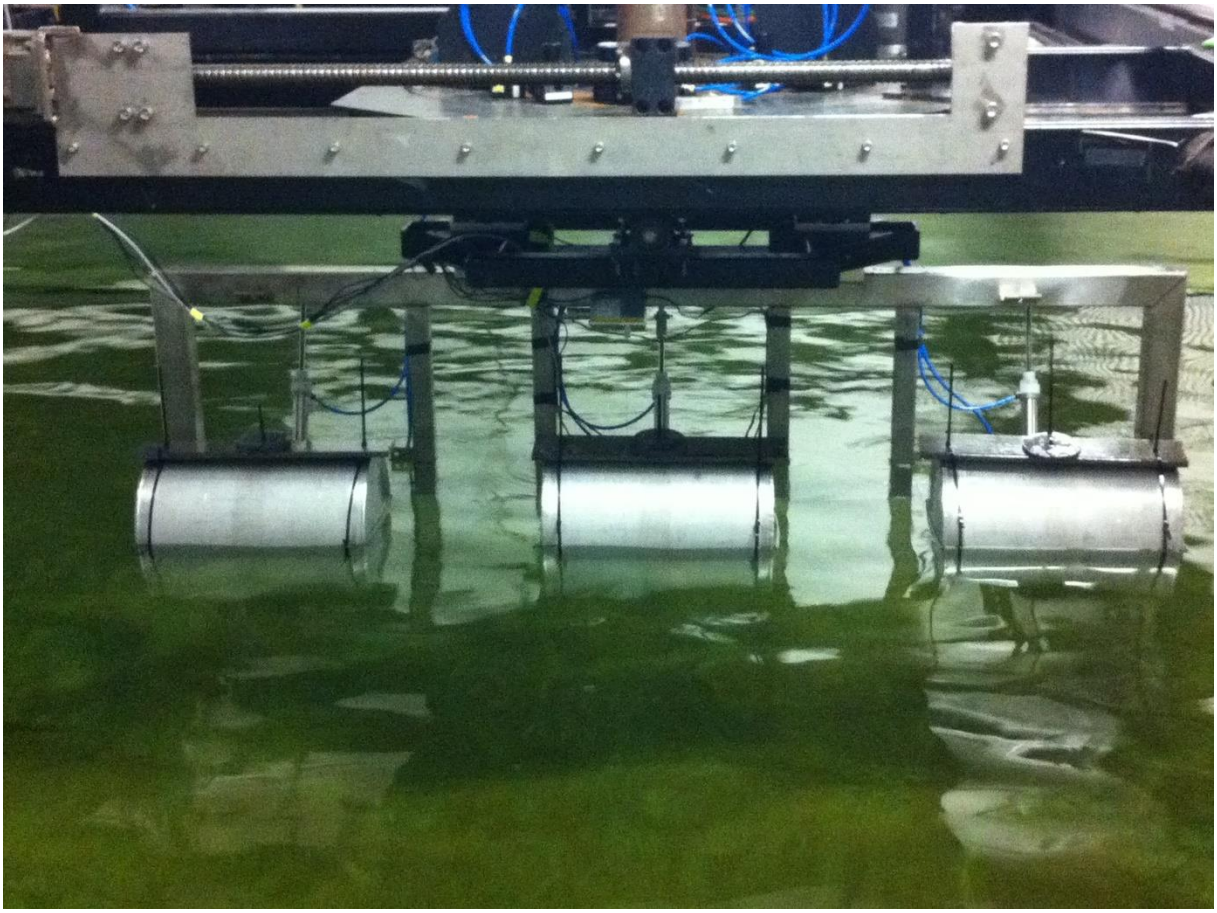

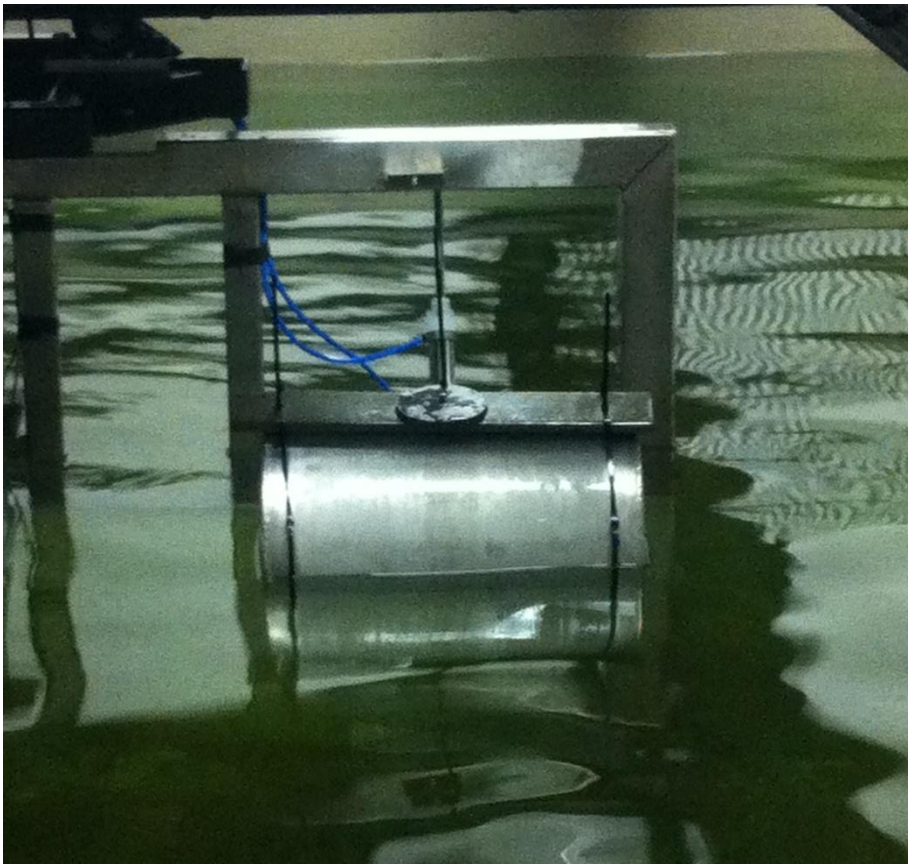

Appendix B: Complete log for experimental campaign

Date	Schedule	Log
Mon 31	weighing of model + Installation of the model	Mostly waiting for things to happen due to sickness and course participation of MARINTEK staff. 13:00: installation of model begins. Nothing is really done.
Tue 1	Calibration of instruments + Ballasting	09:00 – 11:30: calibration of force transducers. All day: Installation of model. A few parts were missing from Inrigo, they will be prepared by MARINTEK for tomorrow. Still no water in tank, ballasting postponed.
Wed 2	Variation of load resistance air cylinder + Decay test	Work on missing/wrong parts from Inrigo continues. Pressure valves ordered online, not possible to buy in town. Everything except valves mounted, hose attached to air cylinders to be connected to valves. Start filling of water 15:30. Have done some measurements of dimensions on the model, not 100 % consistent with drawings.
Thu 3	Regular waves set 1-5	Water filling continues, not finished over night because of slow filling rate by mistake. Ballasting done, around 3.3 kg per buoy. Decay test with and without air cylinder performed, but no logging of position. Must be done again. Buoy 3 does not move as smooth as the others, tried to loosen the screws but with no success. Great help from Ellen, Runa and Hege.
Fri 4	Regular waves set 6-7. Irregular wave set 1-3	Buoy 3 loosened, moves smoothly. Decay tests with and without air cylinder performed again, now with position measurements, with help from Ellen. Post processing of responses, still unable to find present damping. Pressure regulators arrived and installed. Must be tuned tomorrow. Wave probe installed and calibrated.
Sat 5	Irregular wave set 4-7 + change position of buoy	Decay tests with different pressure regulator configurations. Some problems with starting the wave maker. Variation of load resistance air cylinder. Help from Johanne.
Sun 6	Buffer day to finish the week's planned tests.	No time spent in lab, entire day used to analyze Saturday's files and find optimal load resistance,
Mon 7	Regular wave sets 8-12	Regular wave set 1-6. + ekstra struping Installation of GoPro camera Ellen babysitting. Time one wave: Time one set: ~60-70 min

Tue 8	Regular wave set 13-14. Irregular wave set 8-10.	Regular wave set 7 + irregular wave set 1-5 Buoy 1 is has more friction in the rotation point than the others, removed some ballast and shortened the 1N hose (this was longer than the other hoses), didn't help much. Must check if it has been like this the whole time. Sea state B is cut off. Time irregular: ~1h30 Hilde babysitting.
Wed 9	Irregular wave set 11-14 + change position of buoy	Irregular wave set 6-7 + extra runs for sea state A. Position of buoy changed to b2, closest to col B. Not possible to change to b3 due to model defects. Regular wave set 8. 6 hours spent changing position and fixing details to make the responses right. Jørgen came by, helped a lot with the adjustments of the buoys. He was almost surprised that all measurements for b2 is done. Sven Ole babysitting.
Thu 10	Regular wave set 15-19	Irregular wave set 8-12 Regular wave set 9-12 Refill of water in tank, it water level has gone down 1.5 cm during the last week. B2, former b1, had some frictional problems in the morning, but this was solved by loosening one of the screws at the rotation point. Johanne babysitting.
Fri 11	Regular wave set 20-21. Irregular wave set 15-17.	Regular wave set 13-14+21 Irregular wave set 13-14+21 Most interesting for b3 for the largest incoming waves, so this is run first in case there is not enough time to run all the sets. Going home early.
Sat 12	Irregular wave set 18-21.	Regular wave set 19-20 Irregular wave set 18-20 Decay test b3. Diffraction wave measurement. Help from Hege. No problems.
Sun 13	Buffer day to finish the week's planned tests.	
Mon 14	Dismounting + Wave measurements	Regular wave set 15-18 Irregular wave set 16-17 Irregular set 15=set 8, not run. The same applies for regular waves, but this set was run for comparison.
Tue 15	Buffer day	Wave measurements without model in tank. Removed the ballast weights. Dismounting after Easter.

Monday 07.04	Set R1	Zero measurements before each set From wave 3, clear lag/stop when buoy is in top position W 5,6: stops at max and min z position. Looks like the damping is too much. Test wave 5 with no damping: b2_0_5_nodamp. Video 09:38. Not much visible difference. W 7 run with no damping by mistake. W 8: smooth response W 9: staccato response W 10+11: moves easily upwards, works hard to move down W 12: staccato, but smooth. T=2.73 W 13: crazy acceleration, ballast weights displaced. B2_0_13_ballast. Moved wave probe, new zero settings 10:26 W 13: moves smooth, and a lot W 14: t=2.373 too large for wave maker at this height, run for 2.008 instead. Staccato, stops longer in min position W 15: lags going up and down at first, more smoothly after some periods W 16: fast up, slow down, as it supports itself on the rotation arm/air cylinder going down. B2_0_16_nodamp: higher max position, få liksom et kast når den er nesten oppe.
	Set R2 Zero 12:29	W 1,2: moves «normal», a bit staccato W 3,4: short stops/breaks at max z position. fast up, slow down W 6: same, movie phone 12.46 W 8: smooth W 9: fast down, slow up. Longest stop at max z position W 10: longest stop at min z, blir liksom kaste opp derfra W 11,12: slow up and down, stops at min and max W 13: smooth and fast W 15: quite smooth, but “works” to get upward, ser nesten ut som den tar I litt ekstra for å komme over kneika. Movie phone 13.23. W 16: smooth, but stops at min position
	Set R3 Zero 13:47	W 1,2: smooth W 3: falls down, is dragged up W 4: longest stop at min position W 5,6,7: stops almost equally at min and max, moves quite smoothly in between. Mov 6 1408 W 8: first GoPro4 take. Smooth. Wave 9: gopro5. Falls down, dragged up, but smooth Wave 10: gopro6. stops longer at min position W 11: gopro7. stops a bit longer at min, is dragged upwards W 12: gopro8. stops equally at min and max, smooth in between W13: gopro9. Crazy. W14: gopro10. Longer stop at min, a little lag just after mean position on the way down. Kinda gets thrown upwards. W15,16: gopro11,12. Fast down, slow up. Longer stop at min position.
	Set R4	W1: gopro13. Smooth W2: gopro 14. Smooth.

	Zero 15:19	W3: gopro 15. Stop at min and max, smooth in between W4: floats up, pushed down W5,6,7: stops at min and max, smooth in between W8: smooth W9: gopro 16. Dives down, pulled up. W10: gopro 17. Longest stop at min position W11: gopro 18. Stops at min and max equally, drops down, works up W12: gopro19. stops at min and max, smooth in between W13: gopro 20. crazy W14: gopro 21. Smooth, but stops at min pos W15,16: gopro 22,23. Smooth, short stop at min pos, uses some time to accelerate when going up
	Set R5 Zero 17:15	W1,2: smooth W3,4: smooth, but stops at min pos W5: a bit more staccato, stops at min and a little at max W6,7: stops at min and max pos, quite smooth in between W8: smooth W9: smooth, but faster up than down W10: a bit more staccato W11: quite smooth, stops at max and min, a bit slower up W12: smooth, stop at min and max W13: a bit faster down than up, smooth W14: smooth, stops in min pos. almost equal speed up and down W15: slowly up, "falls" down W16: quite smooth, stops at min pos
	Ekstra struping Zero 18:28 0 grader	W8: ser ingen forskjell W10: gopro 24. kanskje bittelitt mindre bevegelse Struper enda mer før w11 W11:gopro 25 W13: gopro 26 W14: gopro 27 W15: gopro 28 Ser ingen forskjell fra uten struping!
	Set R6 Zero 18:52	W1,2: smooth W3,4,5,6,7: lag at max and min pos. Smooth W8: smooth W9,10: fast down, a bit slower up. Takes some time to turn acceleration at min pos W11,12: stop at max and min pos, smooth in between W13: smooth W14,15,16: fast down, slow up
Tuesday 08.04 1.33	Set R7 Zero 08:16	W1,2: gp 29,30. smooth. Buoy 1 moves more staccato than the others. W3,4: gp 31,32. A bit staccato, very short stops at min and max W5,6,7: gp34,33,35. long stops at max and min pos, smooth in between. B1 moves as the others. W8,9: gp 36,37. Smooth. B1 moves more forced (more friction?) W10,11: gp 38,39. Drawn up, falls down. B1 er utafor, ligger ikke på vannlinja lenger. W12: gp 40. a bit smoother.

		W13: gp 41. Smooth. B1 a bit staccato. W14,15,16: gp 42,43,44. Falls down, dragged up, needs some time to change acceleration direction at min pos 0.4 kg ballast removed from b1.
	I1 zero 10:19	A: gp 45. Very small waves, no action. It is clear that b1 and b3 has more friction in their rotation axis. E: gp 46. Ikke kjør for krappere bølger enn dette. B2 and b3 moves equally and alot, b1 is sleeping. The waves occasionally splash over the buoys. For the highest waves the air cylinder stops due to lack of space upward, not because of buoy movement. Ballast on b2 displaced. B: gp 47. As A. Will not run both A and B for the other angles. C: gp 48. Ca 20 sek før bølgene når frem. Some waves splash over. The buoy stops at mean position-ish when the waves are very small. D: gp 49. As C, but less splashing. F: gp 50. Some splashing over the buoys. Calmer than E. Hose to 1N cut, about the same length as the others now.
	I2 Zero 12:22	C,D: moves smooth. B1 still not moving like the others. A: Ganske dødt. B kuttes ut. E: masse action, lots of splash ballast b2 detter nesten av, må ut å fikse. F: ganske smooth, litt splash
	I3 Zero 13:51	Same as I2. E: kjempeutslag mot slutten, all ballast datt av, mulig giver ødelagt. Måtte stoppe etter 9:40.
	I4 Zero 16:06	A: gp 51. Compared with 30_A, everything looks ok. C: gp 52. D: gp 53 F: gp 54 E: gp 55. Lots of splashing, ballast did not move, no crazy forces. Ser ikke ut som at bøyene skygger noe særlig for hverandre så langt
	I5 Zero 17:46	Samma. Fan tut at A har blitt kjørt med feil γ, 3.3 istedenfor 1. kjører 60_A =60_A1 på nytt og sjekker hvor stor forskjellen er. Alle A må kjøres på nytt, forskjellen på spekter er stor.
Wednesday 09.04	1.33 Zero 07:55	New runs for A sea states, angles 0 – 45. Files renamed: 0_A = γ=1, 0_A33=γ=3.3
	I6 Zero 08:54	A: ok C: smooth, b1 is still staccato. In general things are more calm at this angle
	I7 Zero 10:09	A: gp 56. Small and smooth. C: gp 57 D: gp 58 F: gp 59. The biggest waves splashes all the way to b2. E: gp 60.
		Change of buoy position to b1. Lots of trouble with things not being right, small inaccuracies made things not fit at first try. Fixed at 18:00.
	I8 Zero 16:31	Must do again.
	R8 Zero 17:53	All buoys moves more or less equally. Same tendencies as before regarding lagging/stops and unsmooth movements.

Thursday 10.04	1.325 I 8 Zero 08:25	A: gp 61. At 0 deg, all buoys move equally, the response of buoy 1 is therefore directly comparable with b2. Check if there is a difference due to frictional damping at the rotation point. C: gp 62. B2 is a bit looser than the others. Refill of water, 1.345, and new zero 09:15. D: gp 63. B1 and b3 moves equally and smooth, b2 is more staccato. Strange. F: gp 64. 04:00-05:45 on the movie: valves on buoy 2 opened, moved even higher, but still not a fully smooth response. Could be lack of ballast. Doesn't really matter before testing for position b3. Now it's kinda like the problem in R7 when ballast was removed. After almost 10 mins: b2 hardly moves. Crazy friction at rotation point, does not oscillate at decay test E: gp 65. Clearly a lot less friction at rotation point with this configuration, sea state stopped after 2:55 after several crashes between air cylinder and force transducer.
		Decay test of b1 to compare with b2 regarding friction at rotation point.
	R9 Zero 10:02	W4: b1 and b3 moves equally, b2 still stuck. Same for the rest of the set. B2 fixed, loosened the left screw at the rotation point. Check with wave 10, everything looks ok.
	I9 Zero 11:19	A: everything ok, moves smoothly C: smooth, one "crash" at around 520 sec, -120 N D: F: large responses, crash at 330 sec, -400 N E: not run. Afraid of breaking the air cylinders and force transducer.
	R10 Zero 12:24	Everything ok. No surprises. Some skranglelyder from b3.
	I10 Zero 13:17	C: 560 sek, -180 N F: 300, 470, 560 sek, -400 N
	R11 Zero 14:17	W1: gp 66 W2: gp67 W3: gp 68 W4: gp 69 W5: gp 70 W6: gp 71 W7: gp 72 W8:gp 73 W9:gp 74 W10: gp 75 W11: gp 76 W12: gp 77 W13: gp 78 W14: gp 79 W15: gp 80 W16: gp 81 Everything as usual.
	I 11	A: gp 81 ? C: gp 82. Measurement start a bit late.

	Zero 15:08	D: gp 83. No further action. F: gp 85,86. 470 s, -180 N E: gp 87. 52 sec, then finished after crash of -480 N.
	R12 Zero 16:25	Everything ok and normal.
	I12 Zero 17:11 1.34	Everything ok, E not run even though the responses are a bit calmer at this angle.
Friday 11.04	1.34 R13 Zero 08:18	Alles gut. Checking effect of water depth and wave heights. Looks like it matters.
	I13 Zero 09:41	Water depth changed to 1.34 for all spectra. New names: jons_A_134. This is used on all sea states unless specified otherwise. F: ok responses. E: no problem, max forces +- 60N. uncertain if this is because of the angle or the “new” wave spectrum. Compare wave spectra: i13_E and i8_E.
	R14 Zero 11:03	Gopro files transferred to computer. W1: gp 28 W2: gp 29 W3: no go W4:gp 30 W5: gp 31 W6: gp 32 W7: gp 33 W8: gp 34 W9: gp 35 W10:gp 36 W11: gp 37 W12: gp 38 W13: gp 39 W14: gp 40 W15: gp 41 W16: gp 42
	I 14 Zero 12:41	A: gp 43. C: gp 44 D: gp 45 F: gp 46 E: gp 47. Max forces +- 80 N.
	R21 Zero 14:03	Most important to run for the angles where the shadow effect is likely to be significant.
	I21 Zero 14:48	A: ok C: still no surprises, everything as normal. D: F: E: ok, +- 60 N. In the shadow of the two other buoys, should be smaller responses.

Saturday 12.04 1.337	R20 Zero 11:31	Water depth 1.34 has been used for all regular waves throughout the experimental campaign. Alles gut.
	I20 Zero 12:17	A_134 Everything ok, E is quite calm.
	R19 Zero 13:37	Alles gut.
	I 19 Zero 14:20	Alles gut
	I 18 Zero 15:34	
Monday 14.04 1.335	R18 Zero 08:20	20287 har mest negative utslag, oscillerer ikke rundt 0. vanndybde data fortsatt 1.34
	R17 Zero 09:11	W1: 20287 +6 -8 Zero W2: +-6 Zero W3: +- 6, W4: no zero before. +-6 W5: no zero. +-6 W6: no zero. +- 6 W7: no zero. +- 10 W8: no zero. +16 – 20. With zero: +16 – 19 W9: no zero. +- 15 W10: no zero. +10 – 18. With zero: +10 – 18 W11: no zero +-12 W12: no zero +- 15 W13: no zero +20 – 25 W14: no zero + 11 – 27. With zero: +12 – 27 W15: no zero + 20 – 33 W16: no zero +20 – 32
	I17 Zero 10:14	Ok. Two crashes for E_134 at -200 N.
	R16 Zero 11:30	W3: no zero +5 – 7. With zero +-6 W4: no zero +- 6 W5: no zero +-6 W6: no zero +- 6 W7: no zero +- 10 W8: no zero +17 – 19. With zero +17 – 21 W9: no zero +15 – 17 W10: no zero +11 – 20. With zero +11 – 20 W11: no zero + 12 – 14 W12: no zero +15-20. Takes some time to stabilize. W13: no zero +20 – 27. With zero +22 – 26

		W14: no zero +16 -27 W15: no zero +20 – 32 W16: no zero +22 – 30
	I 15 Zero 12:33	E: bøya kræsjer I snorgiveren på ca 190 sek. 7 crashes in total, -200 - -800 N. Ballast falls off, don't know when, most likely at the last crash.
	R15 Zero 14:02	This is the same as R8. W12,w14 uses long time to stabilize. Ballast not put back into position before w13.
	Extra R15 Zero 14:58	W8 and W14 run ten extra times.
Tuesday 15.04 133.5	Waves	Model moved as far back in the tank as possible, waves measured "without" model in tank. Both regular and irregular. Regular zero 08:55 Irregular zero 10:58 134 for both. Have a close look at the longest waves, they seem to be disturbed quite fast, even before the first waves have reached the end of the tank.

Appendix C: RAO in heave, regular waves

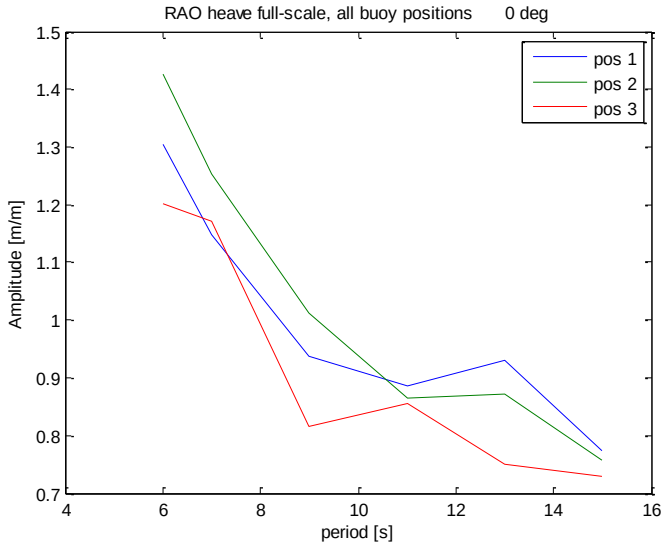

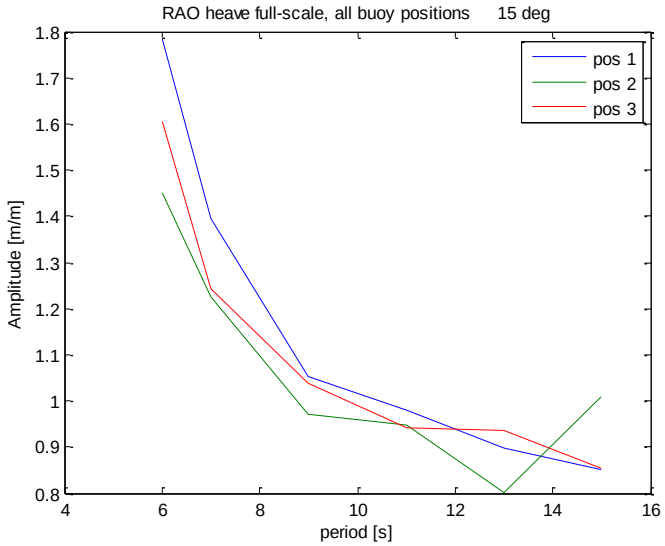

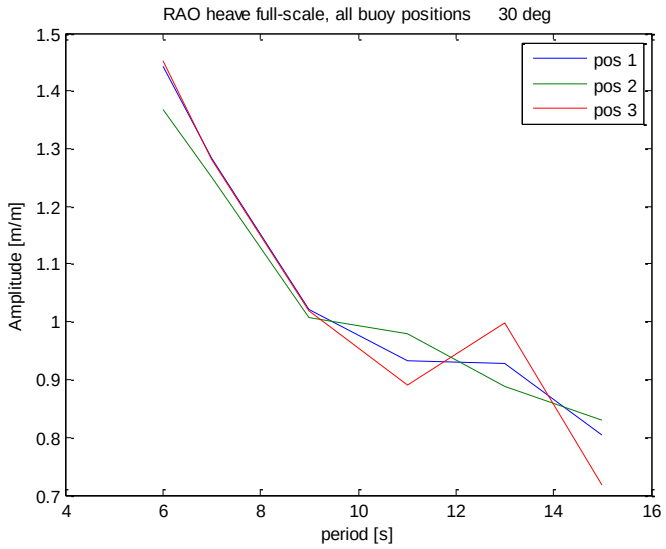

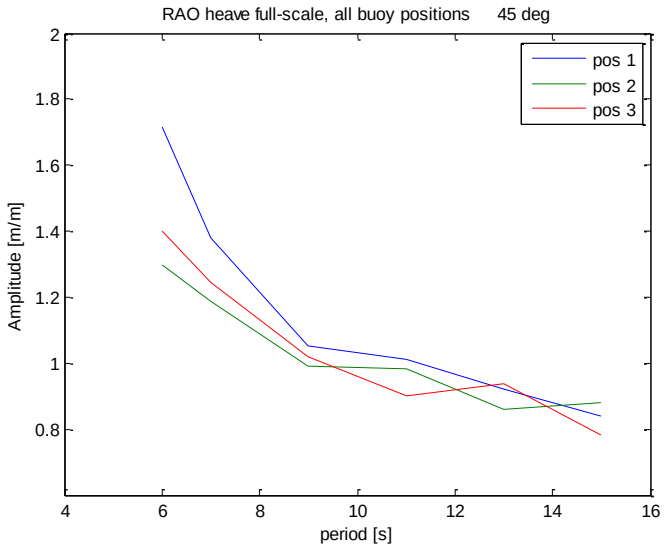

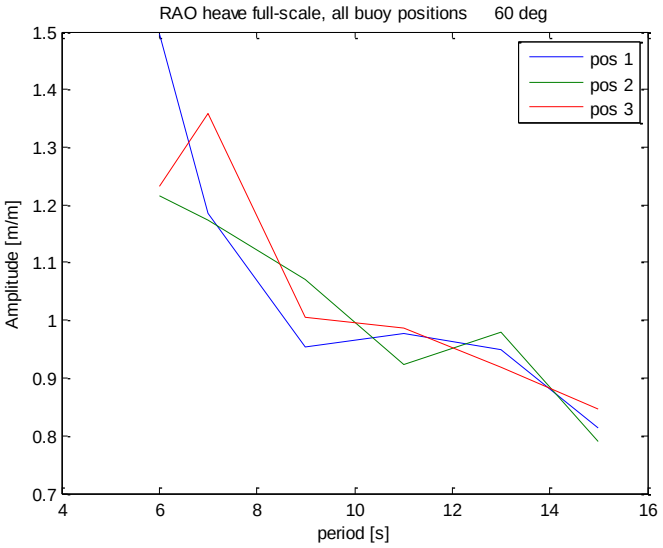
RAO heave full-scale, all buoy positions 60 deg
pos 1
pos 2
pos 3
Amplitude [m/m]
period [s]
1.5
1.4
1.3
1.2
1.1
1
0.9
0.8
0.7
4
6
8
10
12
14
16

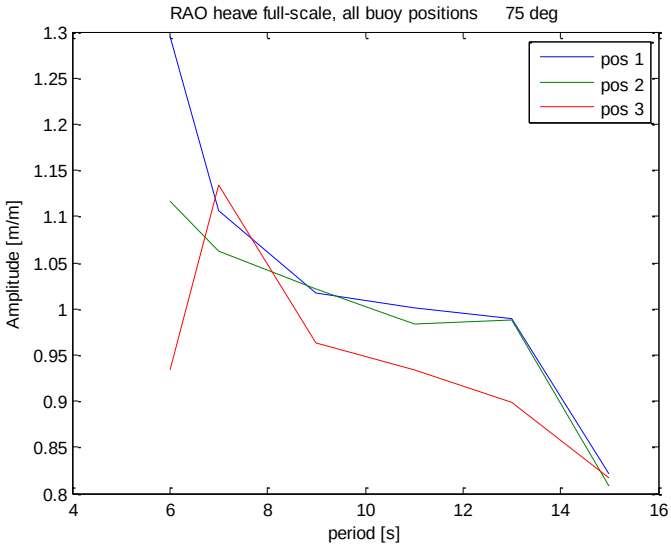
RAO heave full-scale, all buoy positions 75 deg
pos 1
pos 2
pos 3
Amplitude [m/m]
period [s]
1.3
1.25
1.2
1.15
1.1
1.05
1
0.95
0.9
0.85
0.8
4
6
8
10
12
14
16

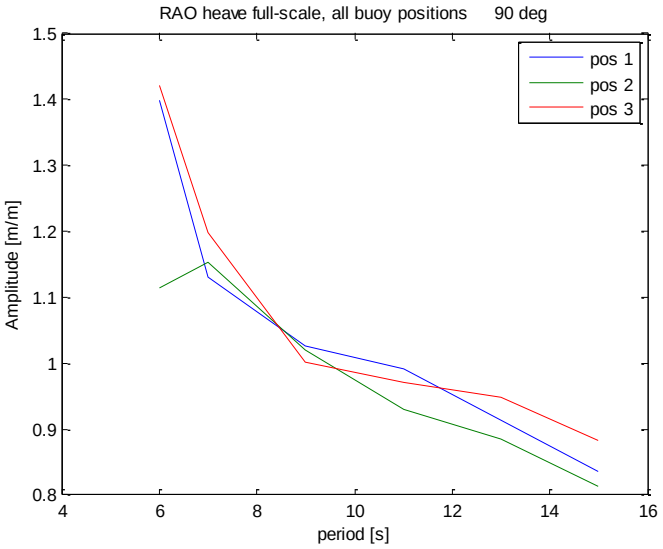
RAO heave full-scale, all buoy positions 90 deg
pos 1
pos 2
pos 3
Amplitude [m/m]
period [s]
1.5
1.4
1.3
1.2
1.1
1
0.9
0.8
4
6
8
10
12
14
16

Appendix D: RAO in surge, regular waves

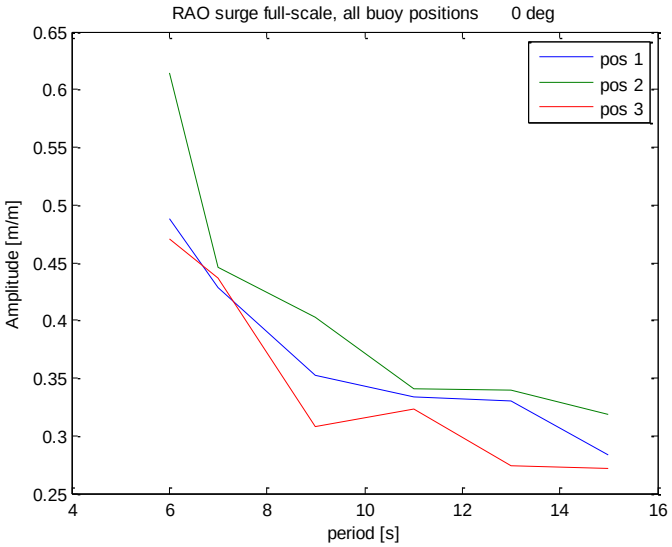

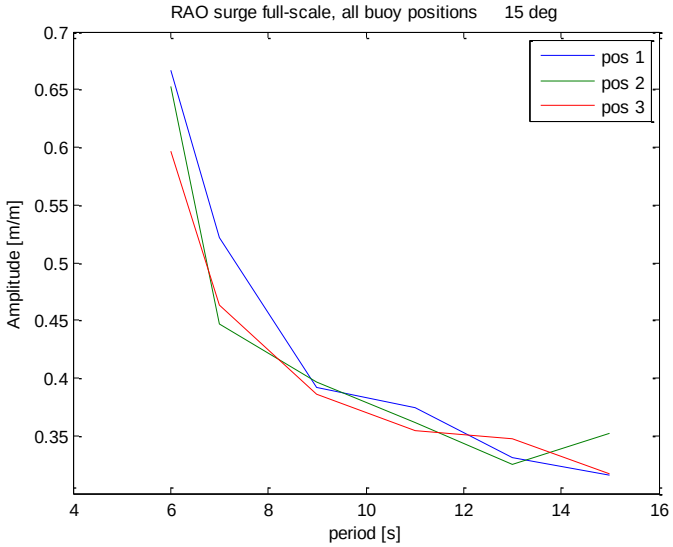

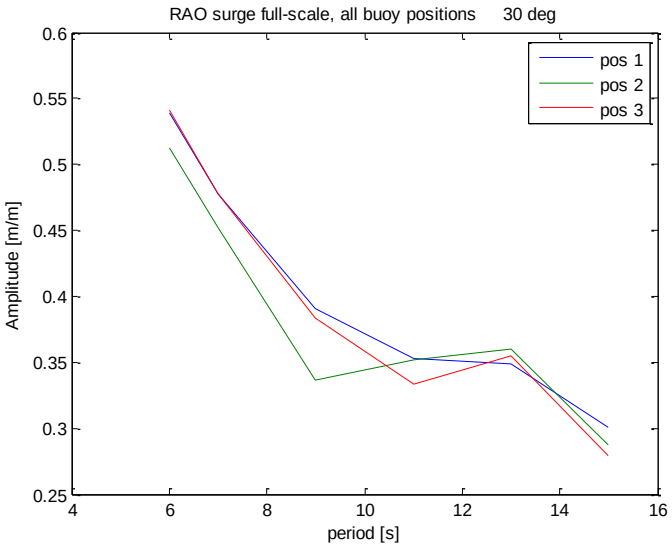

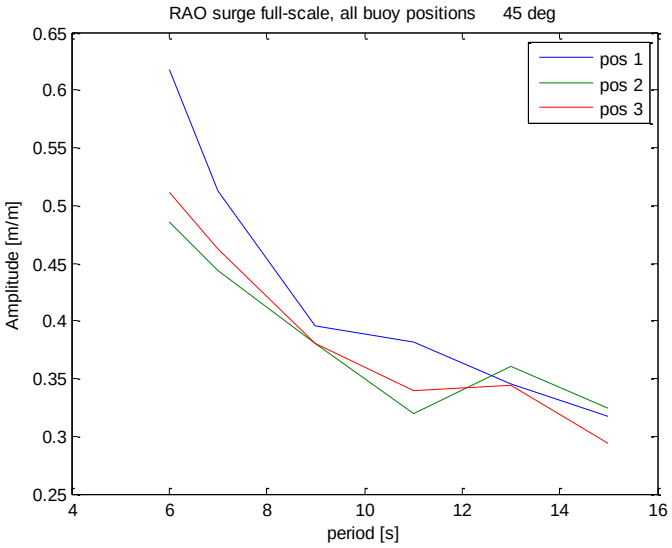

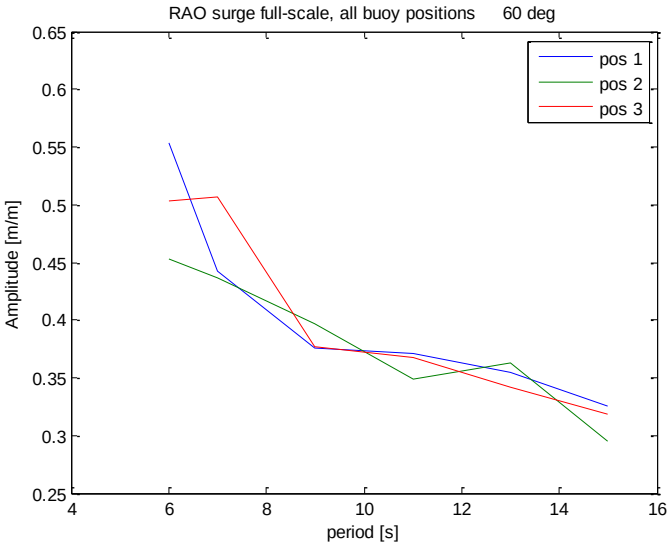
RAO surge full-scale, all buoy positions 60 deg
pos 1
pos 2
pos 3
Amplitude [m/m]
period [s]
0.65
0.6
0.55
0.5
0.45
0.4
0.35
0.3
0.25
4
6
8
10
12
14
16

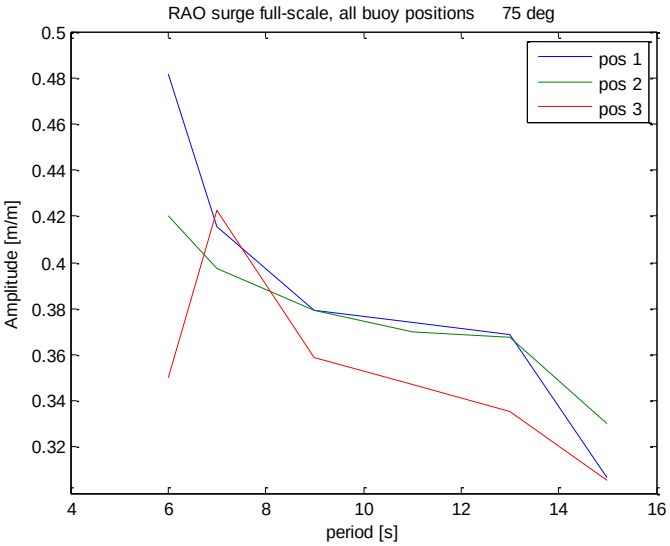
RAO surge full-scale, all buoy positions 75 deg
pos 1
pos 2
pos 3
Amplitude [m/m]
period [s]
0.5
0.48
0.46
0.44
0.42
0.4
0.38
0.36
0.34
0.32
4
6
8
10
12
14
16

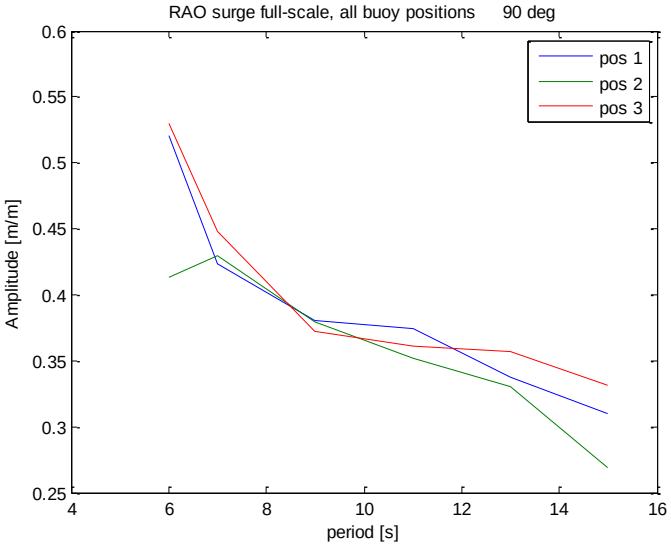
RAO surge full-scale, all buoy positions 90 deg
pos 1
pos 2
pos 3
Amplitude [m/m]
period [s]
0.6
0.55
0.5
0.45
0.4
0.35
0.3
0.25
4
6
8
10
12
14
16

Appendix E: RAO in heave, irregular waves

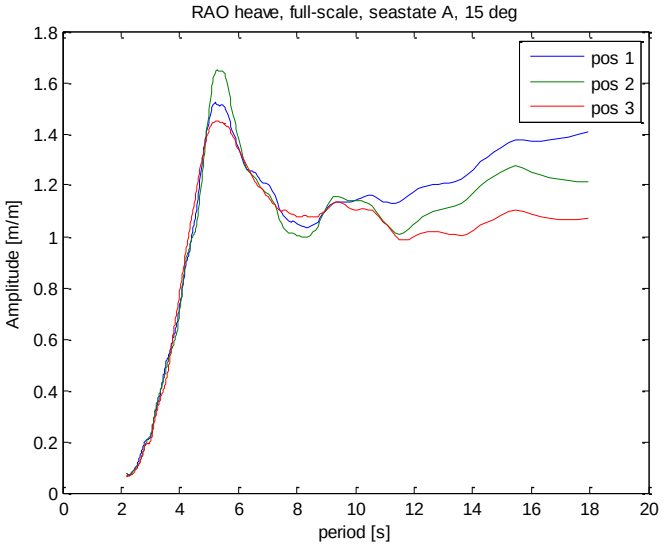

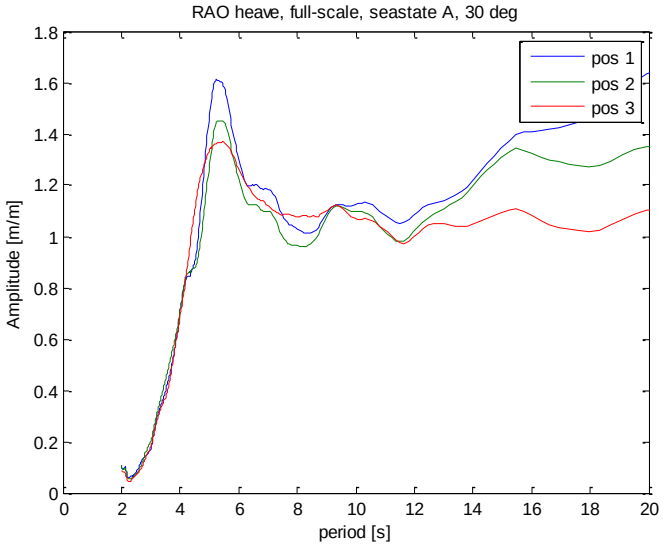

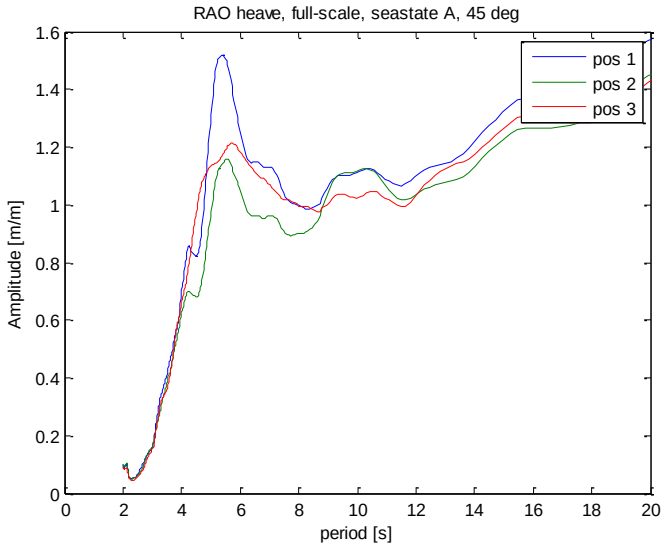

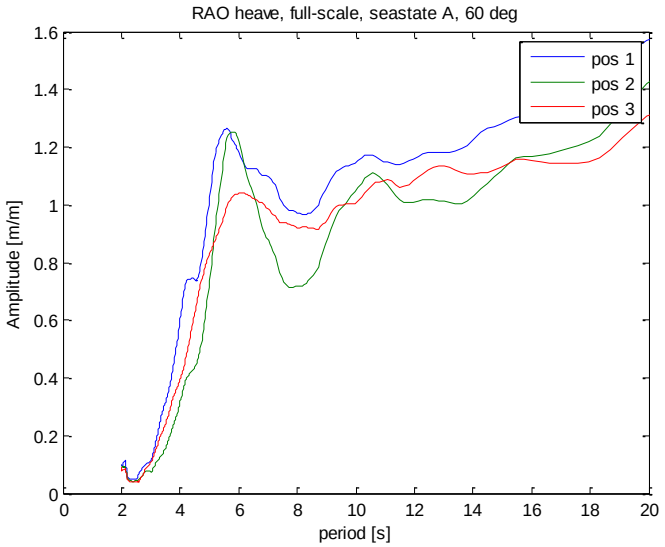

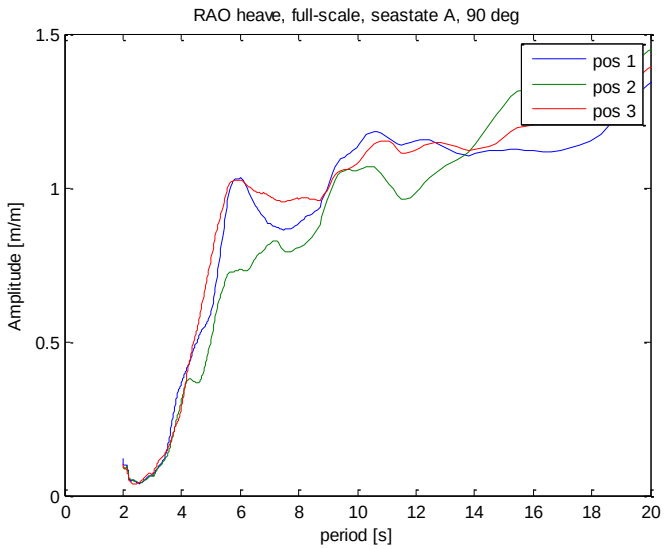

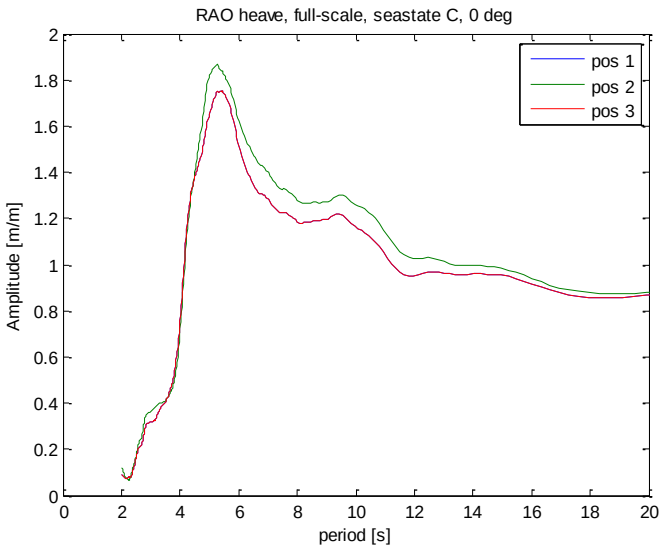

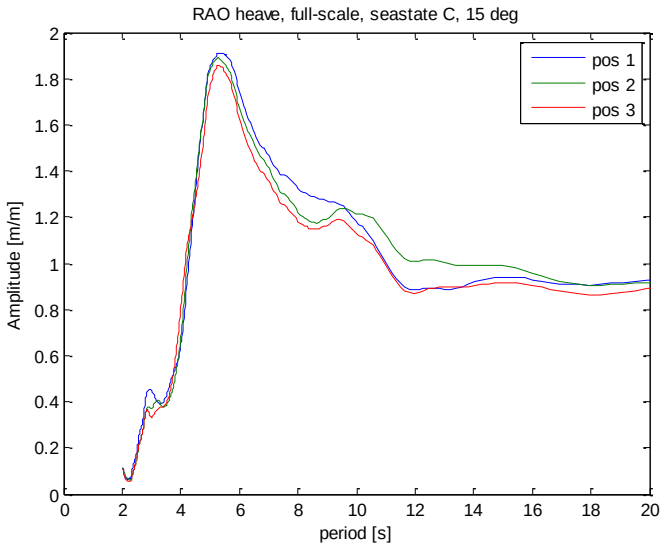
RAO heave, full-scale, seastate C, 15 deg
pos 1
pos 2
pos 3
Amplitude [m/m]
period [s]

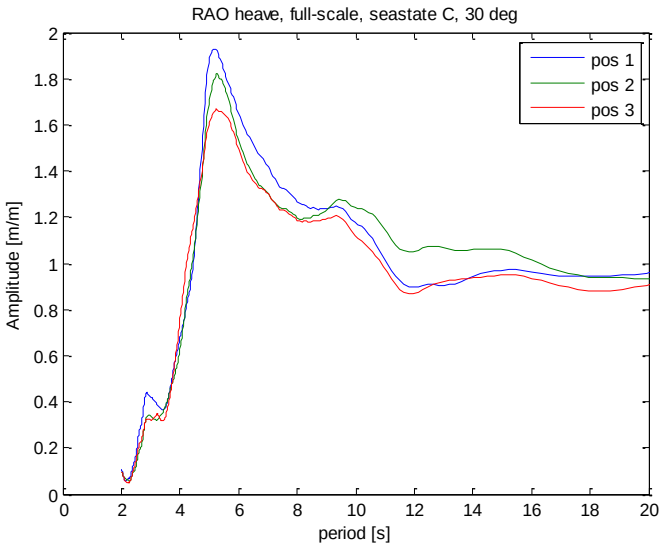
RAO heave, full-scale, seastate C, 30 deg
pos 1
pos 2
pos 3
Amplitude [m/m]
period [s]

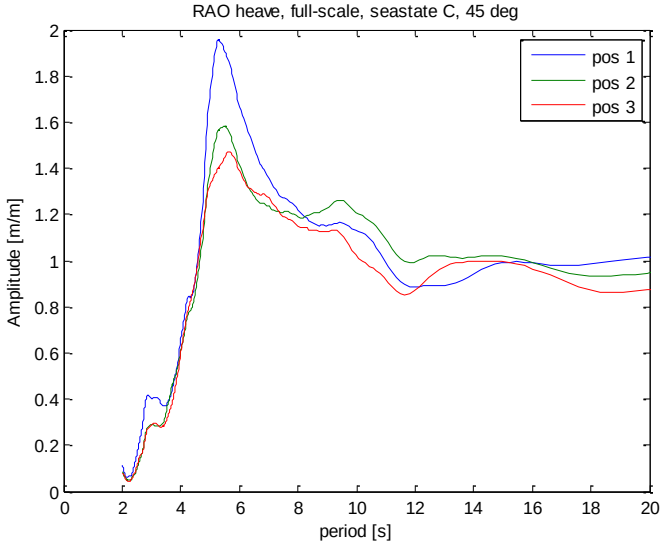
RAO heave, full-scale, seastate C, 45 deg
pos 1
pos 2
pos 3
Amplitude [m/m]
period [s]

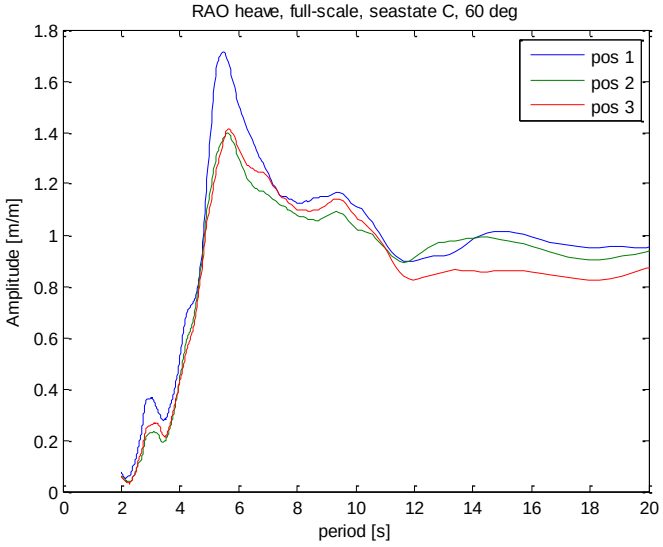
RAO heave, full-scale, seastate C, 60 deg
pos 1
pos 2
pos 3
Amplitude [m/m]
period [s]

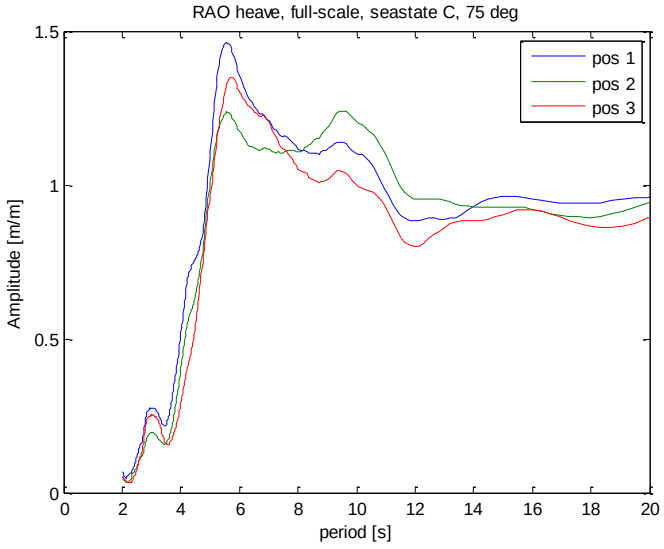
RAO heave, full-scale, seastate C, 75 deg
pos 1
pos 2
pos 3
Amplitude [m/m]
period [s]

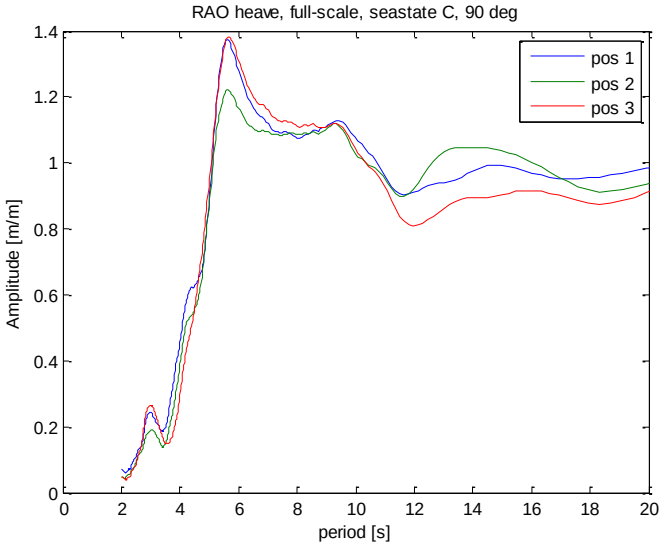
RAO heave, full-scale, seastate C, 90 deg
pos 1
pos 2
pos 3
Amplitude [m/m]
period [s]

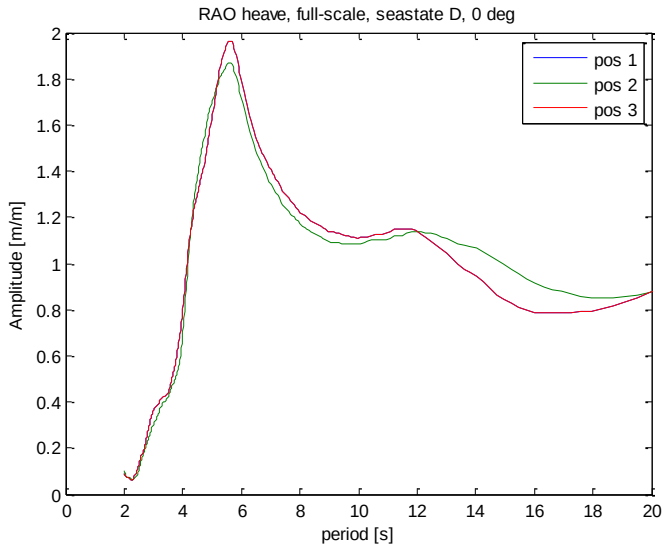
RAO heave, full-scale, seastate D, 0 deg
Amplitude [m/m]
period [s]
pos 1
pos 2
pos 3

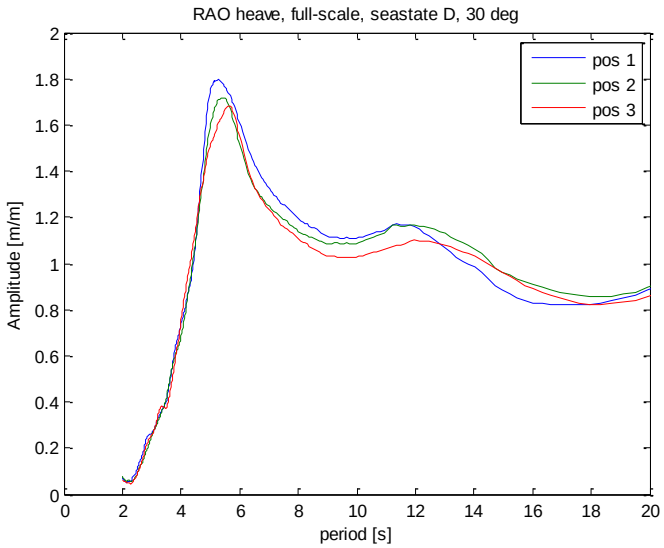
RAO heave, full-scale, seastate D, 30 deg
Amplitude [m/m]
period [s]
pos 1
pos 2
pos 3

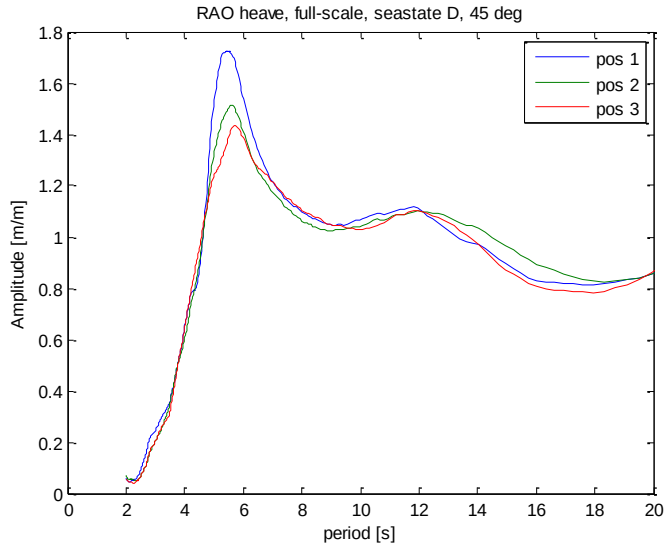
RAO heave, full-scale, seastate D, 45 deg
Amplitude [m/m]
period [s]
pos 1
pos 2
pos 3

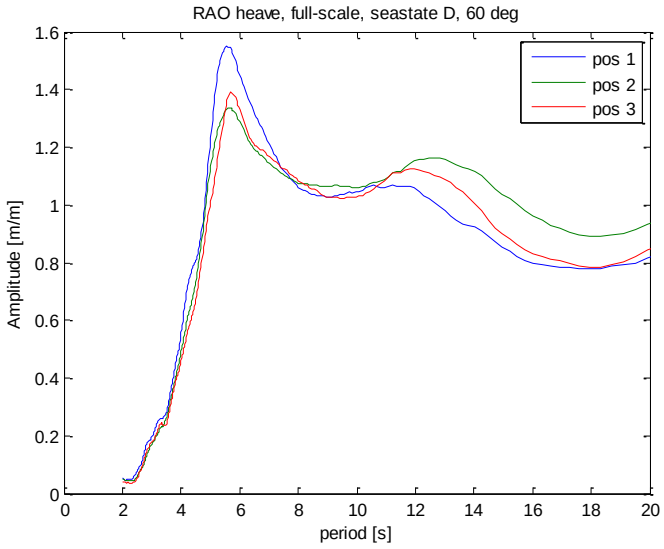
RAO heave, full-scale, seastate D, 60 deg
Amplitude [m/m]
period [s]
pos 1
pos 2
pos 3

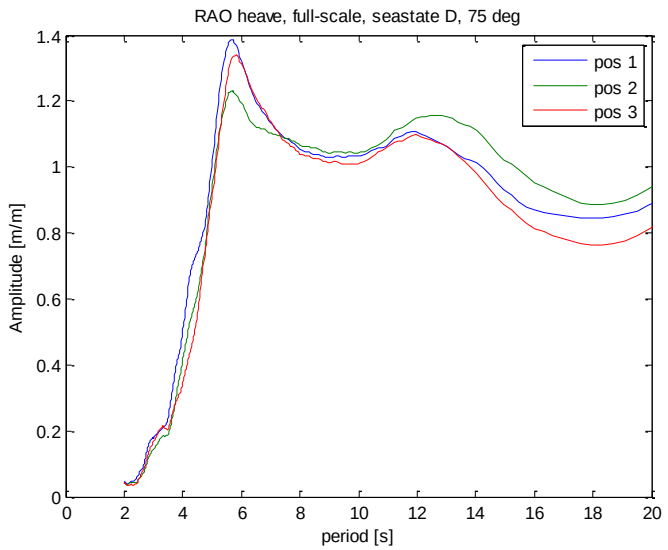
RAO heave, full-scale, seastate D, 75 deg
Amplitude [m/m]
period [s]
pos 1
pos 2
pos 3

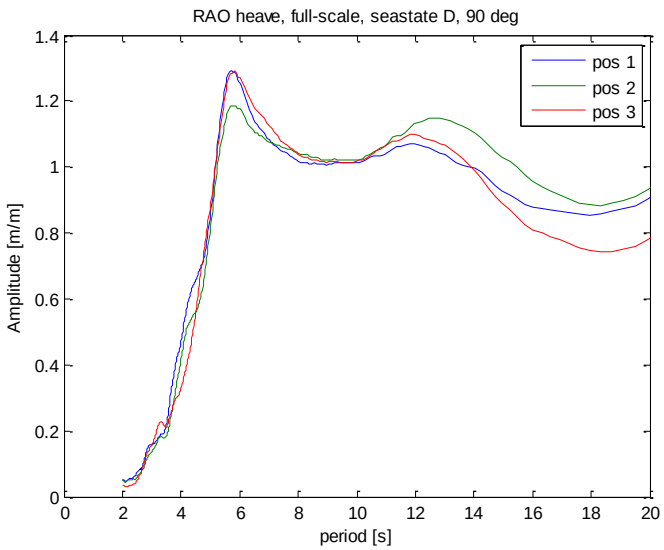
RAO heave, full-scale, seastate D, 90 deg
Amplitude [m/m]
period [s]
pos 1
pos 2
pos 3

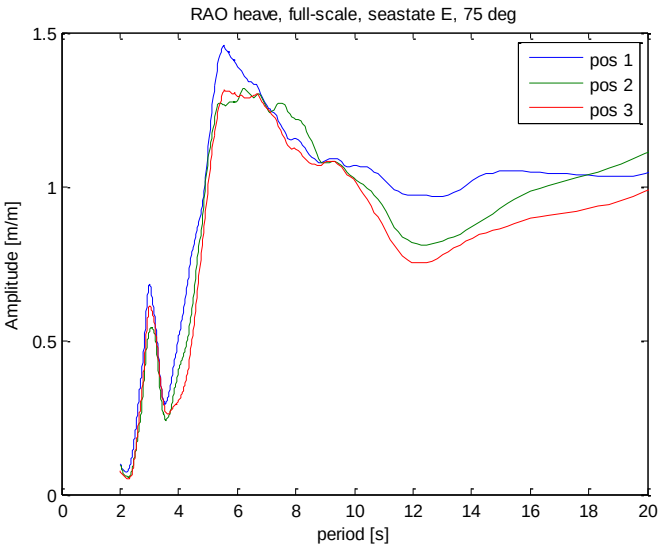
RAO heave, full-scale, seastate E, 75 deg
pos 1
pos 2
pos 3
Amplitude [m/m]
period [s]

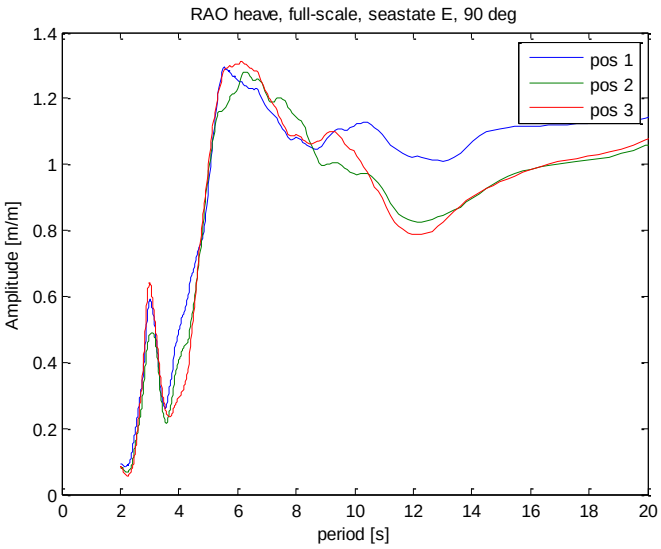
RAO heave, full-scale, seastate E, 90 deg
pos 1
pos 2
pos 3
Amplitude [m/m]
period [s]

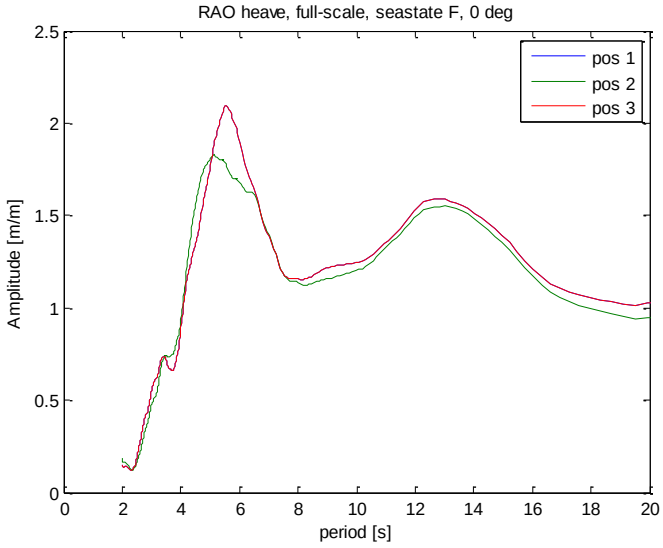
RAO heave, full-scale, seastate F, 0 deg
pos 1
pos 2
pos 3
Amplitude [m/m]
period [s]

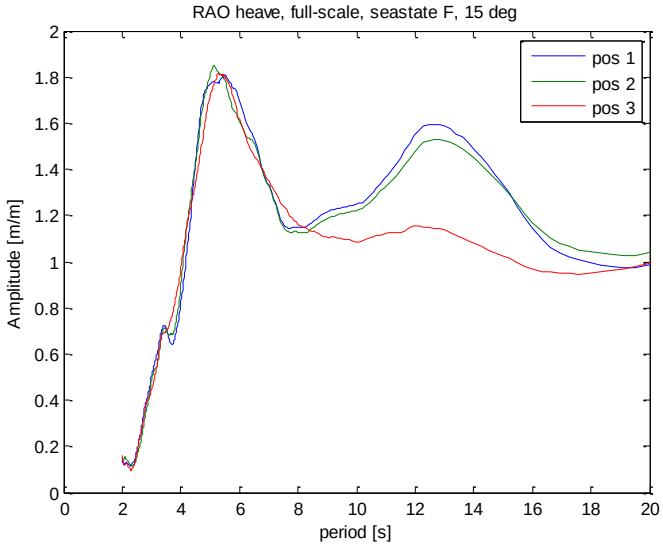
RAO heave, full-scale, seastate F, 15 deg
pos 1
pos 2
pos 3
Amplitude [m/m]
period [s]

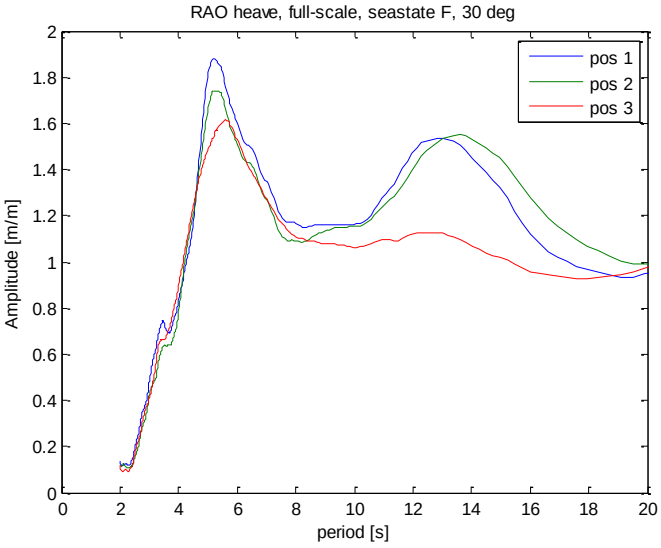
RAO heave, full-scale, seastate F, 30 deg
pos 1
pos 2
pos 3
Amplitude [m/m]
period [s]

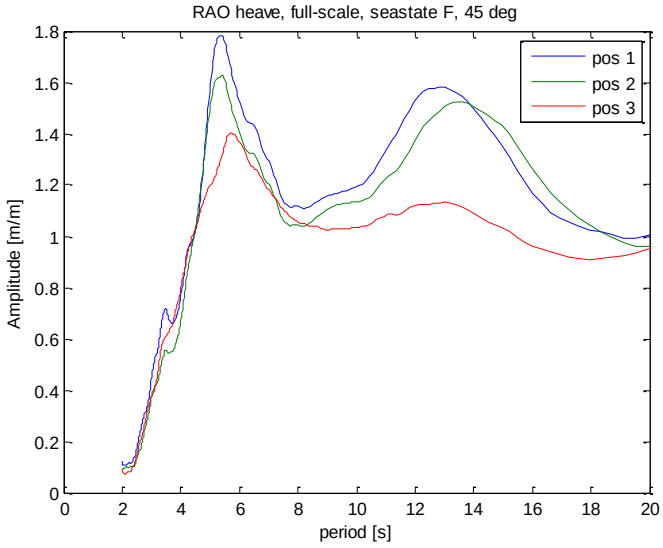
RAO heave, full-scale, seastate F, 45 deg
pos 1
pos 2
pos 3
Amplitude [m/m]
period [s]

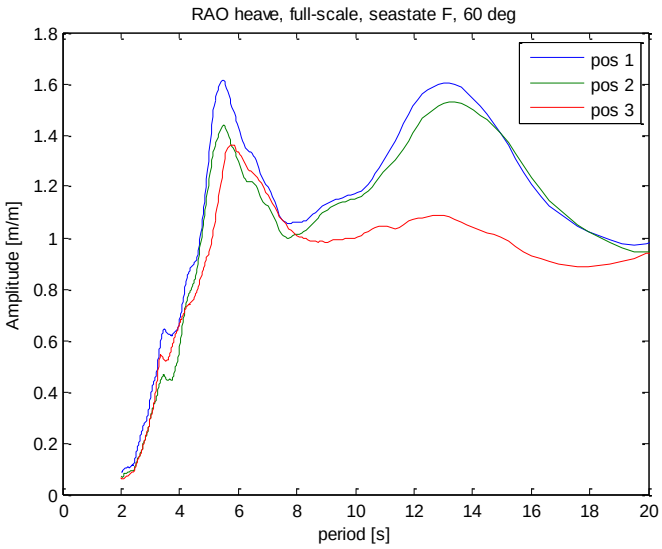
RAO heave, full-scale, seastate F, 60 deg
Amplitude [m/m]
period [s]
pos 1
pos 2
pos 3
0
0.2
0.4
0.6
0.8
1
1.2
1.4
1.6
1.8
0
2
4
6
8
10
12
14
16
18
20

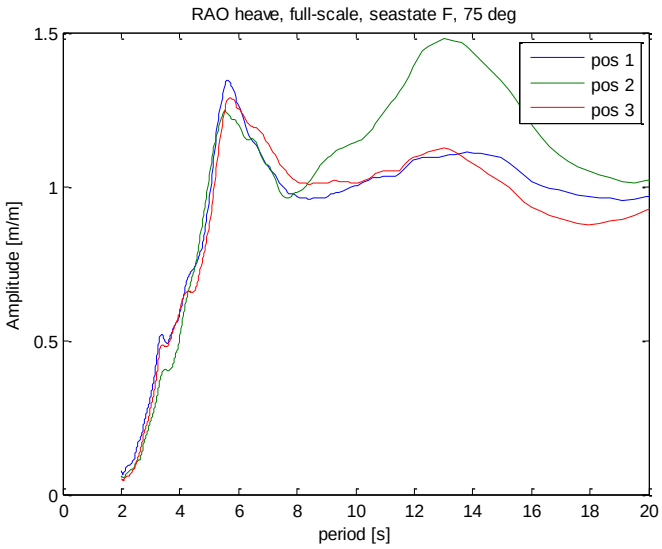
RAO heave, full-scale, seastate F, 75 deg
Amplitude [m/m]
period [s]
pos 1
pos 2
pos 3
0
0.5
1
1.5
0
2
4
6
8
10
12
14
16
18
20

Appendix F: RAO in surge, irregular waves

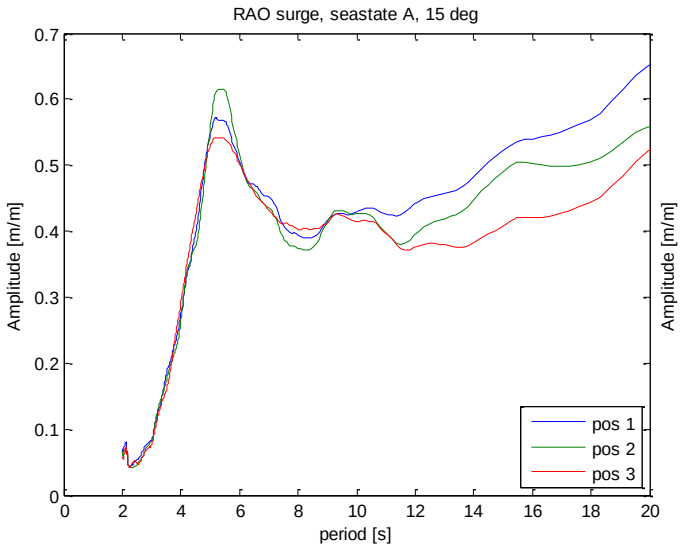

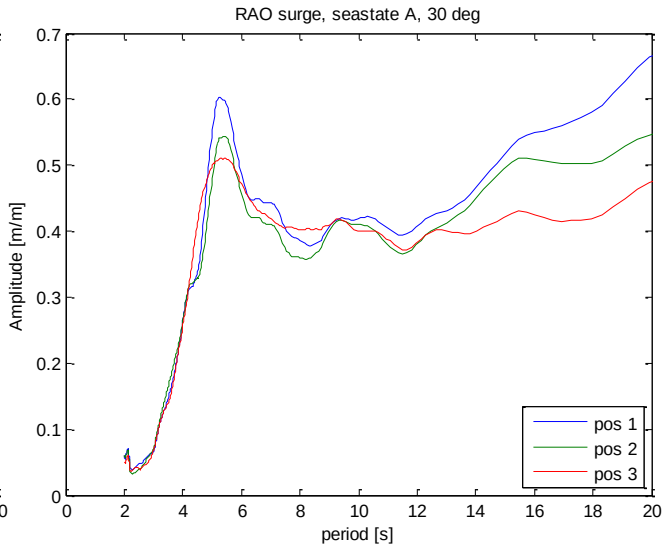

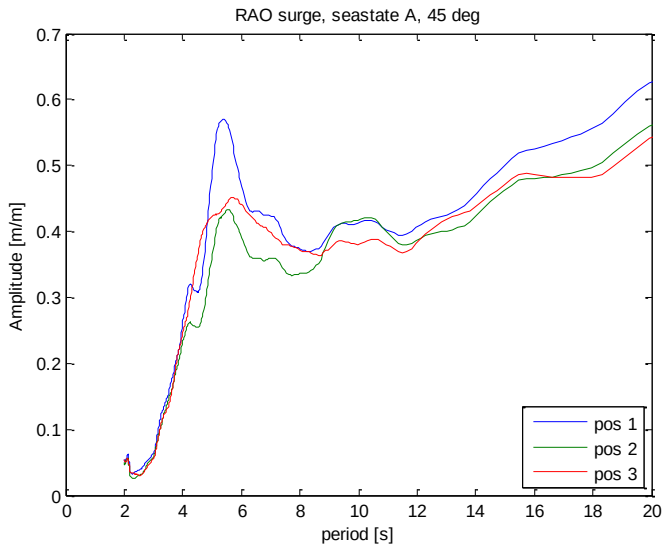

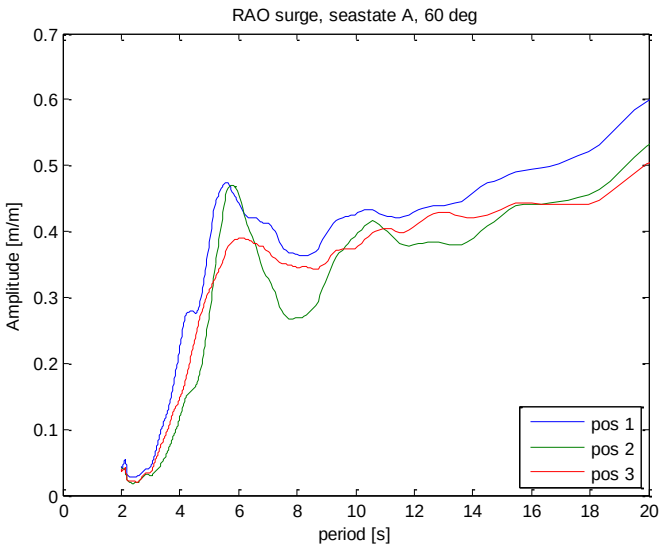

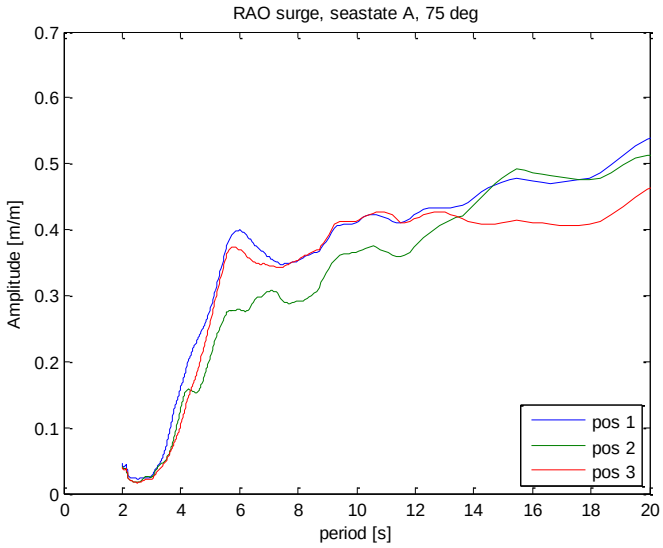

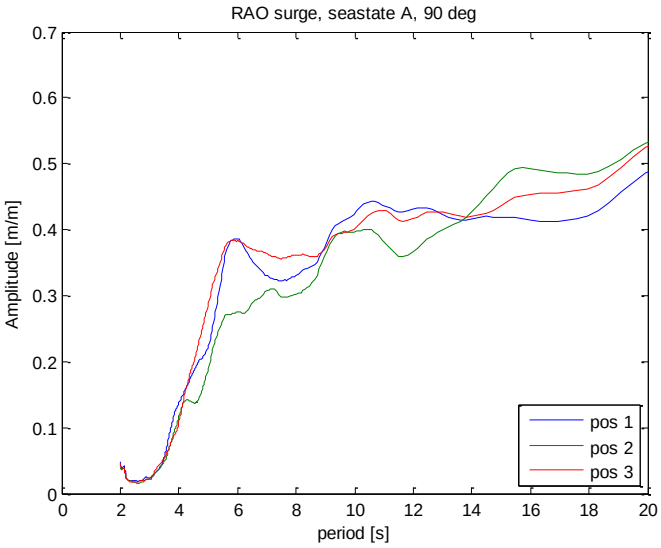

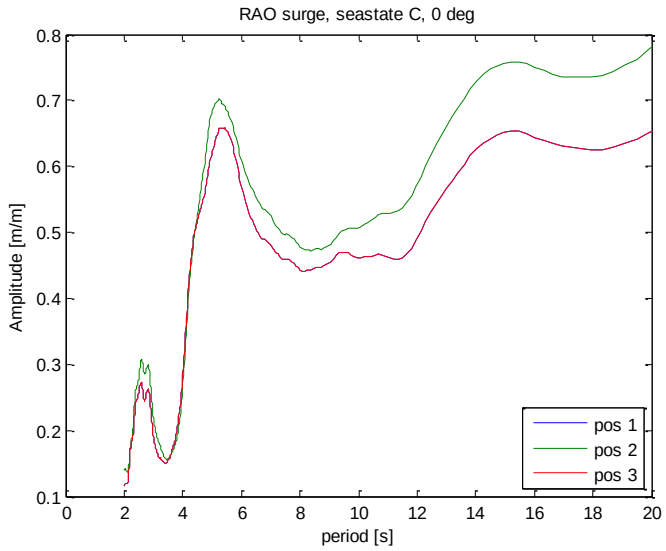
RAO surge, seastate C, 0 deg
Amplitude [m/m]
period [s]
pos 1
pos 2
pos 3

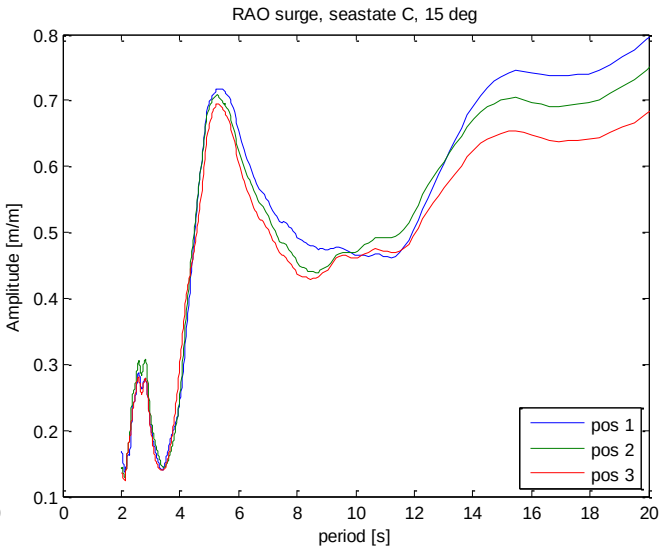
RAO surge, seastate C, 15 deg
Amplitude [m/m]
period [s]
pos 1
pos 2
pos 3

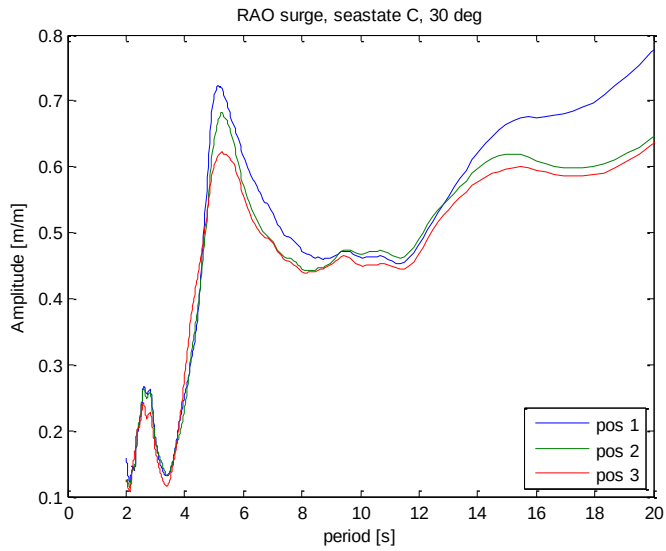
RAO surge, seastate C, 30 deg
Amplitude [m/m]
period [s]
pos 1
pos 2
pos 3

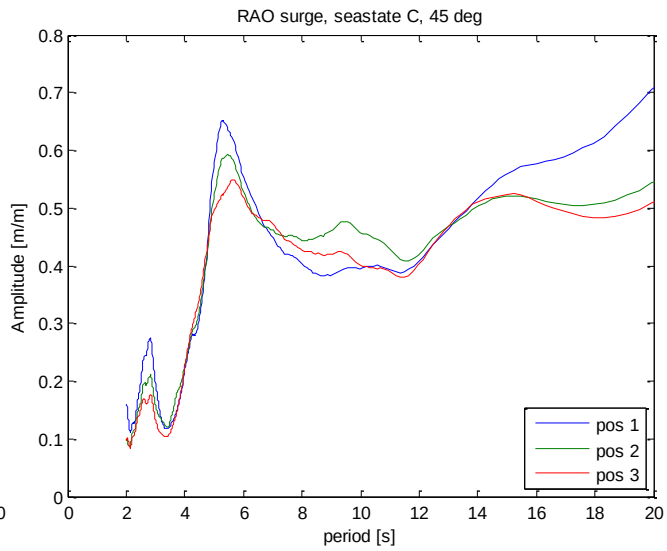
RAO surge, seastate C, 45 deg
Amplitude [m/m]
period [s]
pos 1
pos 2
pos 3

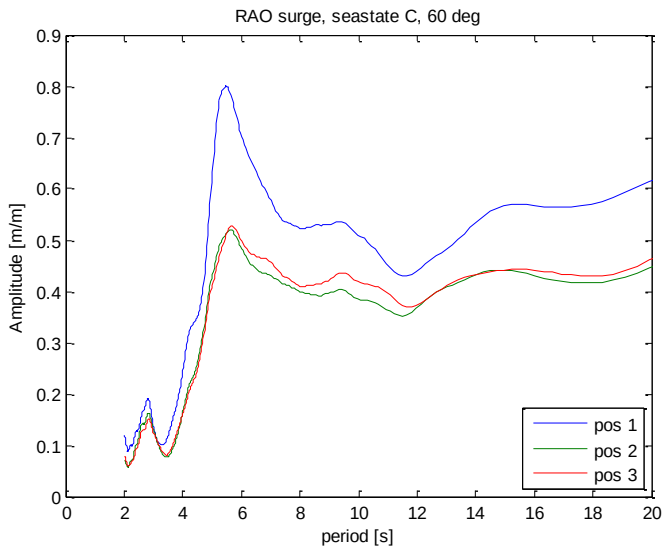
RAO surge, seastate C, 60 deg
Amplitude [m/m]
period [s]
pos 1
pos 2
pos 3

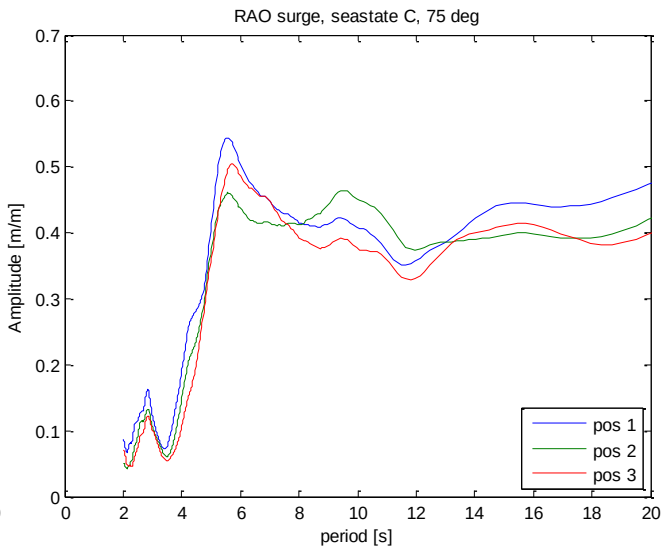
RAO surge, seastate C, 75 deg
Amplitude [m/m]
period [s]
pos 1
pos 2
pos 3

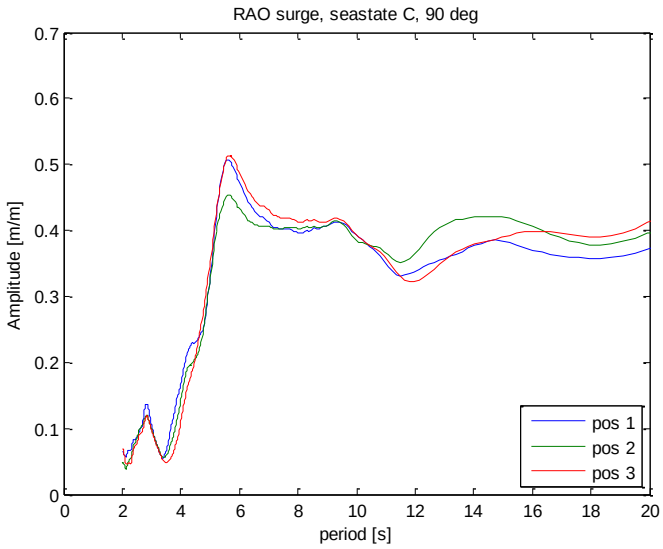
RAO surge, seastate C, 90 deg
Amplitude [m/m]
period [s]
pos 1
pos 2
pos 3

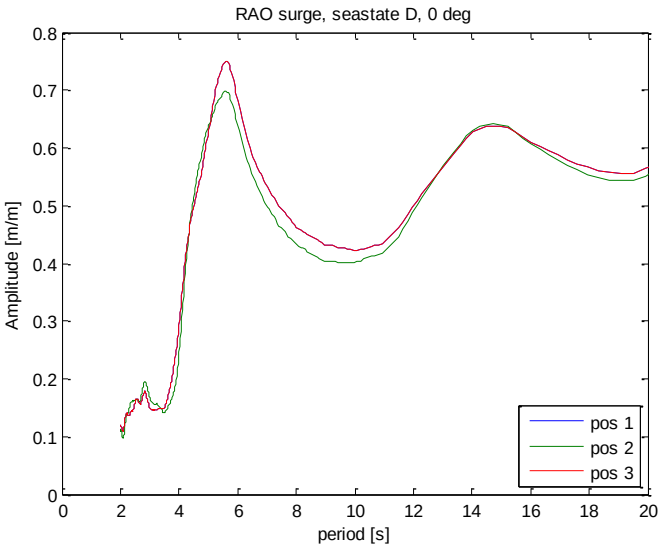
RAO surge, seastate D, 0 deg
Amplitude [m/m]
period [s]
pos 1
pos 2
pos 3

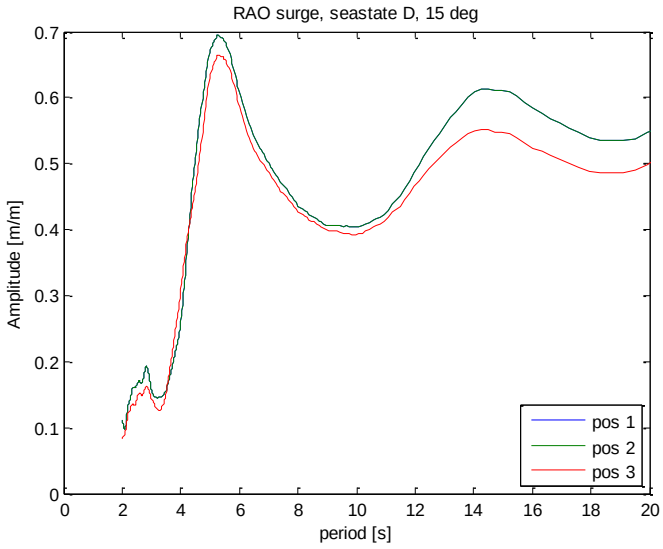
RAO surge, seastate D, 15 deg
Amplitude [m/m]
period [s]
pos 1
pos 2
pos 3

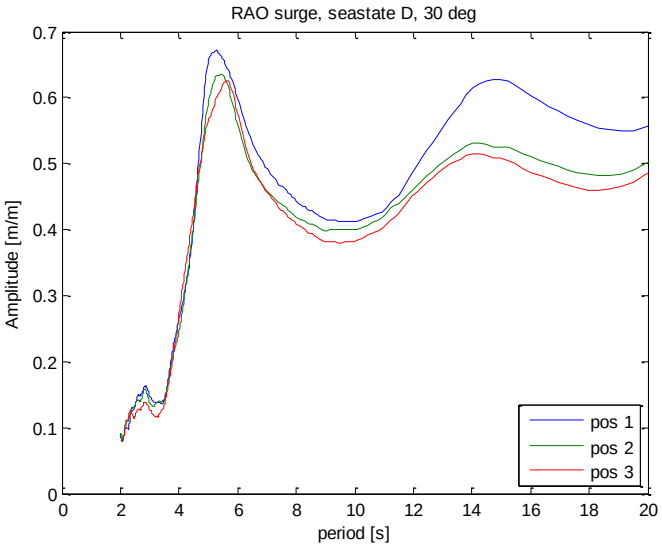
RAO surge, seastate D, 30 deg
Amplitude [m/m]
period [s]
pos 1
pos 2
pos 3

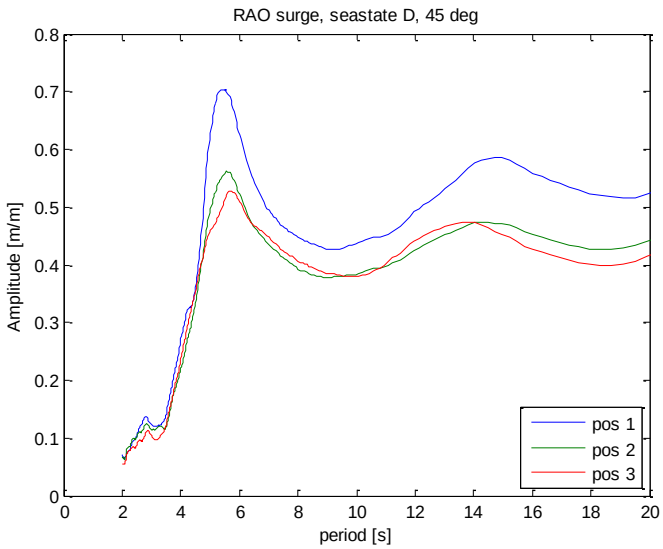
RAO surge, seastate D, 45 deg
Amplitude [m/m]
period [s]
pos 1
pos 2
pos 3

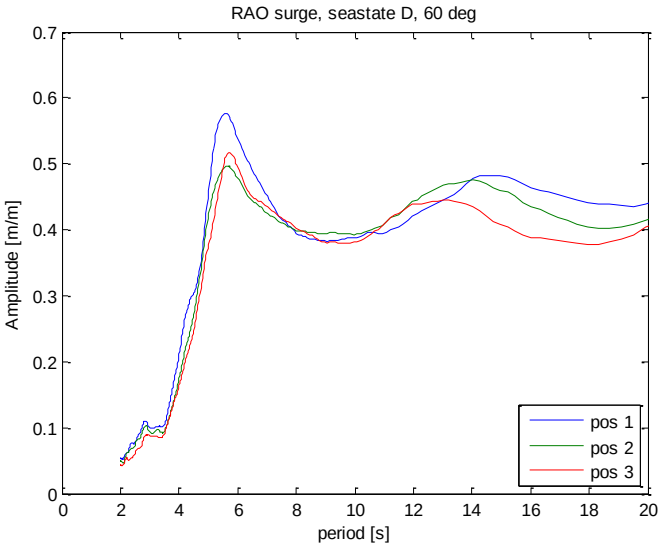
RAO surge, seastate D, 60 deg
Amplitude [m/m]
period [s]
pos 1
pos 2
pos 3

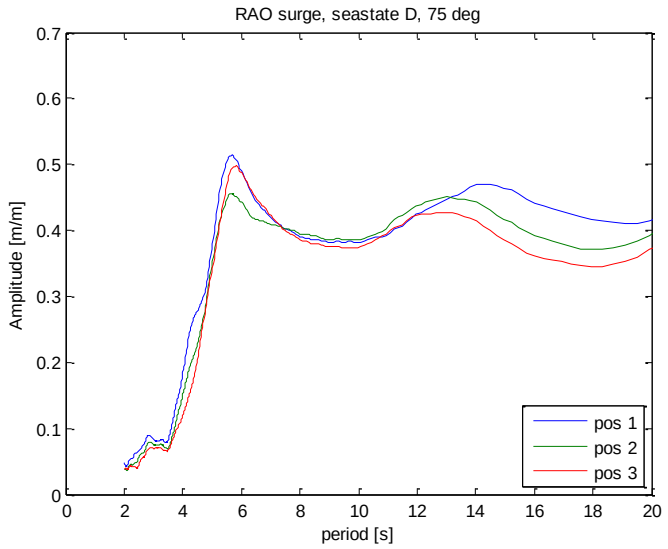
RAO surge, seastate D, 75 deg
Amplitude [m/m]
period [s]
pos 1
pos 2
pos 3

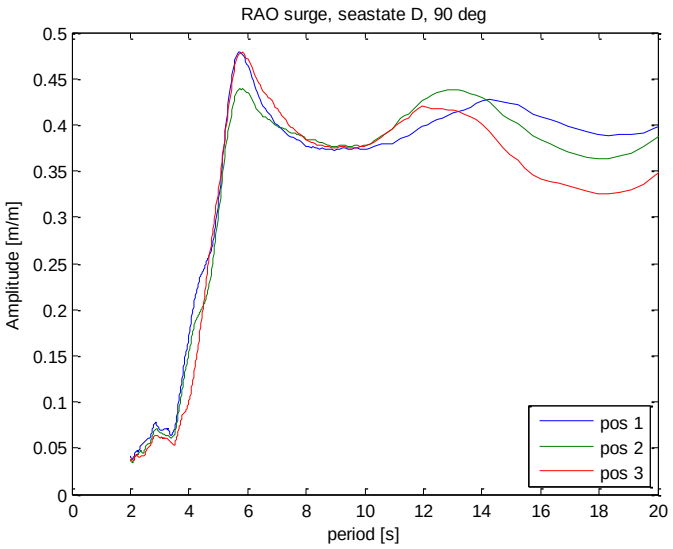
RAO surge, seastate D, 90 deg
Amplitude [m/m]
period [s]
pos 1
pos 2
pos 3

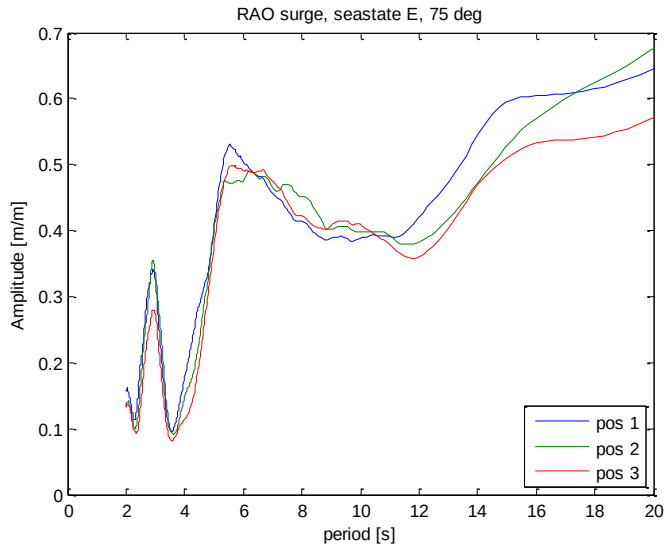
RAO surge, seastate E, 75 deg
Amplitude [m/m]
period [s]
pos 1
pos 2
pos 3

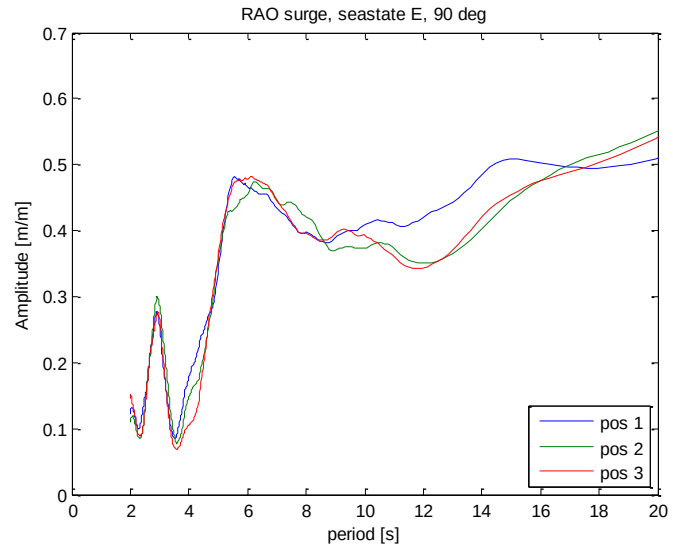
RAO surge, seastate E, 90 deg
Amplitude [m/m]
period [s]
pos 1
pos 2
pos 3

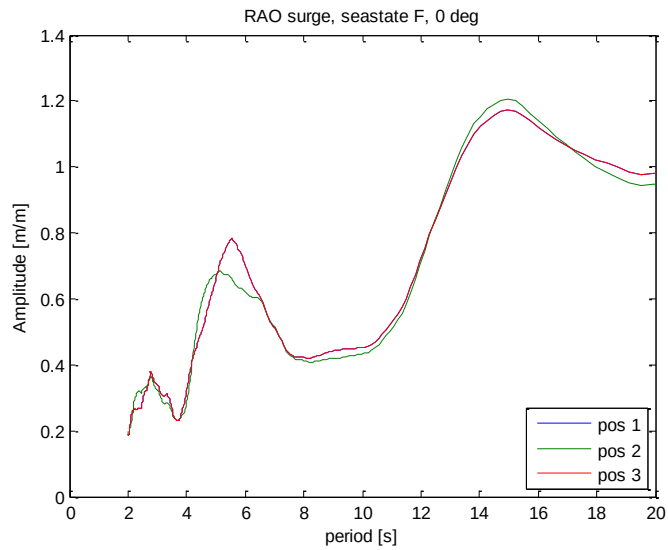
RAO surge, seastate F, 0 deg
Amplitude [m/m]
period [s]
pos 1
pos 2
pos 3

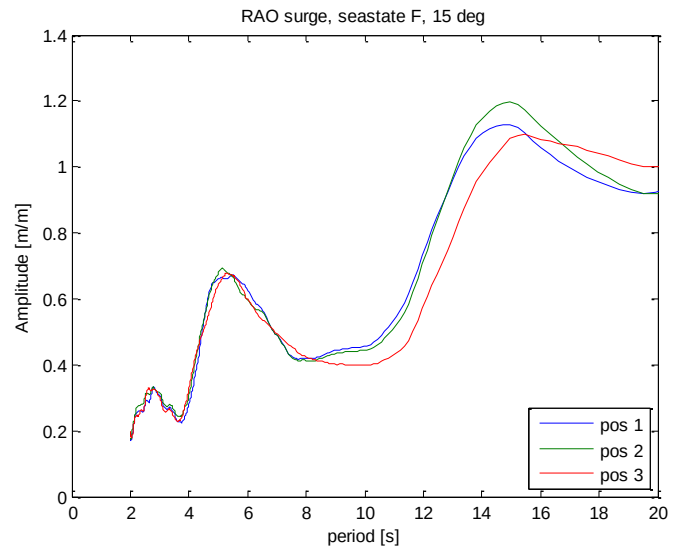
RAO surge, seastate F, 15 deg
Amplitude [m/m]
period [s]
pos 1
pos 2
pos 3

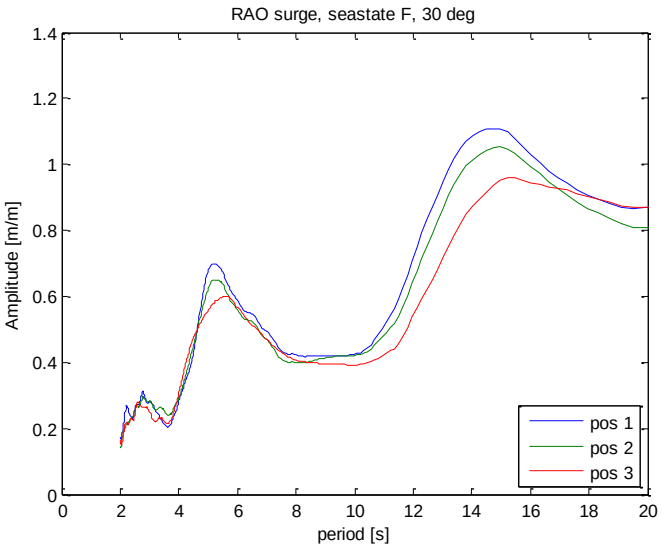
RAO surge, seastate F, 30 deg
Amplitude [m/m]
period [s]
pos 1
pos 2
pos 3

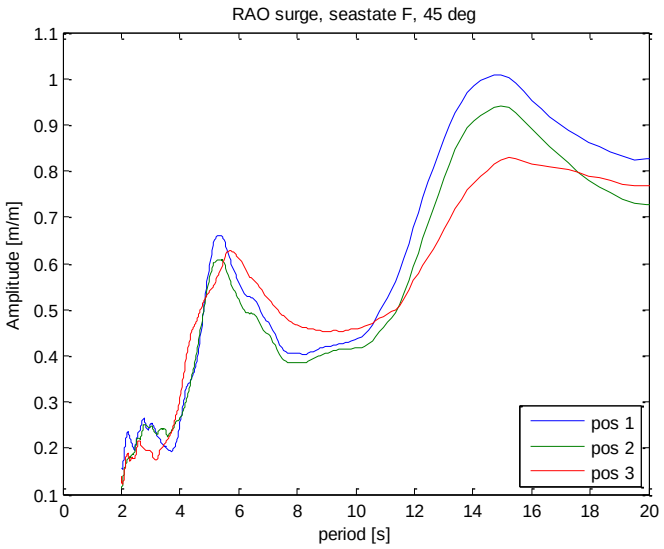
RAO surge, seastate F, 45 deg
Amplitude [m/m]
period [s]
pos 1
pos 2
pos 3

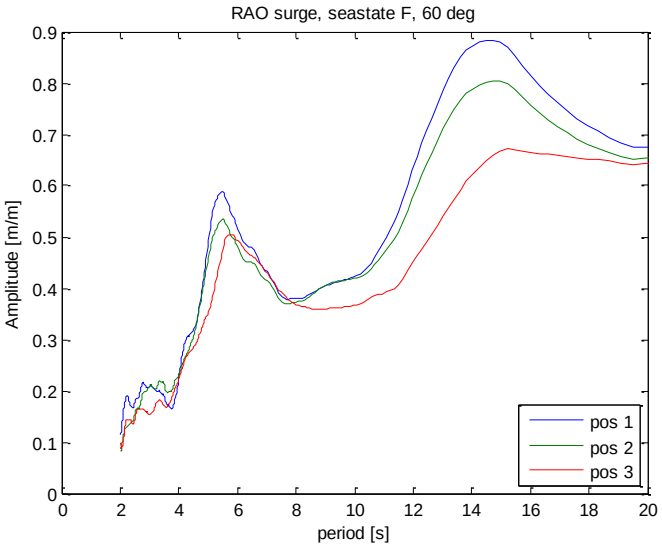
RAO surge, seastate F, 60 deg
Amplitude [m/m]
period [s]
pos 1
pos 2
pos 3

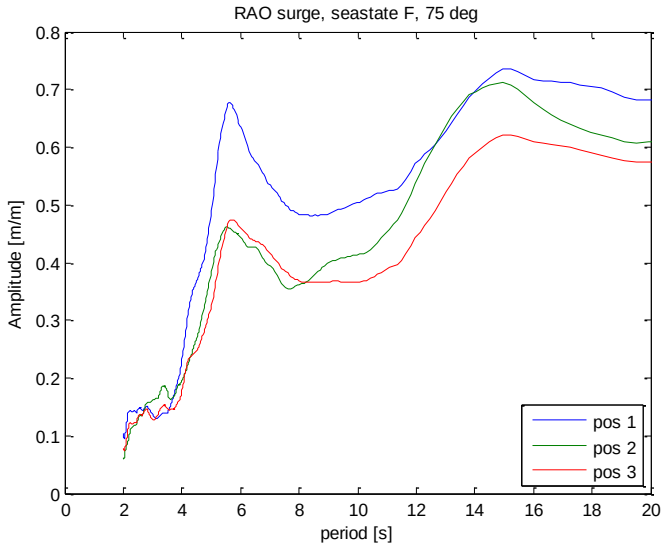
RAO surge, seastate F, 75 deg
Amplitude [m/m]
period [s]
pos 1
pos 2
pos 3

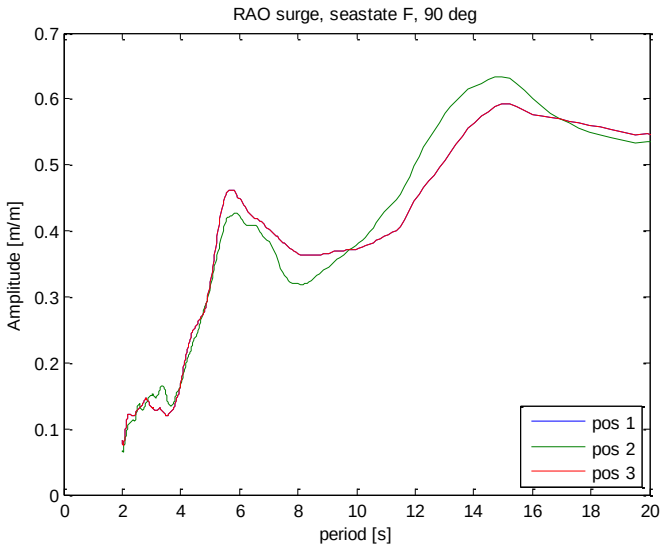
RAO surge, seastate F, 90 deg
Amplitude [m/m]
period [s]
pos 1
pos 2
pos 3

Appendix G: Max vertical force, transducers 8600 and 860. Model scale.

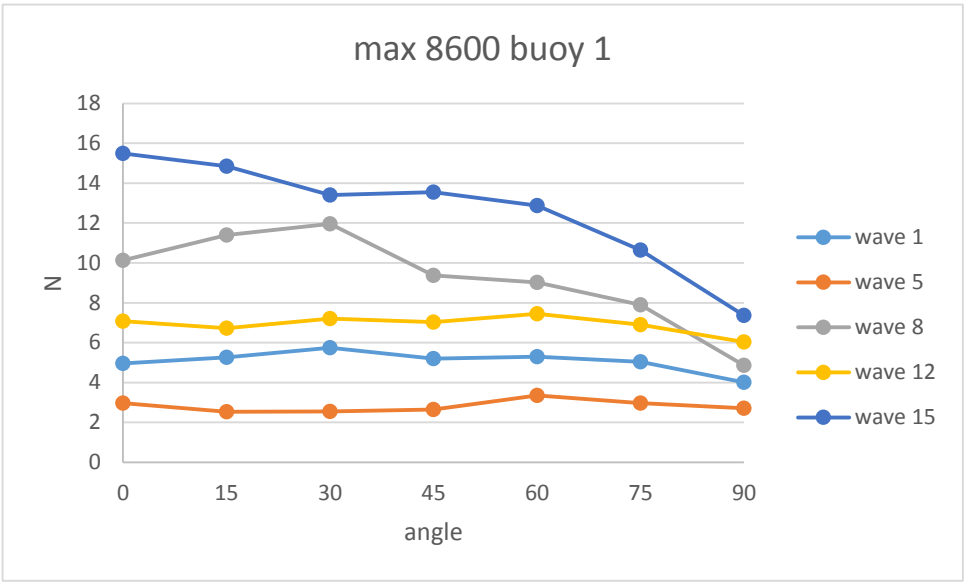

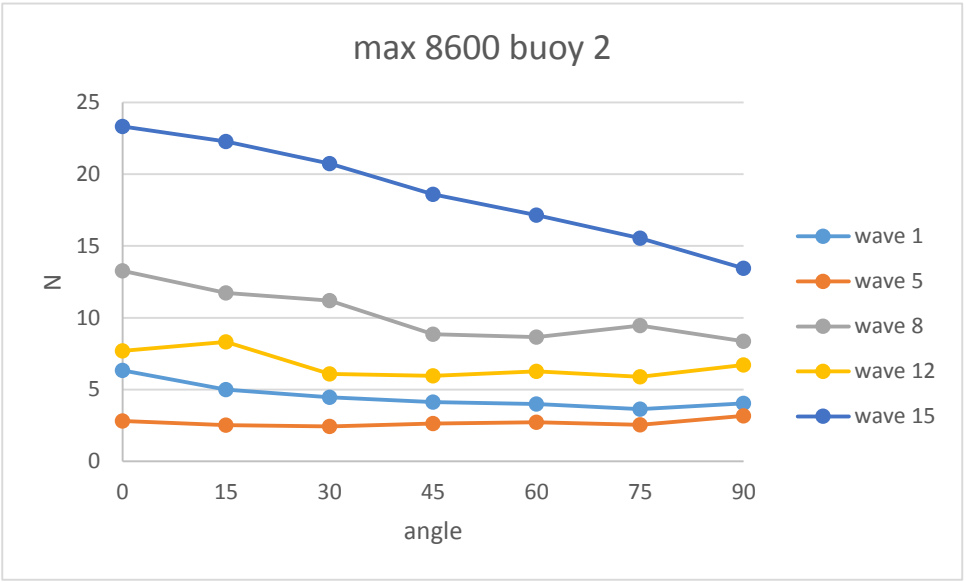

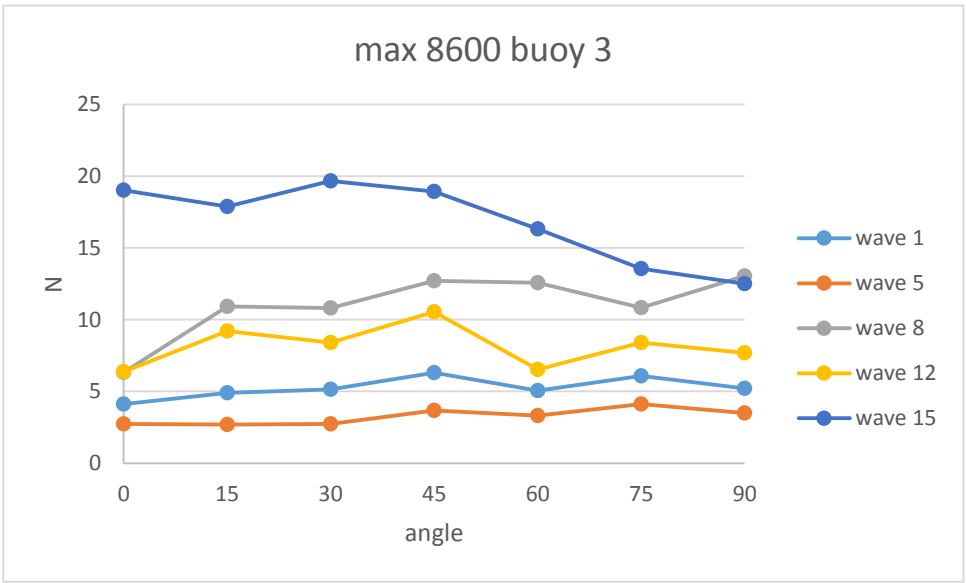


max 8601 buoy 1
25
20
15
10
5
0
N
0
15
30
45
60
75
90
angle
wave 1
wave 5
wave 8
wave 12
wave 15

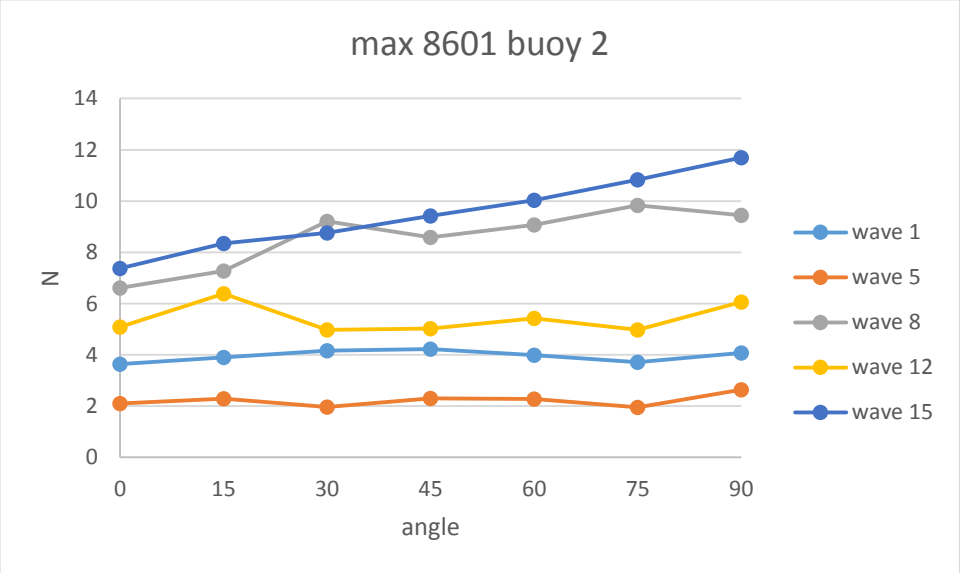
max 8601 buoy 2
14
12
10
8
6
4
2
0
N
0
15
30
45
60
75
90
angle
wave 1
wave 5
wave 8
wave 12
wave 15

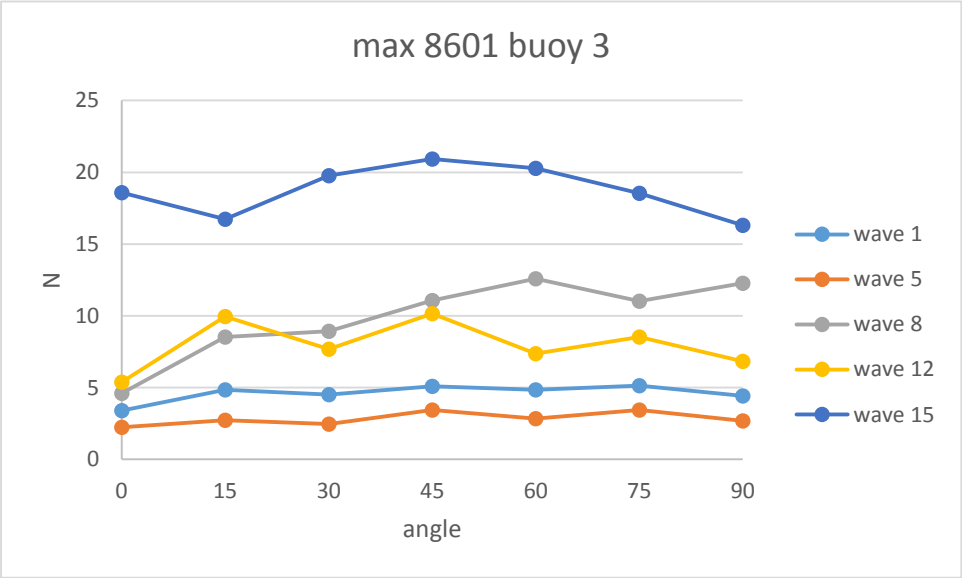
max 8601 buoy 3
25
20
15
10
5
0
N
0
15
30
45
60
75
90
angle
wave 1
wave 5
wave 8
wave 12
wave 15

Appendix H: Significant values, vertical forces. Full-scale values.

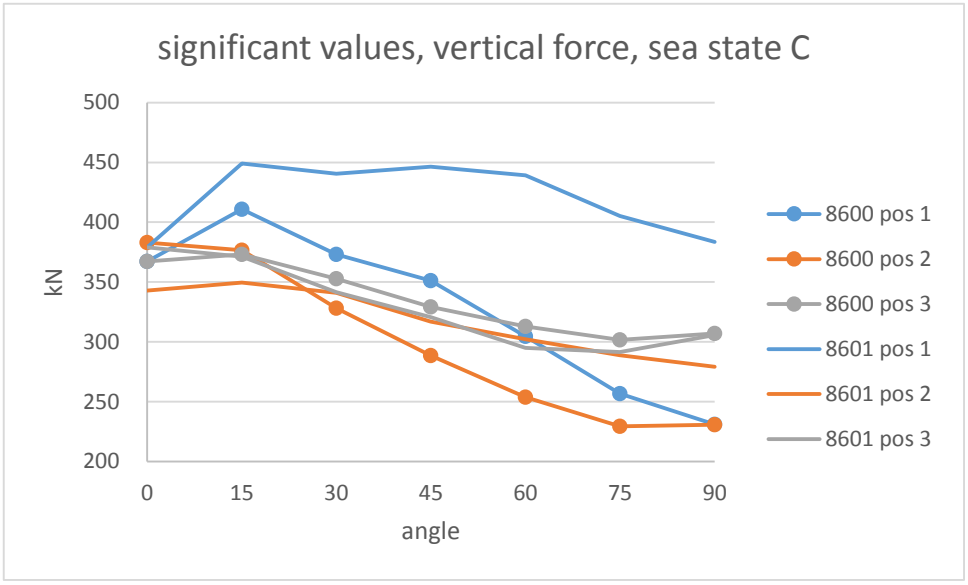

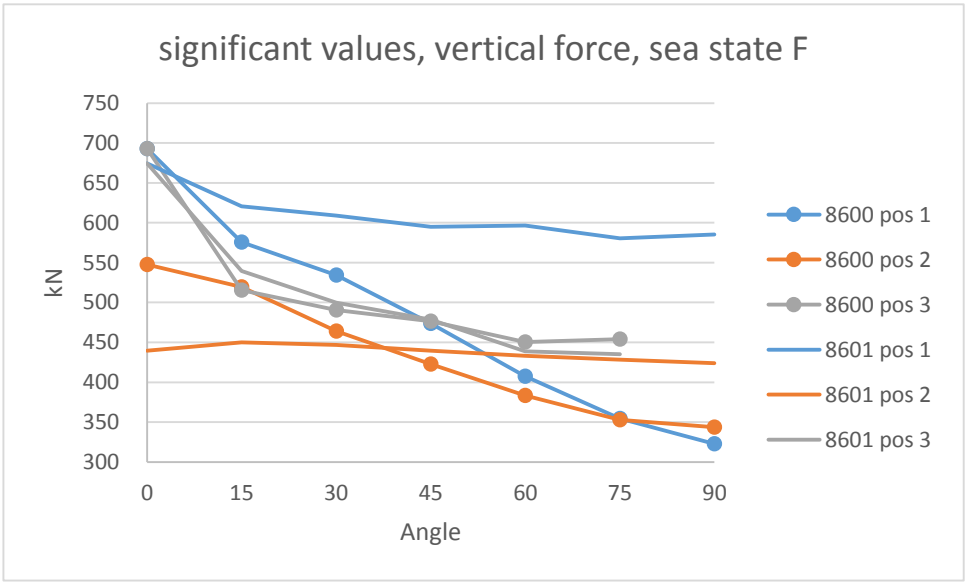

Appendix I: Max horizontal force, transducers 8603 and 8603. Model scale.

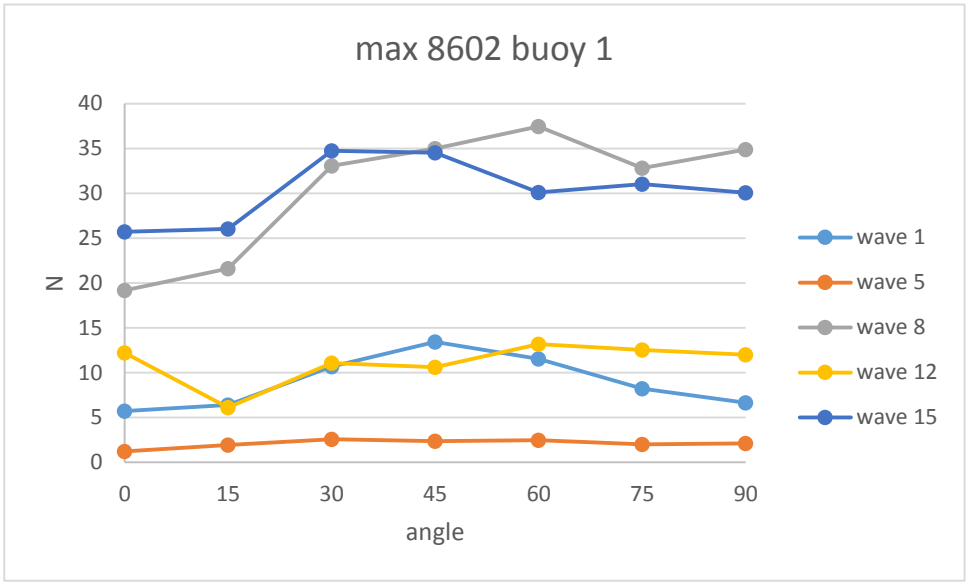

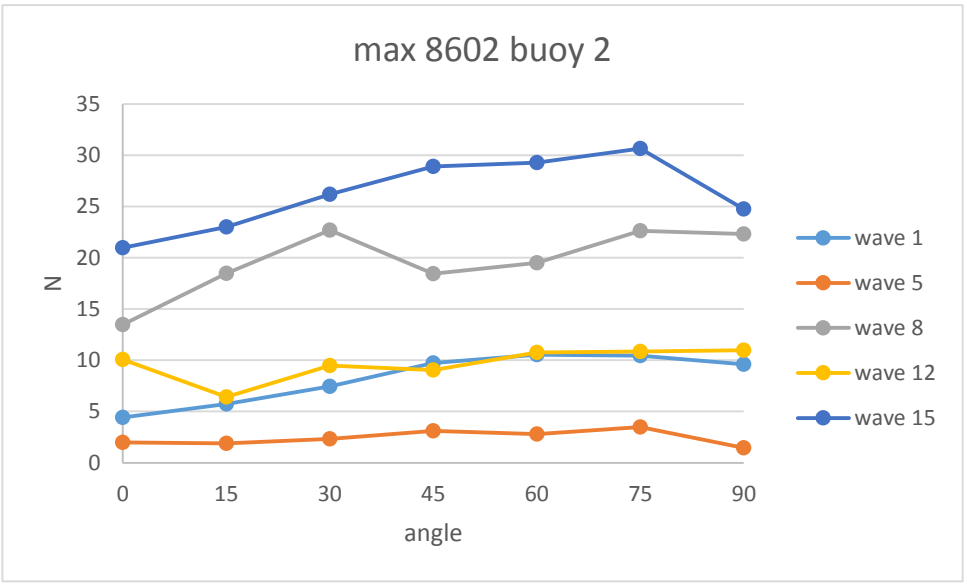

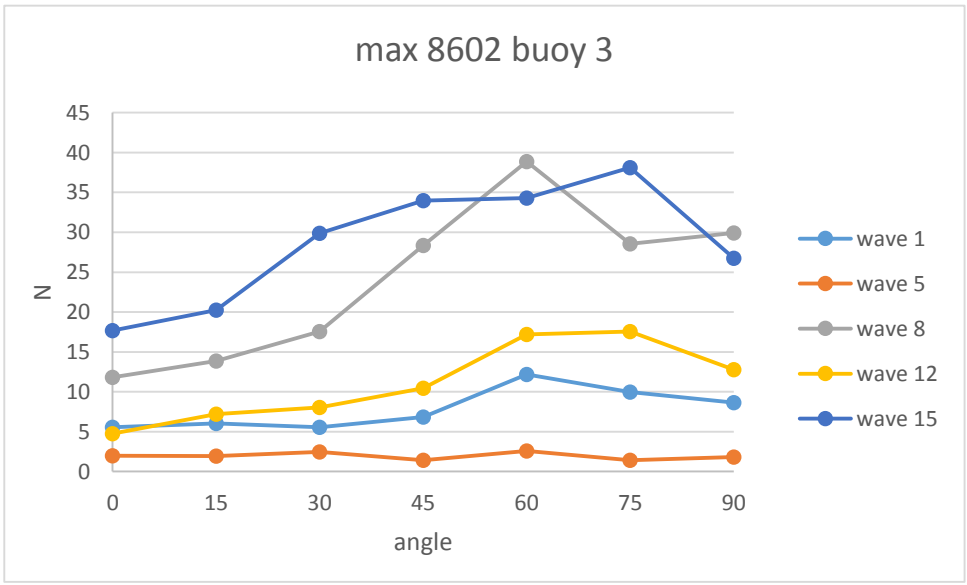

Appendix J: Significant values, horizonal forces. Full-scale values.

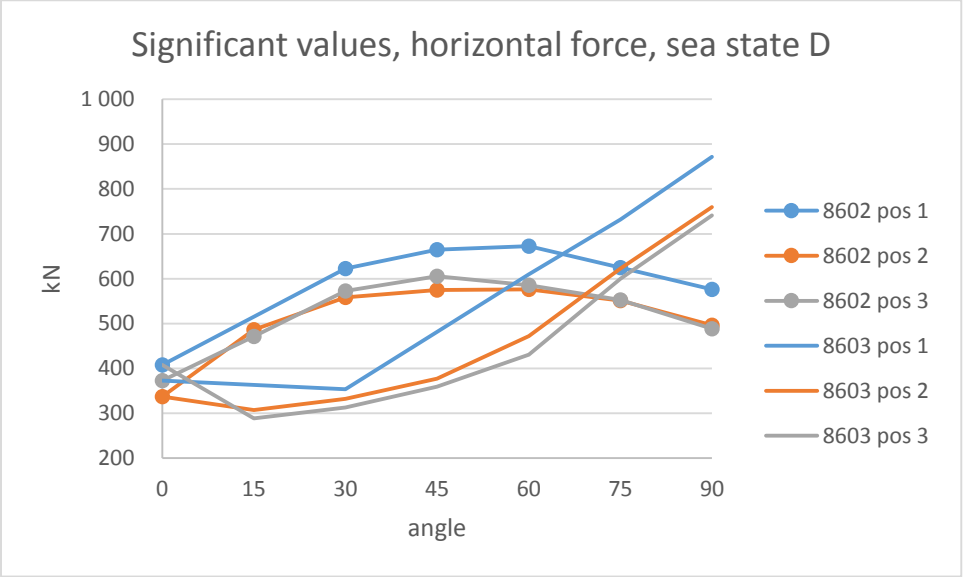

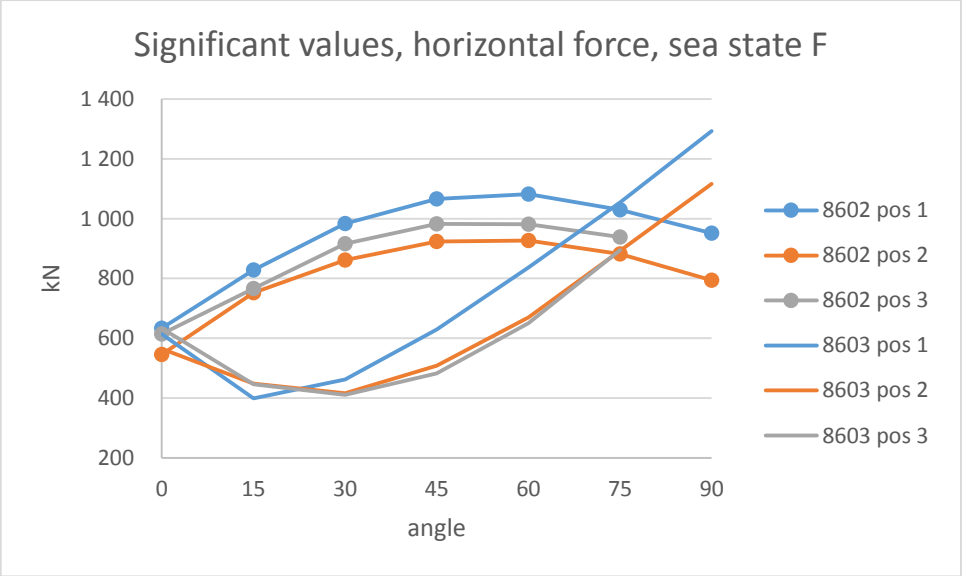

Appendix K: Fixed elongation coupling settings SIMA

buoy 1				buoy 2			
wave 1				wave 1			
No	distance	force	damping	No	distance	force	damping
1	0	1.50E+06	0	1	0	1.50E+06	0
2	19	-7.00E+05	0	2	19	-7.00E+05	0
wave 5				wave 5			
No	distance	force	damping	No	distance	force	damping
1	0	1.00E+06	2.10E+05	1	0	1.00E+06	3.00E+05
2	12.36	-1.00E+04	2.10E+05	2	17	0.00E+00	3.00E+05
wave 8				wave 8			
No	distance	force	damping	No	distance	force	damping
1	0	1.80E+06	0	1	0	1.80E+06	0
2	17	-7.00E+05	0	2	17	-7.00E+05	0
wave 12				wave 12			
No	distance	force	damping	No	distance	force	damping
1	0	1.00E+06	2.10E+05	1	0	1.00E+06	2.10E+05
2	12.36	-1.00E+04	2.10E+05	2	12.36	-1.00E+04	2.10E+05
wave 15				wave 15			
No	distance	force	damping	No	distance	force	damping
1	0	8.00E+05	2.10E+05	1	0	2.00E+06	6.00E+04
2	12.36	-5.00E+05	2.10E+05	2	10	-1.00E+05	6.00E+04
sea state D							
No	distance	force	damping	No	distance	force	damping
1	0	1.80E+06	1.00E+05	1	0	2.00E+06	6.00E+04
2	17	-7.00E+05	1.00E+05	2	10	-1.00E+05	6.00E+04

buoy 3			
wave 1			
No	distance	force	damping
1	0	1.50E+06	0
2	19	-7.00E+05	0
wave 5			
No	distance	force	damping
1	0	1.00E+06	3.00E+05
2	13	-1.00E+04	3.00E+05
wave 8			
No	distance	force	damping
1	0	1.80E+06	0
2	17	-7.00E+05	0
wave 12			
No	distance	force	damping
1	0	1.00E+06	3.00E+05
2	13	-1.00E+04	3.00E+05
wave 15			
No	distance	force	damping
1	0	4.50E+06	2.10E+05
2	15	-1.00E+06	2.10E+05
No	distance	force	damping
1	0	4.50E+06	2.10E+05
2	15	-1.00E+06	2.10E+05